Hera-B experiment:

preparation and first results

Stefania Xella

May 1999

Niels Bohr Institute

University of Copenhagen

Contents

INTRODUCTION

Hera-B is a new and nice experiment, where CP violation and production of heavy quark bound states are just two of the many physical phenomena that can be investigated.
It's an hadronic experiment, it detects proton - nucleus collisions, and the high particle radiation (due to the strength of the strong interactions among quark and gluons) makes the detection and analysis rather challenging.
The Ph.D. work, subject of this report, was done in Hera-B, in a period (1996- 1999) where the detector still had to be assembled, and many things were happening, from the point of view of software and hardware development.
The work has followed the flow of the experiment, and has consisted in first instance on the development of a tracking algorithm for the second level trigger. This has required a thorough study on simulated data, to understand the performances of the code, and ensure that two important points, namely high efficiency and limited processing time, were respected.
In the last few years measurements on production of charmonium (charm-anticharm bound state) have played a very important role in guiding the theoretical community to the understanding of the process of formation of these states. The formation involves several time scales, and therefore demands to be explained with more than one theoretical approach. Hera-B can continue on this line, for example providing interesting measurements of nuclear dependence of cross sections.
The second part of this Ph.D. work has consisted of a study of charmonium measurements in simulation environment with a reduced setup for the detector, in preparation for the data taking run.
The last part of this work is concentrated on analysis of data taken during the period March-April 1999. As one can imagine, the understanding of the detector and of the data at a very short time after the end of data taking can only be preliminary, anyway a search for J/ψ has been attempted, and this is also reported here.
The report is structured in three chapters.
The first chapter is a general introduction to Hera-B detector and trigger system, and to the physics goals Hera-B wants to achieve.
The second chapter describes two studies performed on simulated data, to develop a trigger algorithm for the Second Level Trigger of the experiment and to study the physics potential achievable with a non complete setup of the detector.
The third chapter is a summary of the analysis conducted on the recently taken data.

Comment:
Along the way some symbols will be introduced, for shortness of notation. They will be explained the first time they will be used in the text. Further, one can refer to the glossary at the end of the report.

Chapter 1

A new experiment

1.1 Hera-B and heavy quark physics

Hera-B comes to operation in a period of transition for high energy physics in Europe. The LEP experiments are analyzing their final data, and the Large Hadron Collider (LHC), the next big challenge of CERN, is due to year 2005. So for what concerns precise tests of the Standard Model, Hera-B stands essentially alone in Europe.

Hera-B is a high energy, fixed target pN experiment located at DESY (Hamburg). After several years of operation of the Hera storage ring, which has been providing 920 GeV protons at 10 MHz rate for the last decade for ep interaction studies, Hera-B inserts itself in the panorama of DESY physics by inserting a set of target wires in the region of the halo of the beam, and proposing a physics program concentrated on study of B mesons and their properties. The considerable boost given to the produced particles favors this type of study, enhancing $b\overline{b}$ events in respect to $c\overline{c}$ and minimum bias background of few orders of magnitude higher, where particles essentially come from the region of primary interaction.

The idea of using an hadronic machine for studying heavy quark physics with high statistics is not new, clearly hadronic machines have the advantage to reach more easily high center of mass energies with respect to e^+e^- machines, and even when staying at moderate energies, they can easily reach significantly higher production of heavy quarks compared to e^+e^- storage rings.

However the typical problem hadronic machine encounter is the high background, of several orders of magnitude higher than the interesting signal. The high radiation can constitute a problem for the detector employed, for the trigger system, and finally for the reconstruction off-line. The proof of principle for Hera-B , which allowed with good confidence to proceed with the experiment realization, was the experience with the collider experiments at Fermilab (CDF,D0), and with the fixed target experiments, also at Fermilab, E789 and E791. Especially the last ones share a lot of common features with Hera-B , and have showed to be able to sustain the rate and cleanly isolate the heavy quark signal out of the overwhelming background. For Europe, Hera-B is a good training chance, since it resembles the conditions LHC experiments will be in a few years.

The main goal of Hera-B is to contribute to CP violation measurements in beauty quark decays, since this phenomenon, expected to be quite large for B mesons, has never been accurately measured before and Hera-B has by her side a high statistics production of b quarks, due to the strong interactions operating in pN collisions. Hera-B has access to measurements of $B \to J/\psi K^0_s$, $B \to \pi\pi$ and $B \to \pi K$, and therefore of the 3 angles of the CKM matrix. Another goal, which seems achievable only by this experiment for the next couple of years is the measurement of mixing of the B_s meson. It will be impossible for Babar, since the center

of mass energy is too low, and it will be difficult for CDF, since the cuts on momenta applied for data acquisition purposes and for the bad kaon/pion separation power which oblige CDF to refer to lepton identifications of B's, overall making the statistics available more than 2 orders of magnitude smaller than in Hera-B . Hera-B can also contribute to studies of rare B decays, which are interesting mainly because they provide a good field for discovering effects of physics beyond the Standard Model.

Further, during the run in August-December 1998, and January-April 1999, the incompleteness of the detector has allowed to have milder cuts at trigger level, in particular it has not been necessary to apply a secondary vertex cut. This has provided Hera-B with a sample of directly produced $c\overline{c}$ bound states, and the potential to contribute with new measurements to the theoretical field of charmonium production. I chose this to be the main subject of the data analysis performed in the last period of my Ph.D. work. The analysis I performed on this collected sample is described in chapter 3.

1.1.1 Beauty physics

CP VIOLATION: general introduction

The violation of CP (C= charge conjugation, P= parity) symmetry was observed in electroweak interactions including strange mesons in 1964. Both CERN and Fermilab experiments have provided measurements of CP violation significantly different from zero in K decays. The amount of CP violation is not big ($\sim 10^{-4}$), and it can easily be accommodated in the 3 generation Standard Model (SM) by simply not requiring a CP symmetric lagrangian [4]. The ElectroWeak (EW) Lagrangian expressed in flavour states is:

$$L_{int} = (u'c't')\gamma^{\mu} \begin{pmatrix} d' \\ s' \\ b' \end{pmatrix} W^{\mu} + hc$$

but the flavour states are not the mass states (observables). If one expresses the lagrangian in terms of the mass states, then

$$L_{int} = (uct)\gamma^{\mu} V_{CKM} \begin{pmatrix} d \\ s \\ b \end{pmatrix} W^{\mu} + hc$$

where V_{CKM}, called mixing matrix or Cabibbo Kobayashi Maskawa matrix (by the name of the first people who thought and then formalized the concept of mixing among quark families), expresses the mixing probabilities of quarks of one family into quarks of the other families. Mixing among lepton families has not been yet established to be observed, but can be in principle accommodated in a similar way. Now, the phenomenon of mixing among quark families in itself does not bring CP violation into the SM. But the fact that the number of quark families is 3 does. V is a unitary $n \otimes n$ matrix. An arbitrary $n \otimes n$ matrix has $2n^2$ real parameters, but unitarity ($V^{+}V = 1$) provides n^2 constraints, so only n^2 real parameters remain. We may remove $2n-1$ of these by appropriate redefinitions of relative quark phases. The number of remaining parameters is then $n^2 - (2n-1) = (n-1)^2$. Of these, $n(n-1)/2$ (the number of independent rotations in n dimensions) correspond to angles, while the rest, $(n-1)(n-2)/2$, correspond to phases. Therefore, for $n = 2$ the number of phases is zero, and the V matrix can be made orthogonal. But if $n = 3$, then there is 1 phase, which in general cannot be eliminated. This was what lead Kobayashi and Maskawa to introduce a third quark doublet.

The existence of this phase provides a potential source of CP violation[1] : one can think of the amplitude of an electroweak process as a number A (which is function of V), and saying that CP is a symmetry of the system then means $A = \overline{A}$. This is always true if A is real, but one can imagine to potentially encounter problems if A is complex.

The V_{CKM} is commonly parametrized[3] in terms of $\lambda \simeq 0.22$, , while the phase is expressed as term $(\rho - i\eta)$:

$$V \simeq \begin{bmatrix} 1-\lambda^2/2 & \lambda & A\lambda^3(\rho - i\eta) \\ -\lambda & 1-\lambda^2/2 & A\lambda^2 \\ A\lambda^3(1-\rho-i\eta) & -A\lambda^2 & 1 \end{bmatrix}$$

$A \simeq 0.79 \pm 0.06$, and $(\rho^2+\eta^2)^{1/2} = 0.36 \pm 0.09$. V_{CKM} in this form is an expansion in $\lambda \equiv -V_{cd}$, and it is correct only up to order λ^3.

The unitarity of the matrix implies that $V_{ij}^* V_{ik} = \delta_{jk}$ and $V_{ij}^* V_{kj} = \delta_{ik}$. For example,

$$V_{ud}^* V_{td} + V_{us}^* V_{ts} + V_{ub}^* V_{tb} = 0 \tag{1.1}$$

Since $V_{ud}^* \simeq 1$, $V_{us}^* \simeq \lambda$, $V_{ts} \simeq -A\lambda^2$, and $V_{tb} \simeq 1$, we have $V_{td} + V_{ub}^* = A\lambda^3$. Eq. 1.1 can be represented like a triangle in the complex plane (ρ, η), like in fig. 1.1.

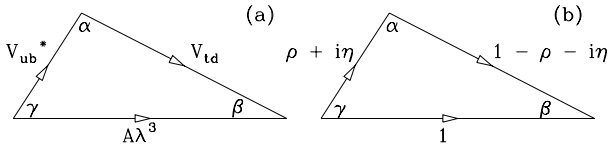

Figure 1.1: *Unitarity triangle for CKM elements. (a) the relation 1.1 in complex plane. (b) the relation 1.1 divided by $A\lambda^3$. The angles α, β, γ are also noted.*

It is important to improve our knowledge of both the sides of the triangle and the angles of it, to check if the SM picture of CP violation is really the one present in nature and to quantify it precisely. At the moment our knowledge can be summarized in fig. 1.2.

As noted in the caption of fig. 1.2, the determination of the amount of CP violation in the SM heavily depends on B mesons measurements like Δm_s,V_{cb}, etc.. Further, our present knowledge of the elements of the triangle tells us that if CP violation can described in the way it is done in the SM, it is expected to be quite larger in the B system than in the K system. Therefore effort from a considerable part of the physics community will be devoted in the next few years to the accurate measurements of the CP violating parameters in the SM, some hoping to confirm the SM picture, others hoping to discover the first signs of new physics, and shake the so well working Model.

CP VIOLATION: the golden decay

For a decay of type $B^0 \to f$, we can define the decays amplitudes A_f and $\overline{A}_f$ as:

$$A_f = \langle f \mid H \mid B \rangle, \overline{A}_f = \langle \overline{f} \mid H \mid \overline{B} \rangle \tag{1.2}$$

If $B = B^0$ and we call the components of the interaction eigenstates in the neutral meson mass eigenstates p and q:

$$\mid B_{1,2} \rangle = p \mid B^0 \rangle \pm q \mid \overline{B}^0 \rangle \tag{1.3}$$

[1]This is a bit too simple, anyway, we will show later on more accurately how this phase can bring CP violation in the system

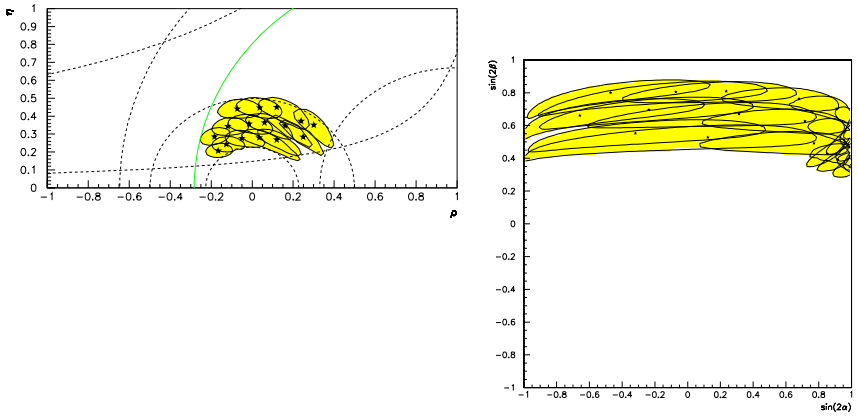

Figure 1.2: *the present allowed range (a) in $\rho - \eta$ plane and (b) in sin2α-sin2β plane, where α, β are the angles showed in fig. 1.1. Constraints come from $\mid V_{cb} \mid$,$\mid V_{ub}/V_{cb} \mid$,ϵ_k,Δm_{B_s}. [5]*

we can finally define a complex quantity λ_f by

$$\lambda_f = \frac{q}{p}\frac{\overline{A}_{\overline{f}}}{A_f} \tag{1.4}$$

The possible manifestations of CP violation can then be classified in a model independent way:

1) CP violation in decay [2] , when the amplitude for a decay and its CP-conjugate process have different magnitudes:
$$\mid \overline{A}_{\overline{f}}/A_f \mid \neq 1$$

2) CP violation in mixing, which occurs when the two neutral mass eigenstates admixtures cannot be chosen to be CP-eigenstates:
$$\mid q/p \mid \neq 1$$

3) CP violation in the interference between decays with and without mixing, which occurs in decays into final states that are common to B^0 and $\overline{B}^0$. It often occurs in combination with the other two types but there are cases when, to an excellent approximation, it is the only effect :
$$Im\lambda_f \neq 0 (\mid \lambda_f \mid \simeq 1)$$

Type 1) normally involves hadronic phases, which are not well known, and is therefore not a clean way of detecting CP violation. Type 2) is how CP violation in kaon decays has been discovered. Hera-B intent is to investigate mainly CP violation manifestations of type 3), in particular $B \to J/\psi K_s$. The reason why this decay is particularly interesting is that $Im\lambda_f$ can be directly accessed through measurements and is directly proportional to sin(2β), without uncertainties due to hadronic phases. Therefore it gives a clean measurement of one of the angles of the CKM triangle (see fig.1.1). We can look at the processes contributing to the $B^0 \to J/\psi K_s$ decay in fig.1.3.

[2]For charged and neutral B mesons

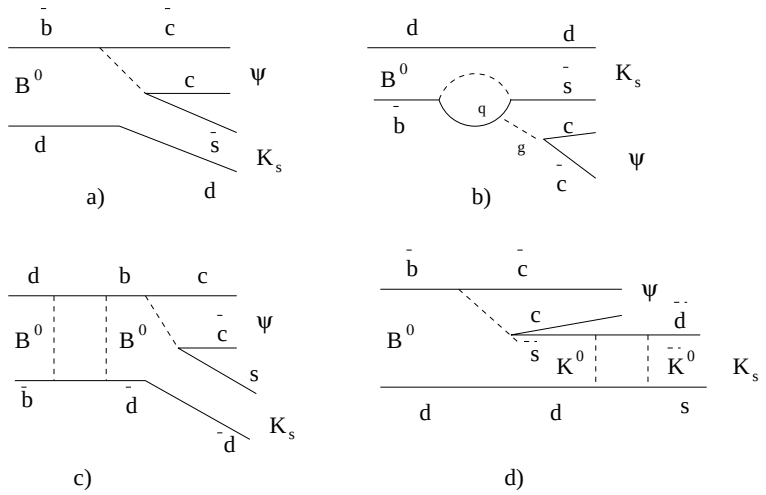

Figure 1.3: *Feynman diagrams for processes contributing to the $B^0 \to J/\psi K_s$ decay*

For the process $B^0 \to J/\psi K_s$ several diagrams interfere. The diagram a) is the tree diagram, and $A_{tree} \simeq V_{cb}V_{cs}^* \simeq \lambda^2$.

The quantity λ_f, already mentioned in eq. 1.4, is in this case

$$\lambda_f = (q/p)_K (q/p)_B (\overline{A}/A) \tag{1.5}$$

where the first term gets contribution from diagram d), the second from diagram c), the last one from diagram b). But, $(\overline{A}/A)$ is essentially 1, and real (the hadronic contributions enter only at order λ^4, therefore can be neglected). Further, $(q/p)_K \simeq 1$ and real as well (also up to order λ^4), so the only contributions remains $(q/p)_B \simeq e^{-2i\beta}$ [5].

How can one try to measure $Im\lambda_f$? By constructing an observable, A_{obs}

$$A_{obs} = \frac{N(B^0 \to f) - N(\overline{B}^0 \to f)}{N(B^0 \to f) + N(\overline{B}^0 \to f)} \tag{1.6}$$

which can be expressed as

$$A_{obs} = M(t_0) A_{CP}, \qquad A_{CP} = \sin(2\beta) \tag{1.7}$$

Depending on the measurement procedure

$$M(t_0) = \begin{cases} \frac{\sin(xt_0)+x\cos(xt_0)}{1+x^2} & \text{meas. of time integrated asymm.} \\ \left(\frac{1+4x^2-\cos(2xt_0)+2x\sin(2xt_0)}{2(1+4x^2)}\right)^{1/2} & \text{meas. of time dependent asymmetry} \end{cases}$$

where t_0 is the minimal proper decay time (distance) one can analyze, due to a necessary experimental cut on secondary vertex position, to isolate a clean sample of B's. $x \equiv \Delta m/\Gamma \simeq 0.75 \pm 0.05$ for B_d, is the mixing parameter, Δm is the mass difference of the B^0 mass eigenstates, and Γ is the inverse lifetime.

The theoretical expectation is $0.3 < \sin(2\beta) < 0.9$ at 95% C.L. [3] One year of run of Hera-B in full setup at 40 MHz should provide enough statistics to get an error of order 0.2 on $\sin(2\beta)$,

[3] There has been recent results published by CDF which probably restrict this region even more

and the potential for a CP discovery measurement. The systematical error is estimated to be of order 0.05. Other measurements of type 3) which can be performed at Hera-B are e.g. decays $B \to \pi^+\pi^-$ and $B \to \phi K_s$, the first one proportional to $\sin(2\alpha)$, the second one again to $\sin(2\beta)$.

B_s MIXING AND RARE B DECAYS

Hera-B can measure other aspects of B physics than CP violation. One example is the measurement of $B - \overline{B}$ oscillations. The B mesons that we observe are not the states which participate to the interaction, rather they are a mixture of them (see also eq. 1.3). The mixing of $B - \overline{B}$ is exactly the same which happen with $K - \overline{K}$. While the 2 observable states for K have big difference in lifetime, and little in mass, the opposite happens for the $B - \overline{B}$. Therefore the $B - \overline{B}$ mixing is normally characterized by the parameter $x = \frac{\Delta m}{\Gamma}$ already met when talking about CP asymmetry. Signatures of mixing of B mesons come from the presence of "wrong-sign" leptons in B semileptonic decays, and more recently from the observation of time dependence of oscillations. Of particular interest are the oscillations of B_s mesons, which now is still poorly determined for limited statistics available. Δm_s goes like $f_B^2 m_t^2 \mid V_{ts} \mid^2$ times a slowly varying function of m_t. f_B is the decay constant of the B meson. Contributions from lower masses up quarks are insignificant. A measurement of Δm_s allows a direct measurement of one of the less known elements of the CKM matrix. A precise knowledge of it will help constraining the CKM triangle parameters. Further, $\mid V_{ts} \mid$ is proportional to $\mid 1 - \rho - i\eta \mid$. Thus, a precise knowledge of Δm_s would mean also a further constrain on the angles of the CKM triangle. Within the SM, $x_s > 14\%$ at 95% c.l. The fact that x_s is so large makes the resolution of the detector become a crucial point. In Hera-B a value of $\sigma_t = \sigma_z/L$ =1/16 can be reached with a significant number of events still reconstructed, where L is the mean decay length ($\gamma = 20$) and $\sigma_z \simeq 500\mu m$. This non zero time resolution smears out the oscillation term of the decay rate, and it can be shown that the number of events required to detect the oscillations increases dramatically beyond $x_s > 1/\sigma_t$. Therefore a limit for Hera-B on the range of values investigable for x_s stands at $x_s < 17$. In a year run, a few hundred events are expected to be reconstructed, and a statistical error of order $\sigma_{x_s} \simeq 0.1 - 0.15$ is achievable.

Some interest will be devoted in Hera-B for rare decays studies, because they can provide evidence for non SM physics. Further, they will also provide measurement of the CKM matrix, and help the CP investigation effort. Of particular interest for Hera-B are rare decays with 2 final state leptons or photons (this is mainly what can survive the trigger requirements). They normally proceed via penguin or box diagrams. Recently this topic has been investigated [6], at the light of the trigger requirements which will be employed, and some of the following decays seem to have good chances to be detectable:

$$B^0 \to K^{0*}\gamma, B^0 \to \mu^+\mu^-, B^0 \to h_1 h_2$$

while some others need some more trigger studies :

$$B^0 \to \gamma\gamma, B^0 \to e^+e^-, B^0 \to B^0 \to \mu^+\mu^-\gamma, B^0 \to h\ell^+\ell^-$$

1.1.2 Charmonium physics

We call charmonium a bound state of $c\overline{c}$ quarks, and more generally quarkonium, a bound state $q\overline{q}$. Several quarkonium states have been already observed, whose masses and quantum

numbers had been already predicted using some hypothesis for the inter-quark model and quantum mechanics [7]. In this work we are mainly interested in $c\overline{c}$ bound states, and therefore the following will be mainly concentrated on them. Some of them are listed in table 1.1.

State	J	P	C
J/ψ	1	-	-
$\psi(2S)$	1	-	-
χ_c	0,1,2	+	+

Table 1.1: *List of some of the charmonium states measurable at Hera-B. J is the total angular momentum, P is the Parity quantum number, C is the Charge conjugation quantum number*

One can argue that $c\overline{c}$ states (together with leptons and photons) are one of the best probes of hard hadronic processes and color dynamics. Why? Their signal is relatively clear : e.g. one sees J/ψ via its decay to a $\ell^+\ell^-$ high transverse momentum pair, and their production is relatively copious in hadronic interactions. The formation mechanism of a $c\overline{c}$ state involves processes happening at several time (energy) scales, and demands for several theoretical approaches to be explained, therefore from its study one can extract a lot of informations about strong interactions.

There exist few models which try to explain the experimental results, and yet none is able to describe all these results that have been produced. The following is meant to be a brief summary of these models. More detailed summaries on charmonium physics (theory and results) can be found in [8, 9, 10].

One of the first hypothesis on cross section for production of a charmonium state of quantum numbers S,L,J in a AB collision (e.q. pp) was that

$$\sigma(AB \rightarrow^{2S+1} L_J + X; s) = F \int_{4m_Q}^{4m_D} ds' \frac{d\sigma}{ds'}(AB \rightarrow Q\overline{Q}X; s; s') \tag{1.8}$$

where Q is a charm quark in this case, s is the center of mass energy, and F is a constant. A similar distribution for rapidity and transverse momentum differential cross sections can be written. This means assuming that the charmonium cross section is proportional to the $c\overline{c}$ cross section below open charm ($D\overline{D}$) threshold, as given by the process $AB \rightarrow Q\overline{Q}X$. In this model, called **Color Evaporation Model (CEM)**, the color exchanges which lead to the color singlet observable $c\overline{c}$ state are assumed to happen over a long time, therefore are factorizable with respect to the hard part of $c\overline{c}$ quarks production through a non perturbative factor F. F has to be determined from data, and it differs from the simple guess $\frac{1}{N}$ where N is the number of possible bound states below open charm threshold. For this assumption to be of any use, it is important that this factor F is "universal", which means, it remains independent of beam energy, charmonium momentum and transverse momentum, and also nature of the target and the beam. This assumption seems to be confirmed by looking at some results on J/ψ elastic photoproduction (fig. 1.4) taken over a wide range of energies and with A=γ, B=p.

When passing to inelastic photoproduction ($\gamma p \rightarrow X\ J/\psi$) and to hadroproduction ($p, \pi N \rightarrow XJ/\psi$, with $qq, gg \rightarrow (g)\ c\overline{c}$) of J/ψ , the model seems to hold still, the factor F is very similar for πN and pp reactions. But the constant F does depend on the $c\overline{c}$ state (e.g. χ_c photoproduction requires a different F factor), and it is not independent of the target (see following). This weakens the power of prediction of the theory.

Two other models, the **Color Singlet Model (CSM)** and the **Color Octet Model (COM)**, try to go more in detail in the description of the formation, in order to achieve a

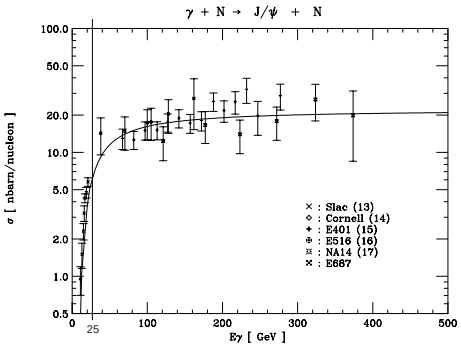

Figure 1.4: *$\gamma p \to p\ J/\psi$ data and fit with eq.1.8 [8]*

better understanding and more predictive power. They think of the production of charmonium as proceeding through two steps.

The first step is the creation of a $c\overline{c}$ pair (hard process, due to m_c) with small relative momentum, of order $m_c v$ or larger, where v is of order 1/2, but not much larger otherwise the pair would fly apart. This first step can be fully described through Perturbative QCD (PQCD). The separation of the pair at production is of order $1/m_c$ or smaller, which is much smaller than the size of a quarkonium state. Therefore the pair is essentially pointlike with respect to the charmonium wave-function.

The second step is the binding of the $c\overline{c}$, which involves momenta $\leq m_c v$, because these are the gluon momenta which can play important role in the binding process. This second step needs a phenomenological model.

One can express the inclusive differential cross section for J/ψ in the following factorized form:

$$d\sigma(J/\psi + X) = \sum_n d\sigma'((c\overline{c})_n + X)\langle O_n^{J/\psi}\rangle \tag{1.9}$$

where $d\sigma'((c\overline{c})_n + X)$ corresponds to the short distance term and can be calculated as a perturbation expansion in $\alpha_s(m_c)$, and $\langle O_n^{J/\psi}\rangle$ corresponds to the long-distance one, the probability for the pointlike $c\overline{c}$ pair in state n to bind to form J/ψ . This matrix element contains all the non perturbative informations. At this point the two models split. The **CSM** assumes that $\langle O_n^{J/\psi}\rangle$ is non zero only if n is a color singlet with the same angular momentum as the dominant state of the meson, for J/ψ is $^3S_1$. The probability is proportional to $\mid R(0) \mid^2$, where R(0) is the radial wave-function at the origin. It can be determined from data on $J/\psi \to e^+e^-$. The color singlet model is very predictive. Using the CSM for explaining photoproduction of J/ψ seems to succeed, as well as the prediction of the ratio $\frac{\sigma(\psi')}{\sigma(J/\psi)}$, similar for photo and hadro production (see fig. 1.5). It also works predicting χ_c hadroproduction.

But the CSM fails badly in predicting hadroproduction of J/ψ and ψ'. In general it seems to fail whenever an additional gluon (to the process $gg, qq \to c\overline{c}$) needs to be emitted to preserve quantum numbers (e.g. $gg \to J/\psi g$). This can be seen in fig. 1.6 and 1.7, where a factor of 30 approximately is needed to reach the magnitude of data from the theoretical prediction. The discrepancy is present both at high and low p_t. More documentation on CSM comparison with data can be found in [14, 12]

How can one account for such a large factor? A relatively simple explanation has been found and described in the **COM** [9, 13]. This model uses the Non Relativistic QCD factorization formalism (NRQCD), and expands the term $\langle O_n^{J/\psi}\rangle$ in powers of $\frac{v}{c}$, and the term $d\sigma'((c\overline{c})_n + X)$

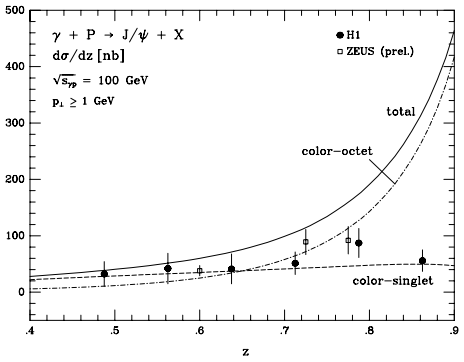

Figure 1.5: *$\gamma p \to J/\psi X$ inelastic data and fit with eq.1.9 for color singlet and color octet [8]*

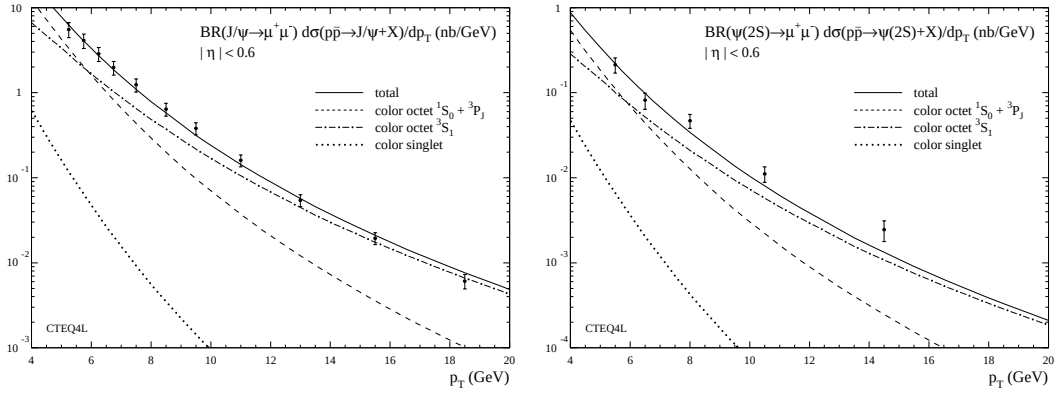

Figure 1.6: *Fit of color octet contributions to CDF data on prompt Jpsi,psi(2s) vs pt [13]*

in powers os $\alpha_s(m_c), \alpha_s(p_t)$ as well. In cases where, for quantum numbers conservation, an extra gluon needs to be emitted ($\alpha_s(m_c)$), the production may be dominated by higher order terms in $\frac{v}{c}$ than the ones considered in the CSM. In other words, for ψ production, if one expands the formula 1.9, the CSM says that the most important term is $\alpha_s(m_c)^3(\frac{v}{c})^3$. But a term of type $\alpha_s(m_c)(\frac{v}{c})^7$ exists as well, and in general a power of $\alpha_s(m_c)$ is more powerful than a term of $(\frac{v}{c})$. Therefore the second term contributes more. The second term is a color octet term of type $\langle O_8^{\psi}(^3S_1)\rangle$.

One can see in fig.1.6 how the COM prediction better accommodates the data for J/ψ production. But once again, this does not seem to be enough. This model fails in estimating the amount of J/ψ photoproduction (see fig. 1.5), fails by predicting strong polarization for J/ψ and ψ', which have been observed to be almost unpolarized instead. Finally it fails predicting the $\Upsilon(3S)$ cross section by an order of magnitude, and since the relativistic corrections in $(\frac{v}{c})$ for bottomonium are much smaller, this result is difficult to accommodate with the COM.

One thing is clear from all this: the theoretical explanation of production of quarkonium systems has not reached a final, unique model, and new data from high energy physics has been the driving progress in the understanding of this physics phenomenon. That's why I think a contribution in this sense from an experiment like Hera-B, which has the potential to do it, has

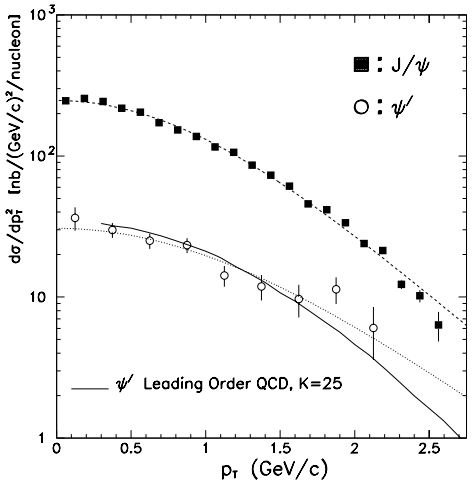

Figure 1.7: *e789 data on prompt J/ψ and ψ' vs pt. The dotted lines are a fit to the data, of the form $(1+(p_t/p_0)^2)^{-6}$, with $p_0 = 3.00 \pm 0.02$ GeV/c for J/ψ and $3.60 \pm 0.32 GeV/c$ for ψ'. The solid line is the CSM prediction for $\psi(2S)$ multiplied with a factor K=25.[12]*

to be pursued, and not taking this chance would be a waste.

Nuclear dependence of charmonium cross section

As a final remark, I would like to present a collection of data on nuclear dependence of the cross section for charmonium production. This gives additional insight into the production process. The cross section can be parametrized as

$$\sigma_A \simeq \sigma_N A^\alpha, with \begin{cases} \alpha \simeq 1.00 & \mu^+\mu^- \\ \alpha \simeq 0.92 \pm 0.008 & J/\psi, \psi' \\ \alpha \simeq 0.962 \pm 0.014 & \Upsilon(1S) \end{cases} \tag{1.10}$$

Further, there is evidence for a p_t broadening induced by the nucleus, depending on the quark mass

$$\langle p_t^2(A)\rangle - \langle p_t^2(H)\rangle = \begin{cases} 0.113 \pm 0.016 GeV^2 & \mu^+\mu^- \\ 0.34 \pm 0.08 GeV^2 & J/\psi, \psi' \\ 0.667 \pm 0.113 GeV^2 & \Upsilon(1S) \end{cases} \tag{1.11}$$

These data are not predictable by any of the models above described, and need an explanation. A first attempt to understand the origin of this phenomenon was presented in [11], where is pointed out that the rescattering of spectators produced by beam and target parton evolution could have important effects in J/ψ production. Additional measurements on this topic, in a larger regime of x_F and p_t, are possible at Hera-B, where the target material can been chosen among several materials.

1.1.3 Hera-B and other B physics experiments

I would like to finish this section by showing the scenario of contemporaneous experiments outside Europe, relevant for beauty physics studies.

Babar,Belle and Cleo are at e^+e^- machines, they are relatively standard detectors (very similar to LEP experiments). The first 2 use beams of different energy, to give a boost to the decay products, and therefore disentangle better the quark content of events.CDF and D0 operate at a $p\overline{p}$ collider with 2 TeV c.m. energy.

Some basic features of these experiments are summarized in table 1.2.

exper. (machine)	**Babar** (PEP II)	**Belle** (KeKb)	**Cleo** (Cesr)	**CDF,DO** (Tevatron)	**Hera-B** (Hera)
energy	3.1 GeV e^+ 9. Gev e^-	3.5 Gev e^+ 8 GeV e^-	5. Gev e^+e^-	2 TeV p$\overline{p}$	920 GeV p
$\beta\gamma$	0.56	0.42	0	0	20
L($cm^{-1}sec^{-1}$)	10^{33}	10^{34}	10^{33}	10^{32}	40MHz IR
$\sigma_{b\bar{b}}$	1nb	1nb	1nb	100 μb	10nb
N_b	10^7	10^7	10^7	10^{11}	10^8
b states acces.	B^0, B^+			$B^0, B^+, B_s, B_c, \Lambda_b$	
N_{ch}	~ 10			≥ 100	
Start	May 1999	1999	sept 1999	2000	oct 1999
Respect to Hera-B : +	clean environment e, μ, ν, γ final states $K/\pi, \gamma/\pi^0$ separation understood detector			experience understood detector	
-	only B^0, B^+			π/K separ. poor selective trigger	

Table 1.2: *Basic features of present experiments relevant for B physics studies*

For discovery of CP violation through the standard channels $B \to J/\psi K^0_s$, $B \to \pi\pi$ and $B \to \pi K$, Babar, Belle and Hera-B have the same potential for equal period of run, while CDF/D0 remain behind for statistics only for 1999, the luminosity upgrade foreseen for year 2000 will put them on the same level as the others. The same can be said for rare B decays studies, with the additional difference that the number of final states detectable by e^+e^- machines is higher than for hadron machines. Further, Hera-B stands essentially alone (up to 2000) in B_s studies, position similar to Babar, Belle and Cleo for what concerns B semileptonic decays studies.

1.2 Hera-B : the experiment

We have already mentioned that Hera-B needs to cope with very high interaction rates, and very high track density per interaction rate. The first factor makes high demands on the trigger system of the experiment, the second one on the detector itself. Let's just mention a couple of numbers.

With five interactions per bunch crossing, which is what Hera-B would need for producing enough B's for CP discovery within a year of run, the track flux varies with the radial distance from the beam-line R like $\frac{3.10^7}{R^2}$ particles per second.

The detector occupancy (the percentage of readout channels busy during one event) is 20%.

The average number of charged tracks per event is more than 100.

The desired interaction rate is 40 MHz, with multiple interactions per event. The distance between 2 interactions is of order 96 ns, and given the length of Hera-B (14 meters), this means

that the particles from 1 interaction have just left the detector, when the flux from the next interaction starts entering it.

One should also remember that Hera-B is not the only user of Hera. Therefore exchange of considerable parts of the detector (i.e. long shutdowns of the machine) are allowed very seldom (of order once a year). The detector should have a minimal lifetime of 1 year (hopefully much more, for cost reasons).

From these few considerations one can understand why Hera-B is considered a difficult experiment.

1.2.1 The halo target

The setup and material for the Hera-B target (see fig. 1.8) has been chosen based on the following requirements:

- In order to keep a high interaction rate, the beam should not be extracted, but instead the target should be placed along the p beam path. Further, a metal wire target is the safest solution, it allows to absorb mainly protons coming from the halo of the beam, if the target is placed at 4-8 σ from the beam line, where σ is the size of the beam. In this way it will not interfere with the other experiments program.

- In order to have well separable interaction points while keeping the interaction rate high, the choice of multiple wires is wiser. With a set of 4+4 and a BX rate of 10MHz, a 40 MHZ interaction rate on the target is achievable.

- For what concerns the choice of material, it has to be based on the following 2 points:

  IR=$\frac{N_p \cdot \epsilon_t}{\tau}$. IR is interaction rate, N_p is typically $2 \cdot 10^{13}$, so being the typical τ of order 100 h, the choice of a material with a proper ϵ_t has to be kept in mind.

  Material should also have not too high atomic number A, because while it's true that $\sigma_{bb} \propto A$, is also true that $\sigma_{tot} \propto \sigma_{pp} \cdot A^{2/3}$ and $< n >= A^{0.2}$. A gain factor can be written down: G=$\frac{A}{\sigma_{pp} \cdot A^{2/3} \cdot A^{0.2}}$. For material like C and Al, a gain of order 10% is achievable. It is not so good to move to higher gains, since the net gain will be anyway small since too many tracks with too soft momentum are very difficult to reconstruct.

- The idea of using several materials is interesting for the physics studies since it allows to perform measurements on dependence of cross sections on A.

- The size of the wire should be comparable with the resolution of the vertex detector on transverse and longitudinal vertex reconstruction precision (respectively 30 and 400 μm).

At present, 4 types of materials for the target wires are employed: Al, C, Fe, Ti.

The setup is done on 2 stations at 4 mm distance in the beam direction, each one furnished with 4 wires.

Their performances and stability have been tested both in 1997 and in 1998-1999 runs, and no problem in getting the desired rate compared to other experiments has been observed.

The interaction rate (or luminosity) is measured by the target group through 4 small scintillating counters (0.2% occupancy), which do not saturate at high rates. The count is performed over 1 sec. This makes the count uncertain for possible rate fluctuations, bunch to bunch variations, coasting beam. The 4 counters are placed at z=1350 cm. from the target, to provide independent measurements of the same quantity. The count is proportional to the interaction

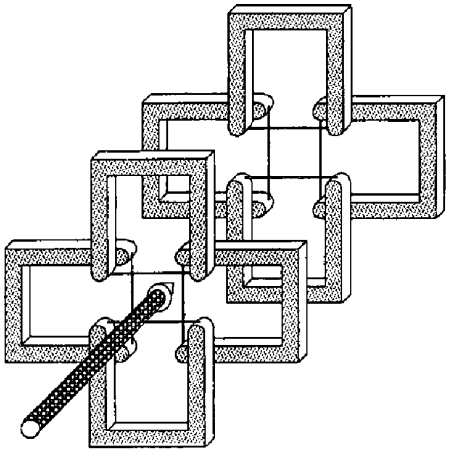

Figure 1.8: *Schematic view of Hera-B target*

rate via the efficiency of the counter. Therefore, to calculate this efficiency, one goes to very low rates (where essentially only single interactions happen) and compares the count of the small counter to the count of a big counter (90% occupancy). The errors on the luminosity is estimated to be about 20%.

Recently some off-line determination of the interaction rate has been performed using the energy sum in the electromagnetic calorimeter and the number of hits in the Cherenkov counter detector. They seem to be in reasonable agreement with each other, and almost a factor of 2 different from the interaction rate as measured by the scintillator target counters. We'll get back to this in chapter 3.

The p background rate is measured by some scintillating counters positioned behind the target station, in opposite direction to the boost of particles. Typical values of the background fluctuate around 10 kHz.

1.2.2 The detector

Hera-B is a rather conventional multi particle spectrometer. The difficult part of the realization of this experiment is the high granularity required to cope with the high particle densities. The main detector components are shown in fig. 1.9

Tables 1.3 and 1.4 show a summary of the detector components properties and performances in the final setup (some voices have been updated with respect to the proposal [1]).

The design of the detector has been based on the following requirements:

- maximal geometrical acceptance for physics decays of interest. 90% center of mass coverage is the final compromise between physics and cost requirements.
- Vertex Detector (VDS) should have maximal acceptance for secondary particles coming from B decays. Therefore it starts at 1cm radius from the beam. A smaller radius would overrule the minimal lifetime requirement of 1 year.
- Tracking system of different granularity, therefore resolution:

  VDS : 12 μm in x,y

  MicroStrip Gaseous Chambers (ITR) : 60 μm in x

  Honeycomb chambers (OTR): 100 μm in x

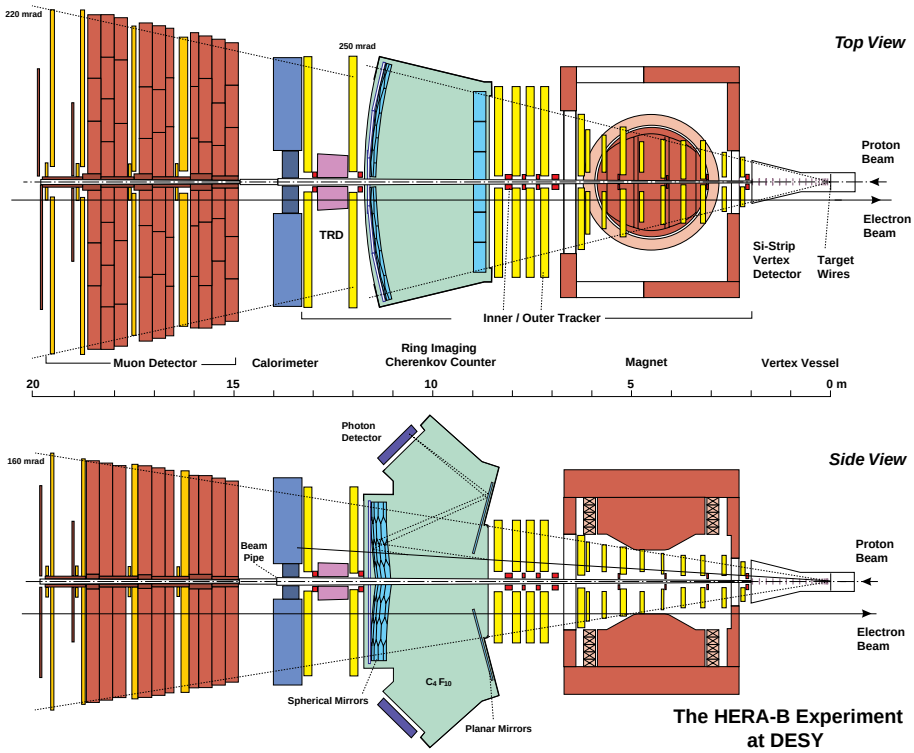

Figure 1.9: *Schematic view of Hera-B*

Detector	*Technology*	*Channels*	*Trig.Lev.*
Vertex detector	Silicon microstrips	176000	2,3
Magnet	Superconducting dipole		
Tracker	Si microstrips (r $\approx$ 2 - 6 cm)		2, 3
	MSGC chambers (r $\approx$ 6 - 20 cm)	135000	1,2,3
	Honeycomb chambers (r $>$ 20 cm)	120000	1,2,3
Transition Rad. det.	Straws	16000	2,3
Cherenkov det.	C_4F_{10} /MA-PMT	27520	-
EM Calorimeter	Pb-W/Scintillator	5800	1,2,3
Muon System	drift chambers	pixel: 7300	1,2,3
		pads: 8000	1
		tubes: 15376	1,2,3
High PT	drift chambers (wires and pads)	8736	1

Table 1.3: *Main components of Hera-B*

- Efficient muon and electron identification. This is very important, to properly reconstruct J/ψ from golden decay, using the dilepton decay channel. This is achieved using muon chambers (MU) in the first case, and Electromagnetic Calorimeter (ECAL) in the second one, using the shape of the shower and the E/p ratio. The Transition Radiation Detector (TRD) also helps in e/π identification.

- Efficient kaon identification. This is important for charged kaon tagging of B's, and for

reconstruction of K_s from golden decay, using the dipion decay channel. This is achieved using the Ring Imaging Cherenkov detector (RICH).

A more detailed description of the different parts of the Hera-B detector can be found in [1] and in [2].

Vertex detection	Impact parameter resolution: $\sigma \approx 25\ \mu\text{m} \oplus 30\ \mu\text{m}/p_t$ (in GeV) B vertex resolution: $\sigma_z \approx 500\ \mu\text{m}, \sigma_{x,y} \approx 25\ \mu\text{m}$
Magnetic analysis	Momentum resolution: $\Delta p/p \approx 2.3 \cdot 10^{-5} p \oplus 5.2 \cdot 10^{-4} \sqrt{p} \oplus 6.7 \cdot 10^{-3}$
π/K separation using RICH	Momentum range ≈ 3 to ≈ 50 GeV $\pi \to K$ misidentification $< 2\%$ at $\approx 90\%$ K efficiency $< 5\%$ at $\approx 95\%$ K efficiency
e/hadron separation using TRD	Momentum range ≈ 1 to ≈ 70 GeV $h \to e$ misidentification $< 5\%$ at 95% e efficiency
EM Calorimetry	Energy resolution: $\Delta E/E \approx 17\%/\sqrt{E} \oplus 1.6\%$ (inner) $\Delta E/E \approx 9.5\%/\sqrt{E} \oplus 1\%$ (mid/out) Position resolution: $\Delta x, y \approx 0.5\ \text{cm}/\sqrt{E} \oplus 0.2$ cm (inner) $\Delta x, y \approx 2.0\ \text{cm}/\sqrt{E} \oplus 0.4$ cm (outer)
e/hadron separation using calorimeter	$h \to e$ misidentification $\approx 7\%$ at $\approx 90\%$ e efficiency
Muon identification	Momentum range > 5 GeV $\pi \to \mu$ misidentification $< 0.3\%$ at 30 GeV $K \to \mu$ misidentification $< 1\%$ at 30 GeV

Table 1.4: *Expected performances of Hera-B*

Some detector performances as measured on recently taken data are reported in chapter 3.

1.2.3 Trigger

Triggering is a difficult task in Hera-B . As already mentioned, the bunch crossing rate is 10MHz, and with the full set of wires (4+4), the interaction rate rises up to 40 MHz. There are 2 main tasks the trigger should fulfill:

- a practical one: no more than 20 Hz can be sustained, as output to tape. The trigger has to provide this reduction factor
- a physics one: the interesting physics channels are suppressed of a factor 10^{-4} (for J/ψ direct) to 10^{-11} (for $B \to J/\psi K_s^0$ decay), and the trigger has therefore to enhance, with its requirements, these signals out of the background.

A schematic overview of the pretrigger-trigger system of Hera-B is shown in fig. 1.10. The reduction factors mentioned in fig. 1.10 refer to the detector in its full setup. The division in several levels is a must, because one needs to do some analysis of the event, in order to

enhance the signal physics signatures, but the input rate to the trigger is very high, so the time (complexity) of analysis has to be splitted in more than 1 level.

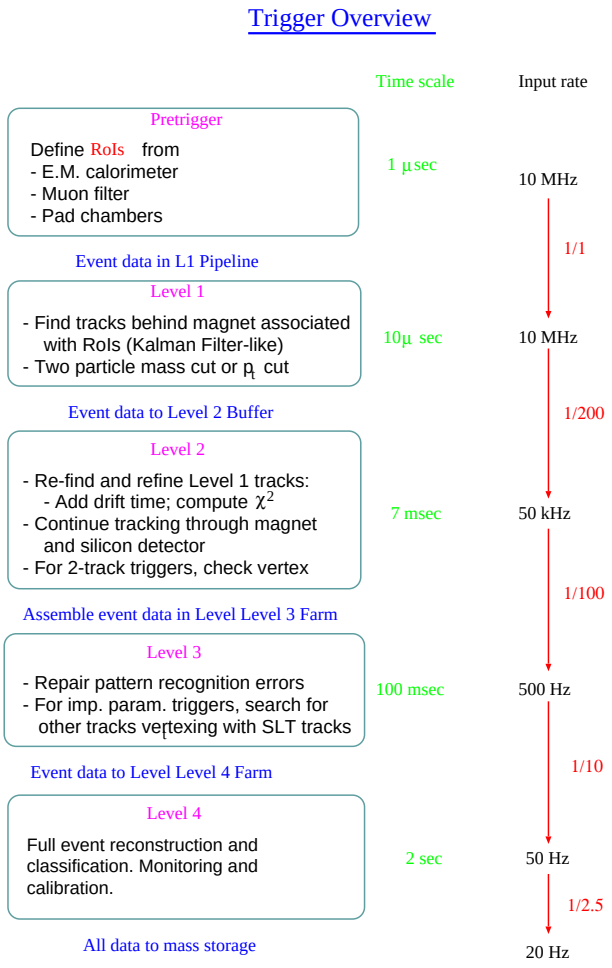

Figure 1.10: *Overview of the trigger scheme of Hera-B*

How should the physics tune the trigger?

For CP violation measurements, one wants to trigger on events with at least one couple of leptons or hadrons of same type but opposite charge, forming a common vertex, to find the J/ψ or the B.

For B_s mixing measurements, one looks for semileptonic B decays, therefore asks for leptons. Because of the demanding reduction factor, one needs to demand at least 2 tracks (but not necessarily restrict the type,charge or ask for a common vertex), or only 1 track but with very selective cuts.

In order to catch these types of physics processes, one needs to look for signal(s) in electromagnetic calorimeter or muon chambers or high-pt chambers. That's what the pretrigger does.

In order to enhance them out of the background (minimum bias, charm), one needs to exalt their kinematic properties: transverse momentum p_t, invariant mass M. Here the First Level Trigger(FLT) starts working.

Further, one needs to require that the trigger candidates are real tracks, therefore leave signals in the tracking chambers before and after the magnet to eliminate background from (converted or not) photons and from decays of primary tracks while they cross the detector. For selecting B decay products, one can then also add the requirement of a detached vertex from the primary vertex. This is the task of both FLT and Second Level Trigger(SLT).

For rare decays searches, which are extremely sensitive to the trigger cuts imposed, the basic idea is to search in the sample selected by the standard triggers or to eventually use other types of trigger decisions based on a higher number of tracks but with weaker requirements. E.g. $B \to \gamma\gamma$, one would ask for 3 tracks: 1 charged track (e.g. from the other B in the event) and 2 seeds in the electromagnetic calorimeter. At the moment is not clear if additional trigger decisions can be accepted, proper MC studies need to be performed.

Here in the following will be described how the pretrigger/triger system will work in the final setup (end 1999 $\to$). For brief information about status of installation, and performances of the system during end of 1998 and beginning of 1999, please refer to chapter 3.

Pretrigger

This is the level at which the seeds for the triggering are searched for. We are interested in ECAL (Electromagnetic CALorimeter) clusters or in track segments in muon and high-pt chambers. These seeds should have some transverse momentum (for $e/\mu > 0.5GeV$, for $\pi > 1.5GeV$). The candidates found are passed to the FLT (First Level Trigger). One can see in fig.1.12 which parts of the detector are used for pretriggering. In fig. 1.11 one can see how the decision is taken [4].

a) Electromagnetic candidates:

   in ECAL, cell 5 hit and $E_5 > E_{th}/2$, and $\sum_{i=1}^{9} E_i > E_{th}$.

   E_{th} is defined in the following way, for accounting for the magnet effect:

$$E_{th} = K_{trig} \cdot (1/R + 1/\sqrt{x^2 + |y^3|})$$

   , where x,y are the center of the reconstructed cluster.

   If a candidate electron is found, a coincidence with TC2 (see fig. 1.12) is required, to suppress photon background. The possibility to also accept photons candidates is foreseen, by requiring a higher E_{th} but no coincidence in TC2.

   The message passed on to the FLT contains energy, position and BX identifier of the electron candidate.

b) For muon and high-pt pretriggers, the signal is generated if hits are found within a pretrigger road, which is defined by a coincidence matrix between certain regions of pads (ROP) in the different chambers. The reason for having a bigger number of pads involved in the downstream pad stations (MU4 or PT2,3) is because of a shift of pads position in y, and for accounting for the effect of the magnetic field in x.

   1) Muon candidates:

   a coincidence of 1 pad in MU3 and 1 of 4 (or 6) in MU4.

   2) Hadron candidates:

   a coincidence of 1 pad in PT1 and 1 of 3 in PT2 and 1 of 2 in PT3.

[4] *The unit for ECAL is a cell, for the muon and high-pt chambers is a pad*

The message passed on to the FLT contains coordinates,direction and BX identifier of the muon/pion candidate.

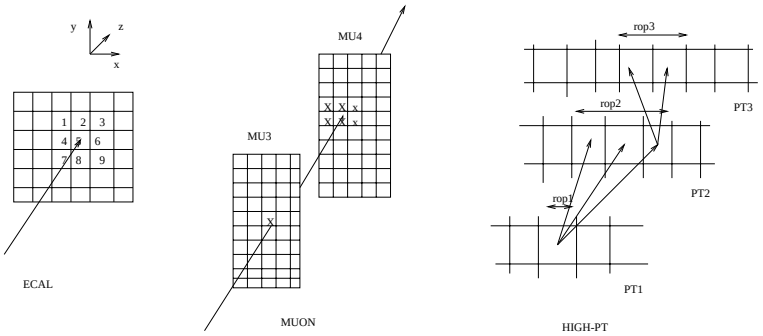

Figure 1.11: *pretrigger requirements*

Level1

The hardware

Detailed information of how the L1 works can be found in [1]. Let us here only mention that analog data at readout are stored in 128 beam crossings long pipelines while the L1 is processing them, and after positive decision about the event, they are translated into digital data and transfered to the second level trigger memory buffers, where PC's are processing the data.

The software

The candidate tracks from the pretrigger define Regions of Interest (ROI) in the tracking chambers of the FLT. To economize processing time, only these regions are searched for tracks.

For an overview of the detectors used by the FLT, refer to fig.1.12. As one can see, the FLT uses informations only from detectors behind the magnet.

What is the FLT doing? Essentially 2 things:

- Tracking:

  Verification of pretrigger ROI's

  Update of track parameters

  Calculation of invariant mass of track pairs

- Decision:

  Count trigger

  Track pair trigger

The tracking algorithm is a Kalman Filter [34]. Starting from the pretrigger ROI extrapolated to the first detector at hand (TC2 or MU1), the algorithm looks in each plane for hits in the ROI. For each hit found, the track parameters are updated, and the track is passed to the next plane. If no hits are found in a superplane[5], the track dies. The parameters of the track, outcome of a fit to a straight line, are: direction in x and y in the region behind the magnet,

[5]A superplane is made of more than one plane

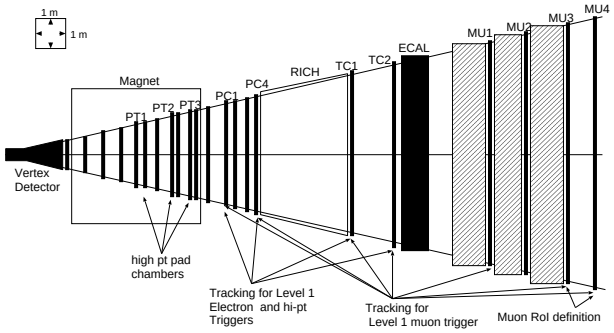

Figure 1.12: *detector used by the first level trigger*

and impact parameter in x, due to the bending in the magnet. If a track survives up to the last plane, then the track parameters are transformed into the kinematic parameters p, θ, ϕ (via look up tables) , and the invariant mass can be calculated. At this point cuts can be applied, and a decision taken.

As mentioned, the FLT can take 2 type of decisions:

- a count trigger. The candidate types are e, μ, π, γ, and for each one the p_t threshold can be set low or high, and the number of tracks of each type required can be 1 or more. The FLT allows 14 types of combinations of these factors, leaving to us to learn how to set the p_t threshold and the number of tracks in order to have a reasonable background rejection.
- a track pair trigger. Based on the type of candidates, one can form 10 pair combinations. In this case the decision is based on quantities dependent on both tracks. E.g. invariant mass, charge combination (+ -,++,- -),etc..

The standard FLT triggers are:

- J/ψ : $\mu\mu/ee$ (+ -) with M>2. GeV
- $\ell\ell$ with $p_t > 1$.GeV
- ℓ with with $p_t > 2.5$ GeV

These 3 alone already give a total output rate of the FLT of 70 KHz, saturating almost completely the threshold allowed for the input to the Second Level trigger. This is not good news, in regard to rare decays studies.

In table 1.5 are given the expected performances of the FLT using track pair decision with hight p_t cut on tracks as estimated on MC events of type $B \to J/\psi K_s^0$, with 5 interactions superimposed, and full detector.

trigg	**eff**	**output rate**
$B \to J/\psi K_s^0, J/\psi \to \mu\mu$	0.60	13KHz
$B \to J/\psi K_s^0, J/\psi \to ee$	0.33	25KHz
$B \to \pi\pi$	0.3	15 KHz

Table 1.5: *FLT performances*

Level2

The hardware

In the beginning of 1996, when this Ph.D. work started, the experiment was pretty much in stage of preparation. In particular, for the second level trigger, the scheme of implementation of the system was still under discussion. It was clear which the basic components needed were : processing units, to analyze the event and take the decision, and memory (buffer) units, to temporarily store the data. But the technology of the first ones, and the way to connect them with the memory units, was not yet decided.

The 2 proposals were:

- The Second Level Trigger (SLT) algorithm is divided in sections, independent from one another, and using independent sets of data [6]. this seemed to favour at first an (historical) idea [20] to develop a pipeline system for processing events coming from the FLT, where the ROI's would be processed in parallel for a given section of the algorithm, and each processing unit at a given algorithm step would be able to see data only useful for that step. The ROI's would then be pushed through the pipeline to the next algorithm step. The system would be made all of SHARC's units (cpu speed: 40MHz, memory: 500 KBytes), which would make it homogeneous and easy to maintain, and further would reduce to zero the problem with interfaces among different components.

- Based on the idea that an event parallel processing is more appealing than a roi parallel processing, and on the consideration that this idea could be implemented, given the cpu speed of 200MHz (nowadays is 500Mhz) and the memory of 64Mbytes of uptodate machines (Pentium Pro), a switch based configuration was proposed [21]. In this scheme, processing units(PC's) would be communicating with memory (SHARC's) through a switch (a system of C104 processors), and would be able to access the whole event.

The switch solution would give a higher performance/cost ratio with respect to the pipeline solution. The strategy used to process an event in the pipeline would require an additional task (more SHARC's) for grouping the informations from different RoI's, and take a decision at a given step. This is not necessary in the switch scheme, where the decision about the event can be taken on the PC processing the event. The only additional task in the switch configuration is the one (SHARC board) to delegate messages to/from PC's from/to buffers. Further, the switch solution reduces the traffic to/from buffers with respect to the first proposal, since multiple requests for the same region in space (same buffer) can be grouped in one message in the PC. Least, but not last, the switch configuration resembles very much (but in a smaller scale) what will be adopted for future experiments like ATLAS,CMS at LHC, and therefore would represent a nice test.

The switch proposal had the best in terms of general structure, but a switch based on SHARC's (instead of C104's) was decided. The final hardware architecture of the trigger system, as it is being installed now, can be seen in fig. 1.13.

The system is presently installed (not in the final size) at DESY, and has been running rather smoothly during the end of 1998, and beginning of 1999.

The software

[6] *except slicer and refit-x*

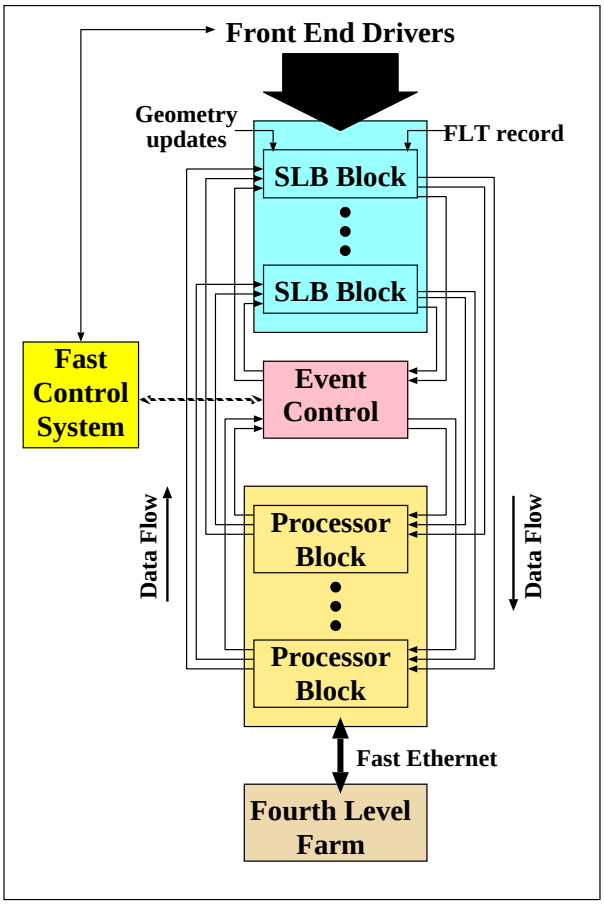

Figure 1.13: *Hardware architecture of the trigger system of Hera-B*

The track candidates surviving the FLT constitute refined ROI's for the SLT to inspect. The SLT code is structured in 5 sections: slicer, refitx, refity, l2magnet, l2sili. A scheme of the detector information used by these sections is in 1.14.

The SLT first attempts to reconstruct tracks in the ROI behind the magnet, adding more hits by use of chambers PC2,3. According to simulation, a factor of 10 rejection is obtained at this step, eliminating ROIs which do not contain real tracks. Surviving ROIs are then projected through the magnet and vertex detector where trigger type dependent vertex cuts are applied. An additional factor of 10 should be coming from this.

For tracking, refit and silicon use simplified kalman filter algorithms, where x and y view are treated separately, while slicer and magnet use histogramming methods. In addition, magnet uses a lookup table, containing values of the magnetic field for different sets of directions in x and y for tracks, to extrapolate tracks from the refit region to the silicon region.

An estimate of the output rate of the SLT using simulated events, with full detector, and several interactions superimposed, could not be performed up to now. The reason is that an amount of data of the order of millions should be generated (rejection factor of flt+slt 10^4), and given the generation time of few seconds required for 1 event, this does not sound realistic, unless a big computer facility becomes available. Some thought has been given to use the SLT farm for this purpose, during shut down periods. Anyway, a study of triggering in 1998-1999 has been attempted (see [22]), and the results, confirmed by the recent data taking period, make us

feel comfortable that no problems should be encountered with the complete detector and setup of wires. Some studies have been performed on $B \to J/\psi K_s^0$, to determine expected efficiency of SLT. The results are listed in table 1.6.

The SLT has been operated during the 1999 run, for magnet off runs, and seemed to cycle properly, and reconstruct tracks online.

For more informations about the SLT code, refer to chapter 2 and 3.

trigg	**eff**
$B \to J/\psi K_s^0, J/\psi \to \mu\mu$	80%
$B \to J/\psi K_s^0, J/\psi \to ee$	70%

Table 1.6: *SLT performances*

Level3

Events surviving SLT cuts are passed to the Third Level Trigger (TLT). The appropriate reduction rate needed when activating the J/ψ trigger can be achieved by FLT+SLT cuts alone. But, as we have mentioned, for other studies than CP violation (e.g. B_s mixing) one wants to use a count trigger at the FLT instead, and no common vertex cut at the SLT, making therefore necessary to get a further reduction. This is the purpose of the TLT. The TLT will not restrict itself to the informations within ROI's given by the SLT, but rather will look through the whole event to find additional tracks to match to the SLT tracks, and form B secondary vertices candidates. At the moment the most realistic solution for the realization of this system is to have it being part of the SLT farm. Each TLT processing unit shall have in memory the entire event. A TLT algorithm has been developed [27] and tested on simulated events. Even more strongly, the point of reduction rate studies brought up for the SLT is valid here. Some more studies are being attempted in this connection [27].

The TLT has been operated at the end of the 1999 run, and could cycle properly, and reconstruct tracks online.

Level4

High track densities and occupancies in the detector require a sophisticated pattern recognition and event reconstruction procedure which needs seconds of computing time per event on present high speed computers. To make most efficient use of computing resources and to minimize time delays between data taking and physics analysis, it is planned to perform full event reconstruction online at the 4th Level Trigger (4LT). In addition, monitoring tasks will be carried out here , before events are routed to mass storage.

The 4LT farm (not in full size) has been operating at DESY during 1998-99, only for logging purposes. Online reconstruction has also been attempted, even if the detectors available constitute less than half the final detector.

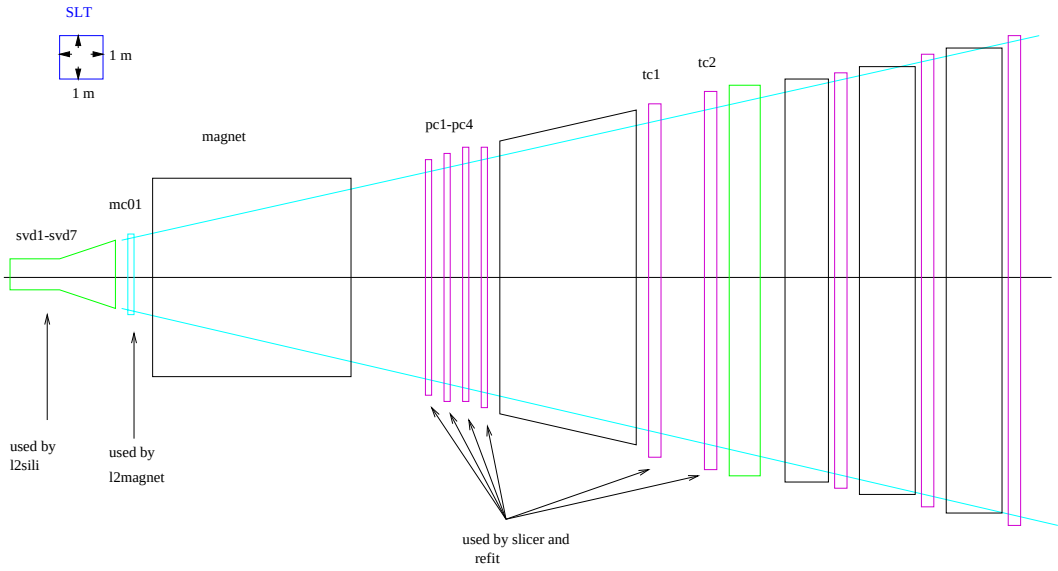

Figure 1.14: *Scheme of the detectors used at the second level trigger*

Chapter 2

Preparation

2.1 The role of Monte Carlo simulation in a high energy physics experiment

Monte Carlo (MC) simulation can be a very useful tool for an experiment, provided that it correctly describe the physics processes of main interest for the experiment. In the following we will show two examples of most common uses of MC in an experiment: to test the efficiency and performances of a physics algorithm (in this case a trigger algorithm), and to understand which type of physics is realistic to investigate within a given setup for the detector, and how the search for it can be optimized.

Let's go back to the first sentence and expand on this point. Which MC generators do we use in Hera-B, and how good really are they to describe the physics of our interest, which means pN hadronic interactions, and in particular hadronic interactions with heavy quark production?

In Hera-B we use a software package called ARTE [32], which contains the MC generators, and the reconstruction and trigger software which can be used on MC/real data analysis. For MC generators we use PYTHIA [30] combined with FRITIOF [31] or FRITIOF alone, for generating respectively heavy quark (high transverse momentum p_t) hadronic interactions and inelastics interactions.

PYTHIA is a parton parton (hard) interaction generator, and makes use of the jet fragmentation routines of JETSET. PYTHIA and JETSET have been created by the theory group at Lund university, and have been used extensively by pp and ee collider experiments in the last several years. PYTHIA uses QCD or strong interaction perturbation theory at finite order. This means that cut off's are introduced, like minimal transverse momentum of the 2 partons, to remove divergences.

FRITIOF is mainly used for simulating nuclear effects like energy loss or multiple scattering of partons crossing the target nucleus. FRITIOF uses PYTHIA and JETSET internally for simulation of hard partonic scattering, but since it is optimized to treat the nuclear environment, it is compromising on the complete implementation of all possible central hard partonic interactions.

That's why for producing special hard processes like $b\overline{b}$ or $c\overline{c}$ events, Hera-B adopts PYTHIA, and once the heavy quark pair is produced, it uses the remaining energy to start FRITIOF, for producing the underlying low p_t part of the event.

Very recently, a carefull study [29] of our MC and a comparison with real data results has been performed. Some interesting changes have been introduced for charmonium and bottomonium production, which can be seen in fig.2.1 and 2.2

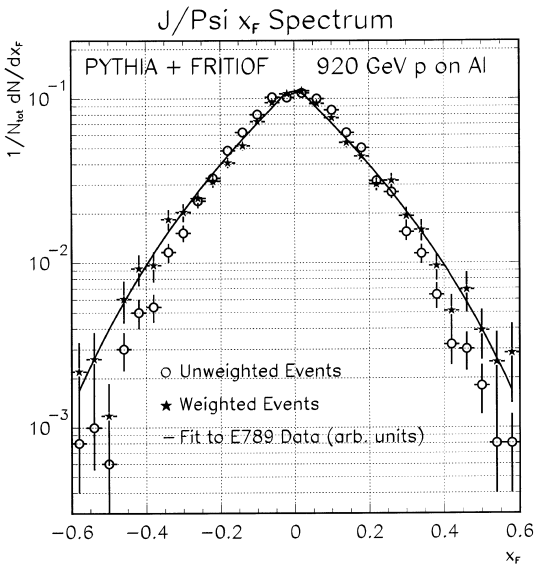

Figure 2.1: *x_f spectrum for direct J/ψ monte carlo events produced with PYTHIA and FRITIOF with the standard PYTHIA processes, compared to fit function to measured data and to correction for MC spectrum after weighting the events for the real data spectrum. [29]*

It turns out that for J/ψ production PYTHIA uses the color singlet model, and the standard processes turned on are via direct creation or via $g\ g \rightarrow \chi_c\ g \rightarrow J/\psi\gamma$. This underestimates the p_t spectra at low p_t ($p_t < 1$), see fig. 2.2. One fast way to correct the MC is either to try to introduce other processes which are important at low p_t like $g\ g \rightarrow \chi_c$, or to try to weight the MC spectrum referring to the spectrum as measured from the data. The last one is the solution chosen in Hera-B at the moment, see [29], and probably it's the best solution, since the introduction of new processes in PYTHIA would correspond also to some fine tuning of the cut off's, which would in turn maybe influence other processes.

For detector simulation, we use GEANT [33], which has been opportunely adapted to describe Hera-B detector. GEANT is also a very standard package, used by both CERN and Fermilab experiments.

2.2 Use of MC simulation to develope a trigger algorithm

When developing a trigger algorithm, the use of MC simulation is fundamental. The trigger is in fact the system which decides which events we should use to do analysis, and therefore its performance has to be checked and optimized on the type of signal we are most interested in. A tool for simulating the Second Level Trigger (SLT) functioning has been developed by the SLT group. This tool is called L2simu, and has been interfaced to the ARTE package. A description of the structure of this package can be found in [23]. Let us here mention that L2simu is a very flexible and usefull tool, built on the same blocks as the real SLT structure: processor, buffer, and switch. This has allowed to prepare the SLT algorithm in simulation mode in such a way that the transportation of it to the online environment would be as easy as possible.

The SLT code is divided in modules, each one using informations from a given part of the detector. These modules are: Slicer, Refitx, Refity, L2Magnet, L2Sili, L2Vertex. We have briefly

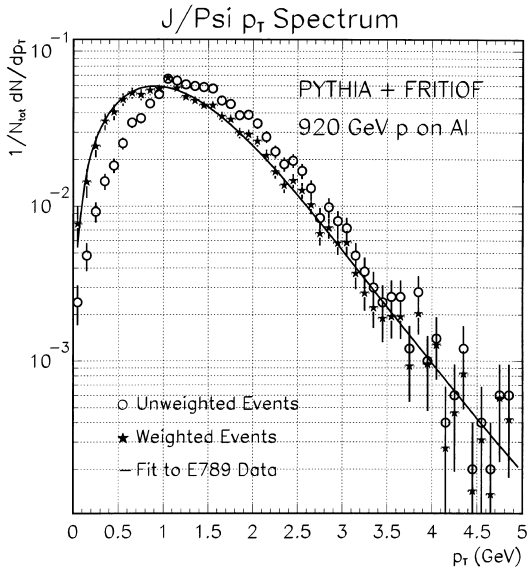

Figure 2.2: *p_t spectrum for direct J/ψ monte carlo events produced with PYTHIA and FRITIOF with the standard PYTHIA processes, compared to fit function to measured data and to correction for MC spectrum after weighting the events for the real data spectrum. [29]*

described these modules in chapter 1, indicating in fig. 1.14 which detector components they use. While L2Magnet will be thouroghly discussed in the next sections, since part of my ph.d. work has consisted in commissioning this code for the SLT, let's now briefly mention the other modules. This will help understanding the function of L2Magnet as well.

The First Level Trigger (FLT) selects events where (e.g. in the J/ψ trigger mode) at least a couple of high p_t tracks has been found, whose invariant mass is above 2 GeV. Since the FLT time for processing an event is of order μsec, its definition of a track cannot be very precise. This implies that "ghost" [1] tracks have good chance of surviving this level, and this cannot be tolerated when the rejection factor required for the trigger is of order 10^6. Further, even for good FLT tracks, only those which seem to come from the target should be considered further and used for decision. Therefore a search in the Silicon Vertex Detector, standing close to the target, should be performed. This is the reason why SLT is needed.

During triggering, the list of FLT high p_t tracks is passed to the SLT. **Slicer** [24] is the first module encountered. Its function is to take a 3 sigma region around the FLT tracks and look for hits in that region using more tracking chambers than the FLT does. This in order to improve the rejection of ghosts. The way Slicer defines "good tracks" is based on a histogramming method: a variable (the direction of a track in the xz plane) is defined to filter hits of a real track, by binning the range of values for this variable opportunely and filling the bins with the hits collected in the 3 sigma region.

Once Slicer has qualified a list of hits as a track, then **Refitx** [25] makes a fit of them to a straight line, using the drift time information as well. Now the track is relatively well known, therefore the y information contained in the hits can be extracted and the track parameters in the yz plane extracted (**Refity**).

[1] e.g. combination of hits which survive the definition of "track" but do not correspond to the path of a physical track

Now we have well defined tracks in the region after the magnet. We said we need to make sure that these tracks are coming from the target (so do the leptons from J/ψ) therefore we need to extrapolate these tracks into the SVD area and try to find hits there. This is the purpose of the **L2Magnet** module.

L2Sili and **L2Vertex** [22] use the hits collected into the 3 sigma region of L2Magnet tracks to reconstruct tracks and calculate their common vertex. L2Sili is using a modified Kalman Filter algorithm [34], where the xz and yz projections of track paramaters are propagated almost separately. This is to reduce computation and therefore gain time. All the possible combinations of hits surviving a cut on the χ^2 probability for the track are propagated. A minimal requirement on the number of hits per view (x or y) collected is also imposed: 1 if the full tracking informations are available for the preceeding SLT steps, 2 if that is not the case.

In the following subsection we will show what the magnet traversal part of the SLT code consists of. Part of this work can be found also in note [22].

2.2.1 Magnet traversal of a charged particle

When a charged particle with momentum $\overrightarrow{p}$ crosses a magnetic field, it is deflected by

$$\frac{d\overrightarrow{p}}{dt} = q\overrightarrow{v} \times \overrightarrow{B} \tag{2.1}$$

In the very simple case of a constant magnetic field, directed along y, the motion of a particle is a superposition of two independent motions : a straight line along the y axis, and a circle in the xz plane. The radius of the circle can be obtained by solving the above eq. of motions

$$\rho = \frac{p_{xz}}{qB_y} \tag{2.2}$$

and the deflection angle is given by

$$\frac{\sin(\delta\phi)}{2} = \frac{LB_y}{2p_{xz}} \tag{2.3}$$

In a more complicated configuration for the magnetic field (inhomogeneous, and with components along the 3 axes), the motion of a particle is more complicated too. In the Hera-B detector, the magnetic field is like the one between two magnetic poles, with the magnetic flux lines around the y direction. The B_y component will be still dominant in respect to the other two. At this point one can think about trying to solve exactly the equations of motion for the particle, or use a parameterization. The second method is less precise, but faster. This is a good candidate idea for a trigger algorithm, where the time at disposal is of order of milliseconds, and that's why we decided to study it via MC simulations, and finally implement it into the SLT official code. This part of the SLT code, which takes care of translating track parameters from the downstream region to the region closer to the target is called L2Magnet.

2.2.2 Implementation of a magnet traversal code

For a given track which we have found (i.e. slope and intercept in x and y measured) in the region after the magnet, L2Magnet determines its charge over momentum, direction and intercept in the region in front of the magnet. In the full detector version the sources of information are the track parameters in the region after the magnet provided by Refitx, Refity, and the target position (or a point in the chambers right at the entrance of the magnet area, at the second

iteration of the code) are the sources of information. The use of tracking devices in front of the magnet improves the precision but L2magnet can give a solution without them. The equations 2.5 and 2.6 used to predict slopes in x and y and charge over momentum form a system of 4 equations with 3 unknowns, using 4 measurements from Refitx, Refity and 2 "measurements" from target or point. The equations are based on the assumption that the shift in angle and position of a particle traversing a magnetic field can be parametrized as polynomials in $\frac{Q}{p_z}$ (see also fig. 2.3).

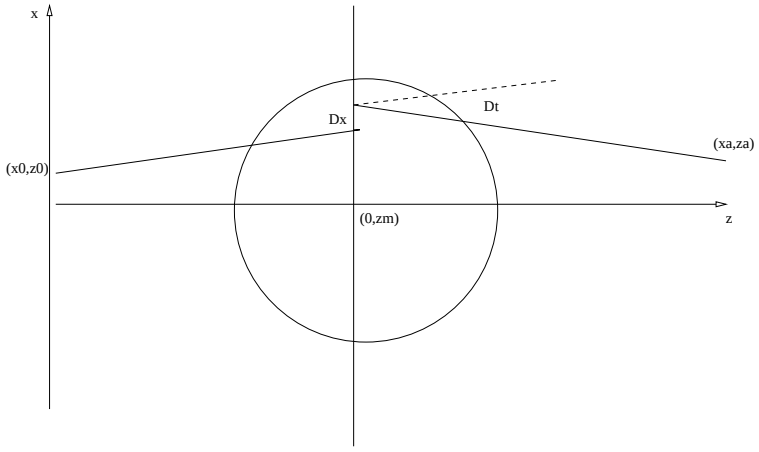

Figure 2.3: *Schematic view of the parametrization L2Magnet uses in the xz plane for describing the motion of a particle.(x0,z0) is the target or the position of the particle as measured at the detector at the entrance of the magnet area, (xa,za) is the position of the particle as measured in Refitx,Refity. During the magnet traversal, the particle suffer a deflection (Dt or $\Delta\theta$) and a displacement (Dx or ΔX). These changes are assumed to happen suddenly at some position z_m within the magnet area.*

The results of the study on the code, in scenarios with full or partial detector, seem to confirm that the assumption is reasonable. For them, see next subsection.

$$\begin{aligned} tx_a &= tx_b + \Delta\theta \\ x_a &= x_b + tx_b \cdot (z_m - z_b) + \Delta X + tx_a \cdot (z_a - z_m) \\ ty_a &= ty_b + \Delta\theta' \\ y_a &= y_b + ty_b \cdot (z_m - z_b) + \Delta Y + ty_a \cdot (z_a - z_m), \end{aligned} \tag{2.4}$$

Indices a and b stand for after and before the magnet, respectively. $\Delta\theta$ and $\Delta\theta'$ are given by:

$$\begin{aligned} \Delta\theta &= \frac{Q}{p_{xz}} \cdot A1(tx, ty) \\ -\Delta\theta \cdot z_m + \Delta X &= \frac{Q}{p_{xz}} \cdot A5(tx, ty) \\ \Delta\theta' &= \frac{Q}{p_{yz}} \cdot B1(tx, ty) \end{aligned} \tag{2.5}$$

$$-\Delta\theta' \cdot z_m + \Delta Y \quad = \quad \frac{Q}{p_{yz}} \cdot B5(tx, ty),$$

where some of the symbols are explained in fig. 2.3, $tx_{a,b}$ is the direction of the particle in the xz plane after, before the magnet (similar for y), and A1, A5, B1, B5 are field maps (lookup tables) and correspond to first (A1, B1) and second (A5, B5) order integrals on the field. How we extracted these field maps from the magnetic field description contained in the MC is the subject of the next section. Their behavior as function of tx,ty can be seen in fig. 2.4.

Corrections for multiple scattering and an average correction of $\frac{Q}{p_z}$ for bremsstrahlung is available in the code. This is also described in the following sections.

THE FIELD MAP

Arte [32] contains a parameterization of the measured Hera-B magnetic field, which is used for simulation of events. We used this to extract the field coefficients of our equations. For doing this, we take eq. 2.5, and use it in the opposite way as we would use it on data: this time we know the x,y parameters of the track and we try to get what the coefficients should be. Which kind of track should we use for doing this? The most natural choice lies on muons, which is one of the two type of trigger tracks we are interested in. We do not choose electrons for our purpose because, due to brehmstrahlung, they do not just change direction, but also emit energy and therefore we would not have a unique definition of momentum for them. We prefer to treat the brehmstrahlung effect as a further effect, to be corrected on average with a separate procedure.

We find it reasonable to treat A_i,B_i not as constants, but as functions of the direction in the xz and yz plane of a particle coming from the target. Therefore we decide for a matrix of values for each coefficient, of size $23 \otimes 15(tx \otimes ty)$, covering the full acceptance of Hera-B detector.

For calculating each element of each matrix, we simulate single muons with high and low energy, with charge positive and negative, 100 times for each case [2], and from the track parameters each time we extract the values of the coefficients. In fig. 2.4 is graphically represented what we obtain. It's interesting to notice how in all pictures one can see the electron beam pipe interference, at high tx and negative ty.

We have tried also to expand eq. 2.5 with higher order terms in Q/p, and calculate the coefficients for those terms as well, but they turn out to be compatible with zero and are therefore not relevant.

IMPLEMENTATION FOR THE 1998-1999 RUN

In August-December 1998, and January-April 1999, Hera-B has run with a number of detector components smaller than the final one. In particular, for triggering, only 50% of ECAL and less than 50% of SVD was instrumented. Therefore, the only measurement available to the trigger in the region after the magnet was a point in ECAL. L2simu has been adapted to accept such a scenario, both in case of magnet on and off, and attempt triggering anyway. This has implied the introduction into the SLT code of a new program, to emulate the function of the FLT of creating a list of tracks above a given p_t threshold and making an invariant mass check on the event. To do this, the ECAL reconstruction program CARE [35] has been used.

In this configuration, if the magnet is off, L2Magnet simply matches the ecal point and the target to give a straight line. No charge estimate is possible. The momentum is simply the

[2] This because multiple scattering was included in the simulation

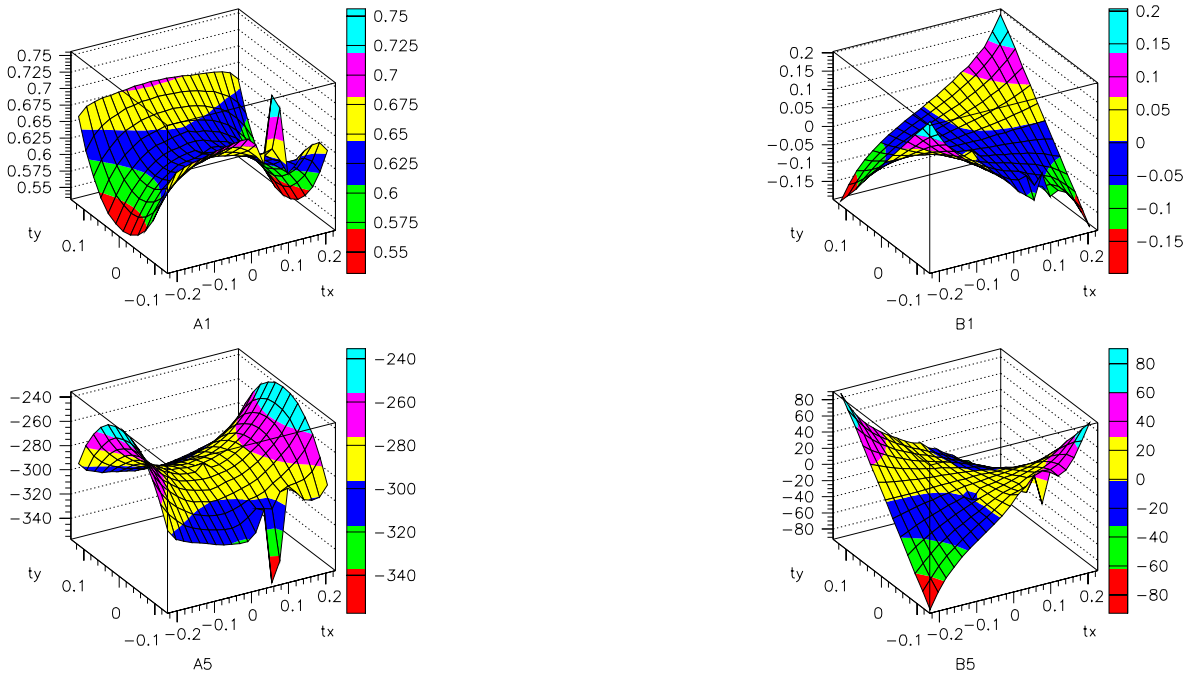

Figure 2.4: *Schematic view of the parameterization of magnetic field in Hera-B, used in L2Magnet. A1 and B1, divided by the momentum of a particle, give the idea of the amount of angular deflection ($\Delta\theta$ in eq. 2.5) in xz and yz plane, while A5 and B5, divided by momentum, give an idea of the spatial deflection ($-\Delta\theta \cdot z_m + \Delta X$ in eq. 2.5) in xz and yz plane.*

energy of the ECAL cluster. To keep the general program flowing smoothly, if the magnet is on the initial 3 sigma regions in the SVD area are created using the ECAL point and the inverted equations of L2Magnet, to get an estimate for the slope in x and y after the magnet (the target position is used at this step). Two regions (Q=+1 and Q=-1) are created for each ECAL cluster. In this procedure L2Magnet will finally give out only 2 new informations: the slope in x and y in front of the magnet, and re-send out the energy measurement of ECAL under the form of Q/pz.

2.2.3 Some performances

Let's summarize the results of performances study on the code. Both for the normal implementation, and for the "ad-hoc" implementation for the 1998-1999 run.

But first a few remarks. While efficiencies will be quoted both for analyzed MC events of type $B \to J/\psi K_s \to \ell\ell\pi\pi$ and direct $J/\psi \to \ell\ell$, the other performances have been estimated on 4 MC samples, containing direct J/ψ only [3], produced with ARTE-01-08-r3 and ARTE-01-07-r1:

a) 2400 events $J/\psi \to e^+e^-$, final setup

[3]The leptons from direct J/ψ are very similar to the ones coming from J/ψ from a B decay. They have a slightly lower p_t and acceptance in the SVD detector, because of the mass and of the non zero decay distance of the B. One channel is as good as the other one for studying L2Magnet performance. The distinction becomes more important for L2Vertex studies, which is not subject of this section

b) 2000 events $J/\psi \to \mu^+\mu^-$, final setup

c) 2000 $J/\psi \to e^+e^-$, 1998 setup: magnet off, no OTR/ITR chambers

d) 1800 $J/\psi \to e^+e^-$, 1998 setup: magnet on, no OTR/ITR chambers

Let us here look at the results of the test of the code on p_t above 1. GeV tracks. This is because it is the typical type of tracks the trigger will be requested to work on. Importance will be given mainly to the study of errors and pull[4] distributions (pull is the quantity given by the spread of the measured quantity divided by the error on that quantity). We look at efficiency of reconstructing J/ψ (i.e. properly reconstructing both leptons) for events where both leptons from J/ψ are within the acceptance of the detector. We define a lepton from J/ψ as reconstructed at a given trigger step if, once compared the reconstructed track with the "true" track, the discrepancy lies within 3 sigma for all the 4 parameters (direction in x and y and position in x and y). We therefore distinguish, in the following tables, between "passed" and "good", the first just counting events at output of a trigger level, and the last denoting the fact that both leptons from J/ψ are reconstructed, as explained above.

Last remark, the x, y, z coordinates in the following plot are measured in centimeters.

Final setup

Within the final Hera-B setup, as already mentioned, L2magnet will as a first step try to get an idea of where the particle is coming from, in the region in front of the magnet, by using the Refit tracks (defined after the magnet) , the knowledge of the field through the field maps, and by constraining the track to come from the target. At the end of this step, an estimate of the parameters: slope in x and y, and Q/p, is obtained.

This involves a first assumption on the error to assign to the target position, in order to include properly J/ψ from B's, which on average come from a point 1 cm displaced with respect to the target. With a set of 4+4 target wires, symmetrically placed around the beam line, displaced 7 cm from one another along the beam line, we chose a point between the 2 stations, and at (x,y)=(0,0), and with an "error" given by the half distance (in x or y) between the 2 targets plus some additional width for accepting J/ψ from B (2 times the average flight distance along z times the average angle). This seems to give a reasonable efficiency (see table 2.2).

Some results of the estimation of the parameters at the first step of L2magnet operation, on $\mu\mu$ and ee final states for J/ψ decay are shown in fig. 2.5, and in table 2.1. Please, note that the cuts at FLT/pretrigger applied for electrons and muons are different. For muons, one requires a ktrig of 1000 and a minimal p_t of 1. GeV and a minimal mass of 2.5GeV. For electrons, one requires a ktrig [5] of 500 and a minimal p_t of 0.5 GeV, and a mass of 2.2 GeV.

Already at this step one encounters two effects, which need to be taken into account: multiple scattering and brehmstrahlung. Multiple scattering of a particle in the detector material gives a momentum dependent spread of the track parameters around the value they have before traversing the given material. The error assigned to the track parameter has therefore to account for this phenomenon properly. This is important for afterwards, where we will be using the parameter and the error to collect hits to reconstruct the track. The way we found the correction was by looking at the spread in track parameters (slope in x and y and momentum) for low and high energy candidates, and hypothizing a correction of the type $A + \frac{B}{p}$. In fig. 2.6 we can see how the resulting pull distributions look like.

[4]We call pull of the quantity x the variable: $\frac{(x-x_{true})}{\sigma_x}$

[5]ktrig is related to the magnetic field, and wil be described in the section "magnet on"

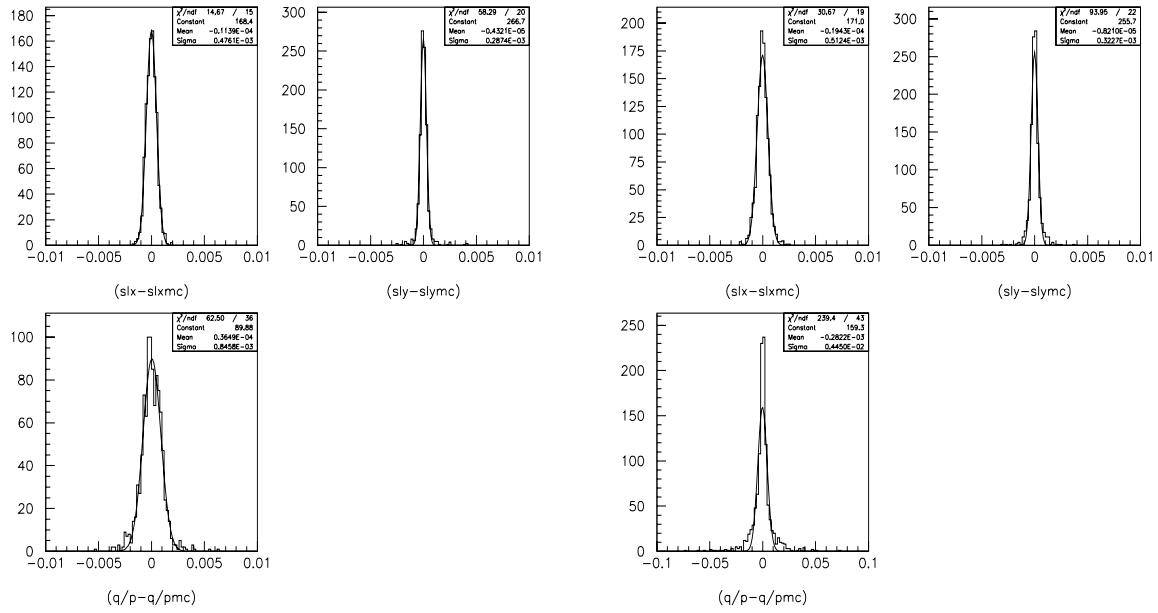

Figure 2.5: *Spread for muon (left) and electrons (right) tracks parameters from J/ψ reconstructed by L2magnet at first step of operation. slx,y represent the direction of the track in the xz, yz plane*

level	**N μ events**	**N e events**
start	2000	2400
pretr-FLT passed	574	649
slt-refit,slicer passed	543	564
pretr-FLT good	540	549
slt-refit,slicer good	538	531
L2magnet good	471	482
L2magnet eff	87%	90 %

Table 2.1: *SLT performances on J/ψ direct events. Please note that on muon and electron sample, different p_t,mass cut were applied, as will happen in real life. Good means that the J/ψ leptons are both reconstructed, i.e. they lay within 3 sigma from the extrapolated track parameters*

Brehmstrahlung, which affects electrons, is radiation loss of electrons being accelerated. This happens when electrons traverse the magnetic field. This produces a underestimate of the momentum of the track, when the measurement is based on the parameters of the track after the magnet. We tried to correct on average for this phenomenon, and in fig. 2.7 one can see on the left the situation before correction, for high(up) and low (bottom) momentum negative (left) and positive (right) particles, and on the right how the situation changes after the correction, separated for positive and negative particles.

While the spread plots (hopefully centered at zero!), see fig. 2.5, give an idea of how big will be the search region for hits in the chambers right at the entrance of the magnet will be, the pull plots, see fig. 2.6 tell us if we are going to have the appropriate search region size or not.

level	N μ events	N e events
start	710	1400
pretr/FLT passed	250	486
slt/ refit,slicer passed	236	415
pretr/FLT good	226	382
slt/refit,slicer good	223	367
L2magnet	206	334
L2magnet eff	92%	91%

Table 2.2: *SLT performances on $B \to J/\psi K_s \to \ell\ell\pi\pi$ events. Please note that on muon and electron sample, different p_t,mass cut were applied, as will happen in real life. Good means that the J/ψ leptons are both reconstructed, i.e. they lay within 3 sigma from the extrapolated track parameters*

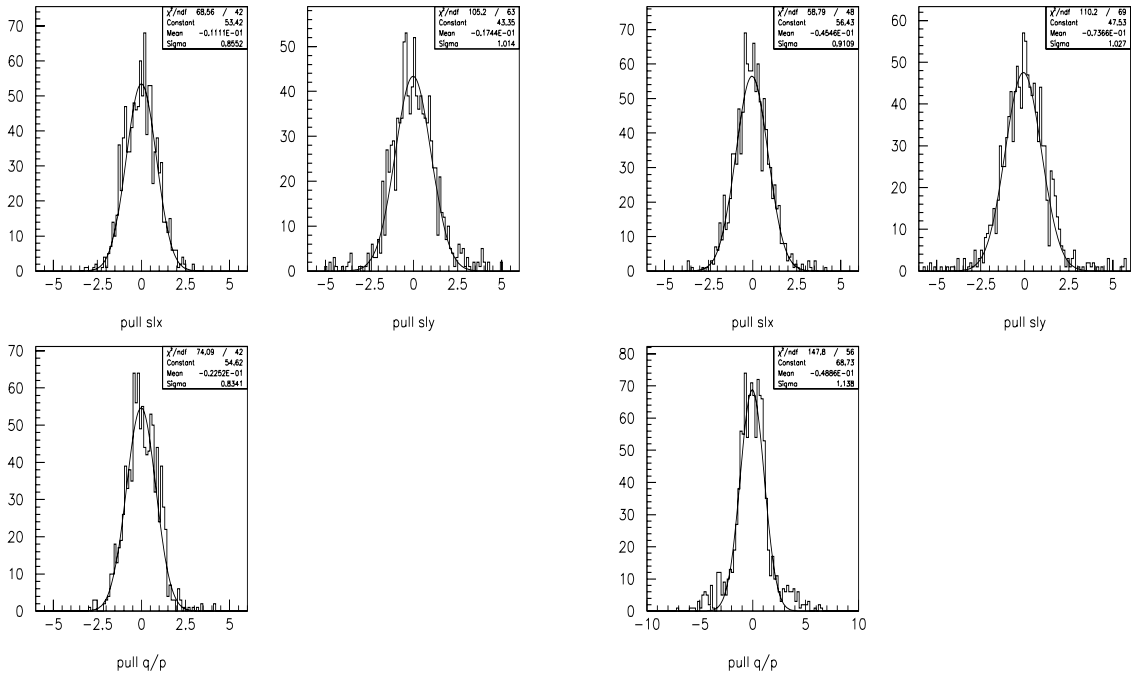

Figure 2.6: *Pull (see text for explanation) distributions for L2magnet estimated parameters at first step of operation. muons (left) and electrons (right). We can see that the pulls have width 1., which tells us that the errors are properly accounting for the spread of the quantities above.*

This seems to be case.

After the first step, L2magnet uses the estimated parameters to define a search region in the chambers at the entrance of the magnet, and try to find a point for the track. The use of the measured point will make the estimate on the parameters of the track more precise, and therefore the search region for l2sili smaller. This will make the operation of l2sili faster and more precise. The procedure L2magnet uses to find the point is at first to "slice" the hits collected in the region of interest corresponding to their slope value in the xz (yz) plane. The bin size has been chosen opportunely by calculating the spread of the slopes in xz (yz) for hits

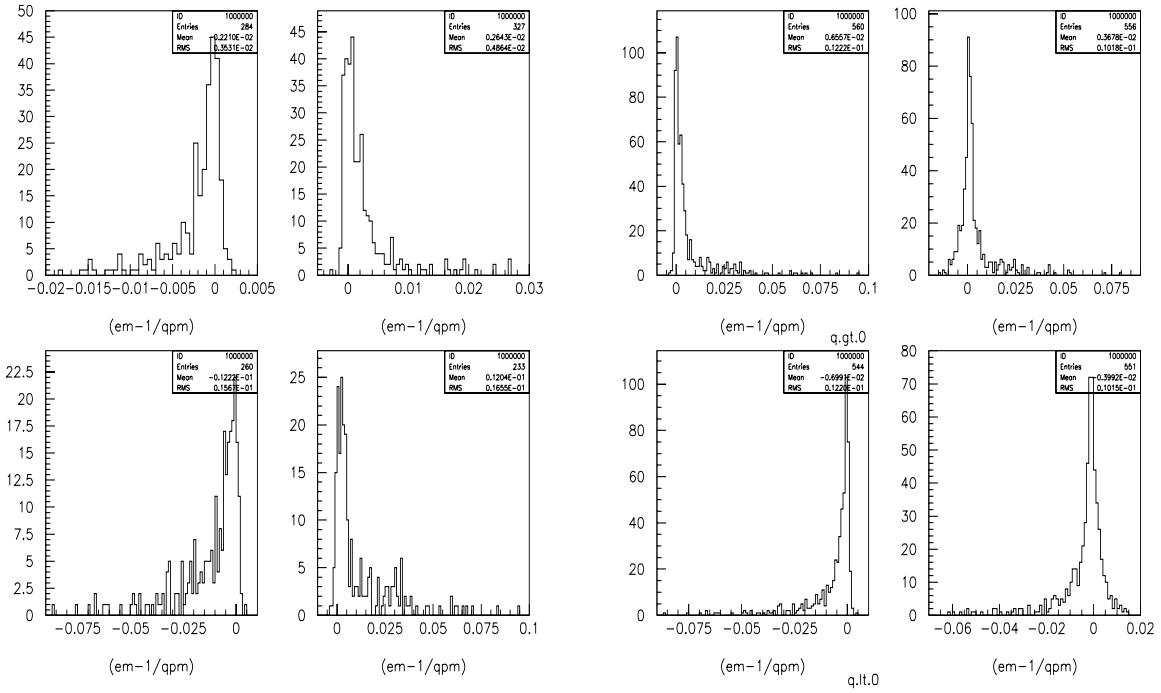

Figure 2.7: *Effect of brehmstrahlung on momentum estimation. On the left we can see the situation for the spread of* $\frac{Q}{p}$ *before correction, for high(up) and low (bottom) momentum negative (left) and positive (right) particles. Then a correction is applied, and on the right we can see how the mean of the momentum spread plot for particles with charge Q greater/less than 0 suffer a change (left to right) when applying the correction*

coming from J/ψ leptons. Then the procedure for estimating slopes in xz and yz and Q/p is repeated, now having a real measured point instead of the "target" guess. The result is shown in fig 2.8. We can notice that the resolution on $\frac{Q}{p}$ at this step is $\simeq 5 \cdot 10^{-4}$, which is only 1 order of magnitude less precise than by using the reconstruction off-line, but is more than an order of magnitude faster to be obtained via L2magnet than off-line. The efficiency for point finding is about 95%. The pulls for the track parameters are shown in fig 2.9.

At this point, another interesting thing to check is how good the error matrix calculation is. We check this by trying to extrapolate to the starting point of l2sili (100. cm away from the target) and see if at that place still the pull distributions have width $\simeq 1$. That means the correlations are treated properly. This seems to be case, see fig. 2.10.

1998, magnet off

For the end 1998-beginning 1999 run, a FLT emulator has been introduced, and the use of the ECAL reconstruction package has been needed. For an electromagnetic cluster, the quantities to use are defined in a class called RCCL in the Arte software, and the entries are x,y and cve[0],[2] for position and width respectively.

When a cluster is reconstructed, a certain width is assigned to the cluster. This width is not necessarily to be considered an "error" on the position of the track, therefore we need to check how to define a proper ECAL error, which is fundamental for the definition of the search region

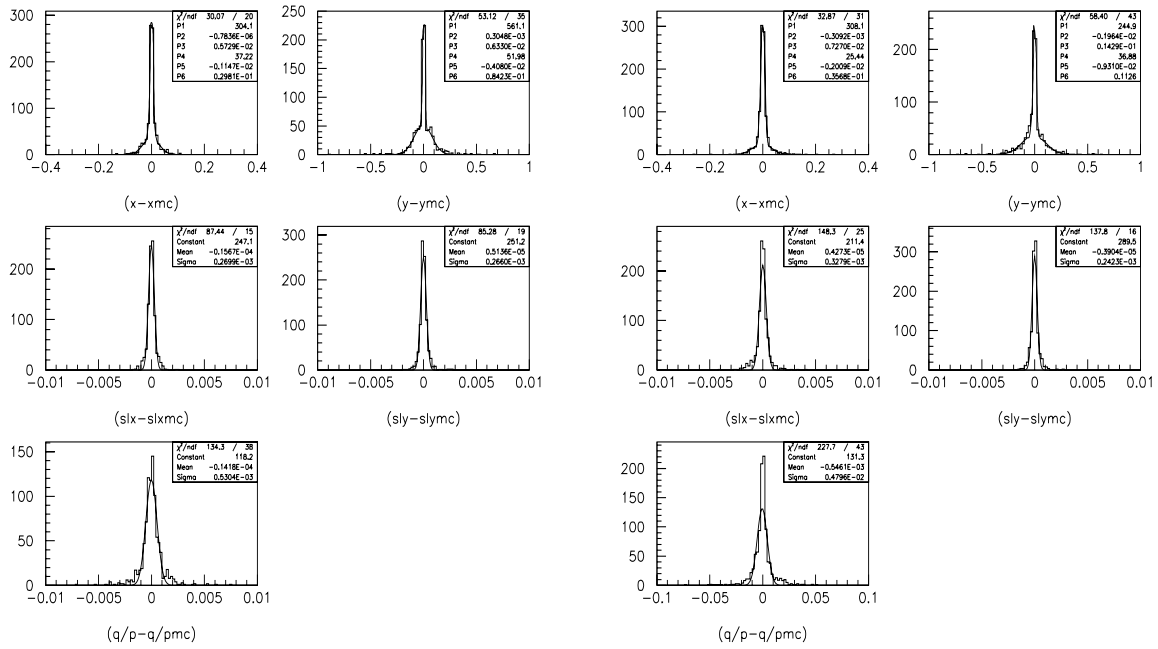

Figure 2.8: *Spread distributions for L2magnet estimated parameters at second step of L2magnet operation. Muons(left) and electrons(right)*

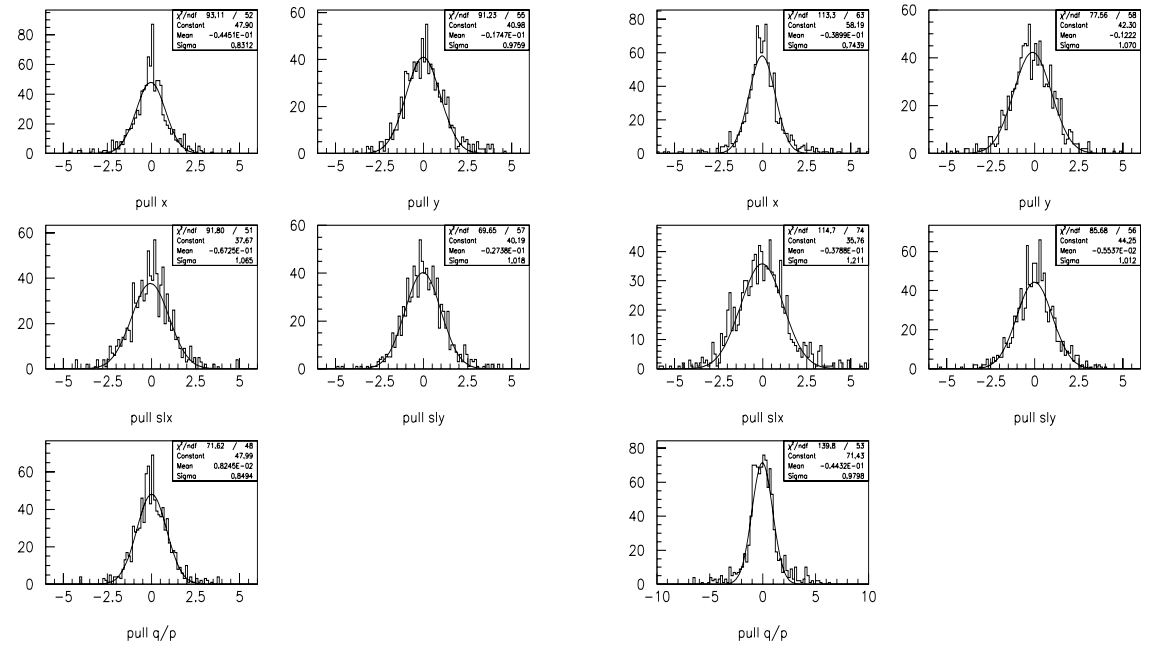

Figure 2.9: *Pull distributions for L2magnet estimated parameters at second step of L2magnet operation. Muons(left) and electrons(right)*

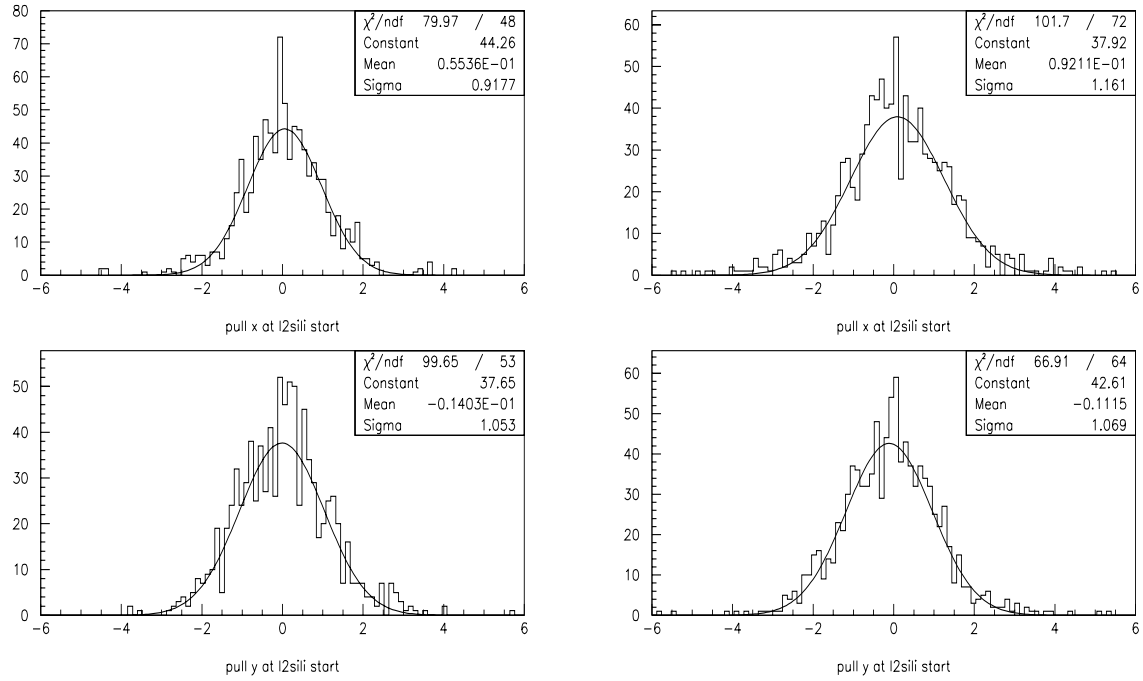

Figure 2.10: *Pull distributions for L2magnet estimated parameters at second step, extrapolated to l2sili starting point. Muons (left), electrons (right)*

of L2Sili. In fig. 2.11 we can see how the cluster position matches the real impact point of a track at the ECAL station for different energies of the track, and a comparison with the given width is shown as well. Clearly an energy dependent correction has to be introduced. We get:

$$\sigma_x(E) = \frac{A}{\sqrt{E}} \oplus B \tag{2.6}$$

where (A,B)=(1.1,0.16) for the inner calorimeter, and (2.,0.2) the for middle/outer calorimeter. This seems to be consistent with what found by the ECAL group in [38].

With this correction we get the efficiency shown in table 2.3.

The efficiency is defined on tracks which are checked, at the impact point level of the simulation to have sufficient hits to be reconstructed (at least 2 points in the calorimeter, and at least 4 points in the SVD). A small part (few %) of the inefficiency can be accounted for by the fact that one is triggering on a cluster which is not due to the J/ψ lepton but typically a photon, and that the J/ψ lepton in this very event is having a p_t which is lower than the threshold. Another few percent can be accounted for by the fact that maybe the amount of impact points required is not enough to reconstruct really a track.

The resolution of the parameters of J/ψ leptons, as observed at the magnet stage, are shown in fig. 2.12. The SLT in this setup has been tested online, some results will be shown in chapter 3.

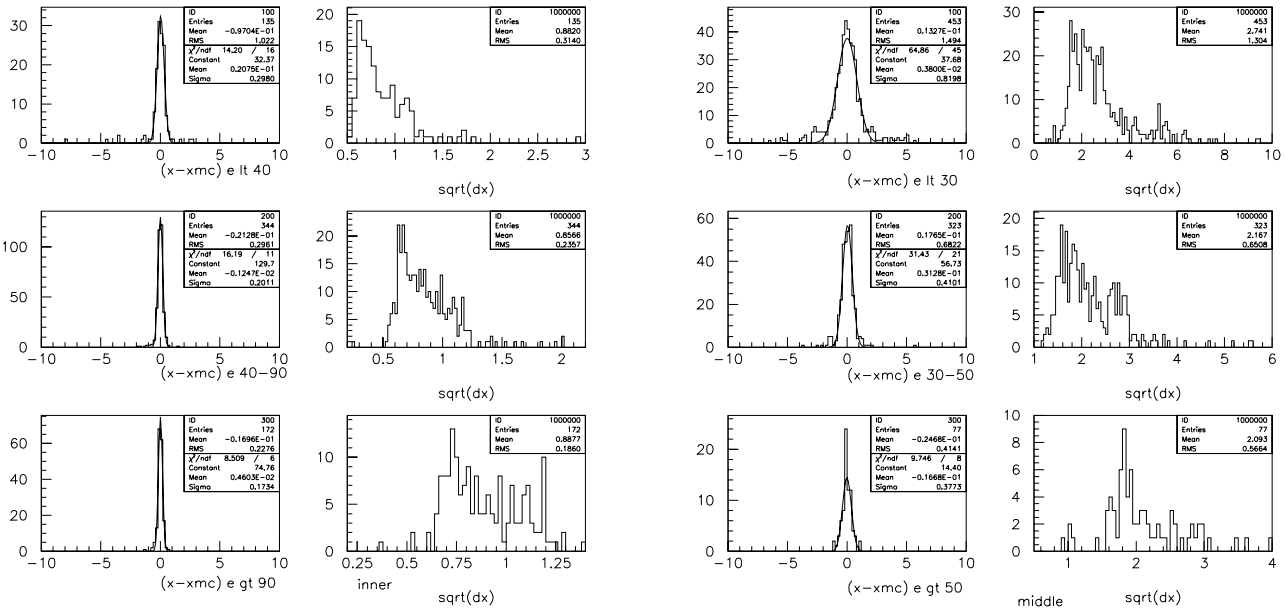

Figure 2.11: *Spread in x position for tracks of different energies, ending up in the inner (left) or middle/outer (right) calorimeter. The spread is compared with the "error" assigned to the cluster, sqrt(dx), and one can see how this error does not follow the energy dependence of the spread.*

level	**events**
start	2000
pretr. passed	1296
FLT passed	1282
slt-before l2mag	1282
within geo	988
L2magnet	886
eff l2mag	88 %

Table 2.3: *SLT performances in the magnet off 1998 scenario. Pretrigger p_t cut above 1. GeV. FLT mass cut at 2.2 GeV applied at the SLT. One can see that no reduction is given by slt-before magnet, since no tracking chambers are available for these trigger steps. In order to have have more statistics to look at, the whole calorimeter and SVD were considered.*

1998, magnet on

A further modification to the FLT emulator was done once it became clear that there would be a period of run where the magnet would be switched on, for detector studies purposes. Therefore some changes were introduced into the FLT emulator, to account for the magnet, and two charge hypothesis for each cluster were generated [6]. Only tracks passing a "ktrig" cut are considered

[6] when magnet is on and tracking chambers are present in the region after the magnet, then the direction in the region in front of the magnet is uniquely determined, but in 1998 no tracking chamber were available

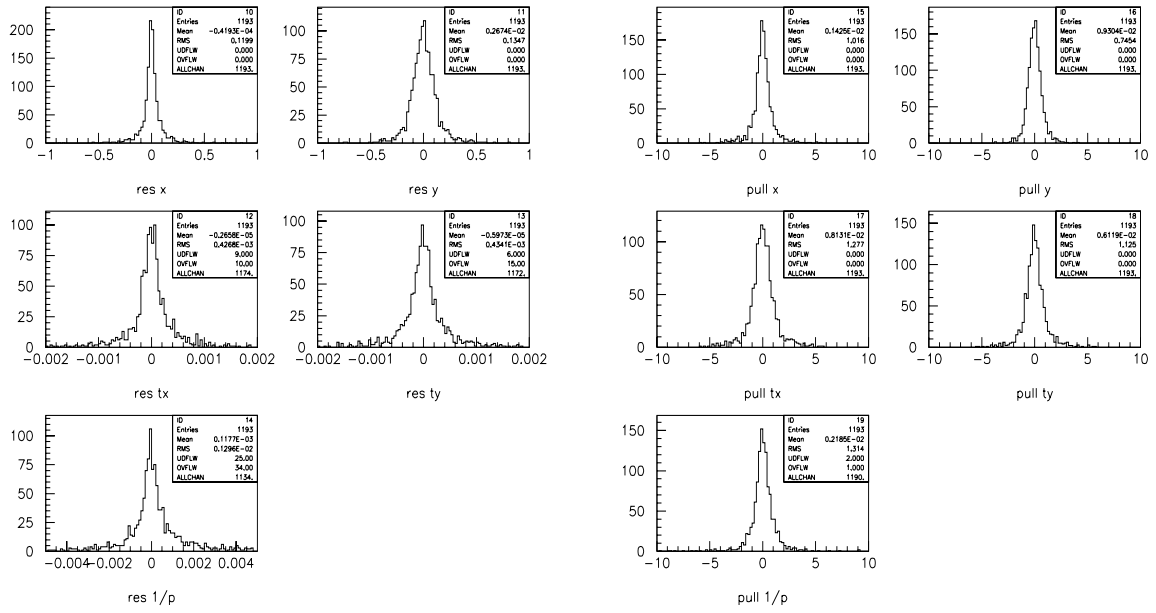

Figure 2.12: *Spread and pull of L2magnet estimates for track parameters in the 1998 magnet off scenario*

by the SLT, where ktrig is used to define a threshold for p_t of the type

$$R = \sqrt{x^2 + y^2} \tag{2.7}$$

$$p_t = ktrig \cdot (\frac{1}{R} + \frac{1}{\sqrt{x^2 + \mid y^3 \mid}})$$

The performance of the SLT with magnet on, with no real FLT filter (no tracking chamber check), is of course expected to decrease, absorbing the inefficiency which normally is sorted out at FLT level (see also some studies done by [19] for FLT with tracking chambers available), due to triggering on photons from brehmstrahlung instead of J/ψ leptons. L2Magnet in this configuration is producing only two new informations, the direction in the xz and yz plane. The momentum is the energy from ECAL, and it is known in this setup.

The resolution of the parameters of J/ψ leptons, as observed at the magnet stage, are shown in fig. 2.13.

2.2.4 Conclusion

We have developed a tracking algorithm for the second level trigger, to extrapolate tracks from the region after the magnet area to the region in front of it, and in this way we provide the initial region for SVD tracking for L2Sili. The precision achieved is reasonable, considering that we need to respect the time window of 1 millisecond for operating on one event. L2magnet is flexible to more than 1 detector scenario, and in particular the SLT code has been used online during the beginning of 1999 run [7]. During this run the magnetic field was switched off, therefore

[7] see chapter 3

level	events
start	1800
pretr passed	677
FLT passed	579
slt-before l2mag	579
within geo	422
L2magnet	260
eff l2mag	62%

Table 2.4: *SLT performances in the magnet on 1998 scenario. Pretrigger p_t cut above 1. GeV. FLT mass cut at 2.2 GeV applied at the SLT. One can see that no reduction is given by slt-before magnet, since no tracking chambers are available for these trigger steps. In order to have more statistics to look at, the whole calorimeter and svd were considered.*

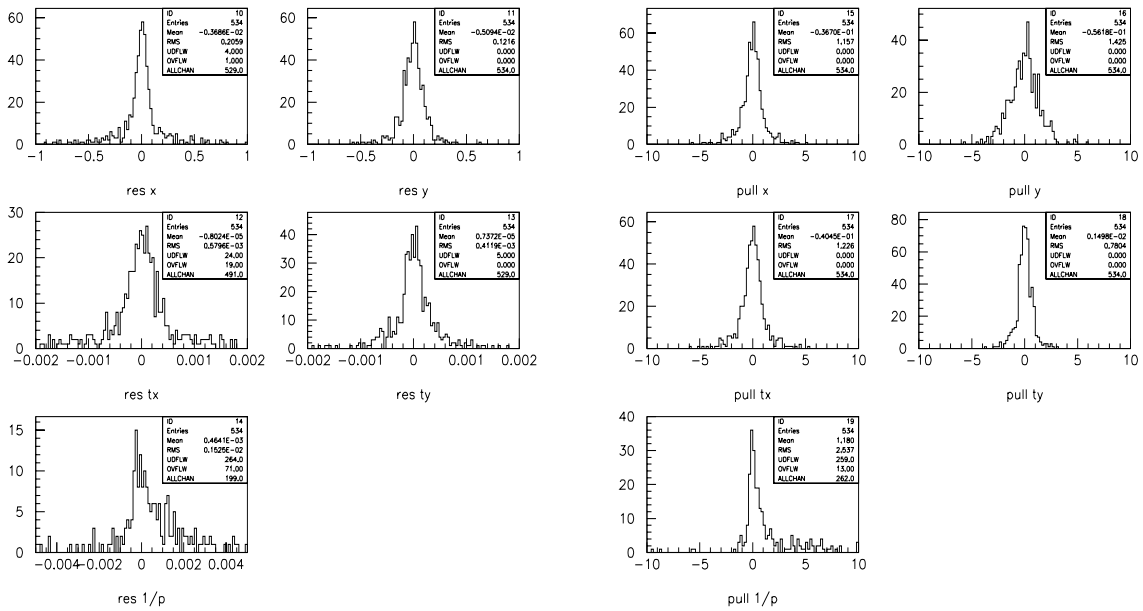

Figure 2.13: *Spread and pull for L2magnet estimates for track parameters in the magnet on 1998 scenario*

real online tests of l2magnet need to wait for the next data taking period, starting at the end of 1999.

2.3 Use of MC simulation to study the physics potential of the experiment

2.3.1 Studies of charmonium production with the expected setup for the Hera-B detector in 1998

In the beginning of 1998, few months before data taking started, we conducted a study, whose aim was understanding which physics possibilities would be worth investigating during the 1998

data taking run. We summarize here this study.

This work is reported as part of [28].

Unfortunately, few months later it became clear that the Hera machine and the Hera-B detector efficiency and amount of installed components we would be running with was lower than expected, and therefore the estimates here obtained need to be opportunely rescaled to keep this into account. We will see this in chapter 3.

Why charmonium ?

Charmonium physics in the last years has particularly attracted the attention of experimentalists and theoreticians, since results from CDF and even earlier fixed target experiments (e.g. E789,E771) have pointed out a large discrepancy between measurements and theoretical expectations of the process of charmonium production. A lot of theoretical effort has been devoted to try to interpret the latest measurements. Any further experimental results on this topic is clearly very welcome and very important.

At Hera-B one can try to perform interesting charmonium measurements already in 1998. For example, one can measure the total and differential cross section for direct $\psi(1s)$ and $\psi(2s)$ production, or the dependence of the cross section on the atomic number A of the target, In order to perform these measurements, it is necessary first of all to distinguish in the $\psi(1s)$ sample collected, the part coming from direct production, and the part coming from χ_c or $\psi(2s)$ production. A preliminary study presented here on this point gives us good hope to be able to disentangle the χ_c source, and therefore give a measurement on the fraction of $\psi(1s)$ originating from that source, and from direct production.

Analysis Tools

The MC data sample analyzed consists of 4 samples of approximately 4000 events each, where an initial $c\bar{c}$ pair produced in a pN interaction has decayed into $\psi(1s)$, χ_{c1}, χ_{c2} or $\psi(2s)$. As main background to charmonium signal, we look at 4000 MC events where the initial $c\bar{c}$ pair has decayed into 2 D mesons, both decayed semileptonically. The final observable state is a pair e^+e^-. Unfortunately the very strong background (high p_t inelastic interactions not containing heavy quarks), which is several orders of magnitude higher than J/ψ production, cannot be seriously studied via Monte Carlo simulation, since it would require an enormous effort of MC generation, which is surely not available at the time of the study. Real data will tell us. Some attempt to study this problem has anyway been attempted by the NBI group, and can be found in [22].

The simulation package used to generate the events is ARTE. The data have been generated using a special 1998 version for the detector [32]. Further, the data have been produced with the magnetic field switched off. Only 1 target wire was used.

The simulation of the pretrigger and trigger system is performed by the SLT software simulation package l2simu [23] with the additional use of the electromagnetic calorimeter reconstruction package CARE [35]. What we will indicate by **PRE** in the tables will be a p_t requirement above a certain threshold for at least 2 clusters in the event, as the pretrigger would do, **FLT** will mean a mass requirement above a certain threshold for at least 1 pair of clusters in the event, and **SLT** means requiring that at least 2 tracks satisfy a mild matching to SVD requirement, with 1 hit per view at least collected.

No offline reconstruction program in SVD is used, since it was not available at the time this study was done. Instead the analysis is done on the tracks passing the reconstruction done by

L2Sili in l2simu [8]. To make a vertex fit of the triggered pairs, L2Vertex has been used. No RICH reconstruction program was publicly available, therefore could not be included.

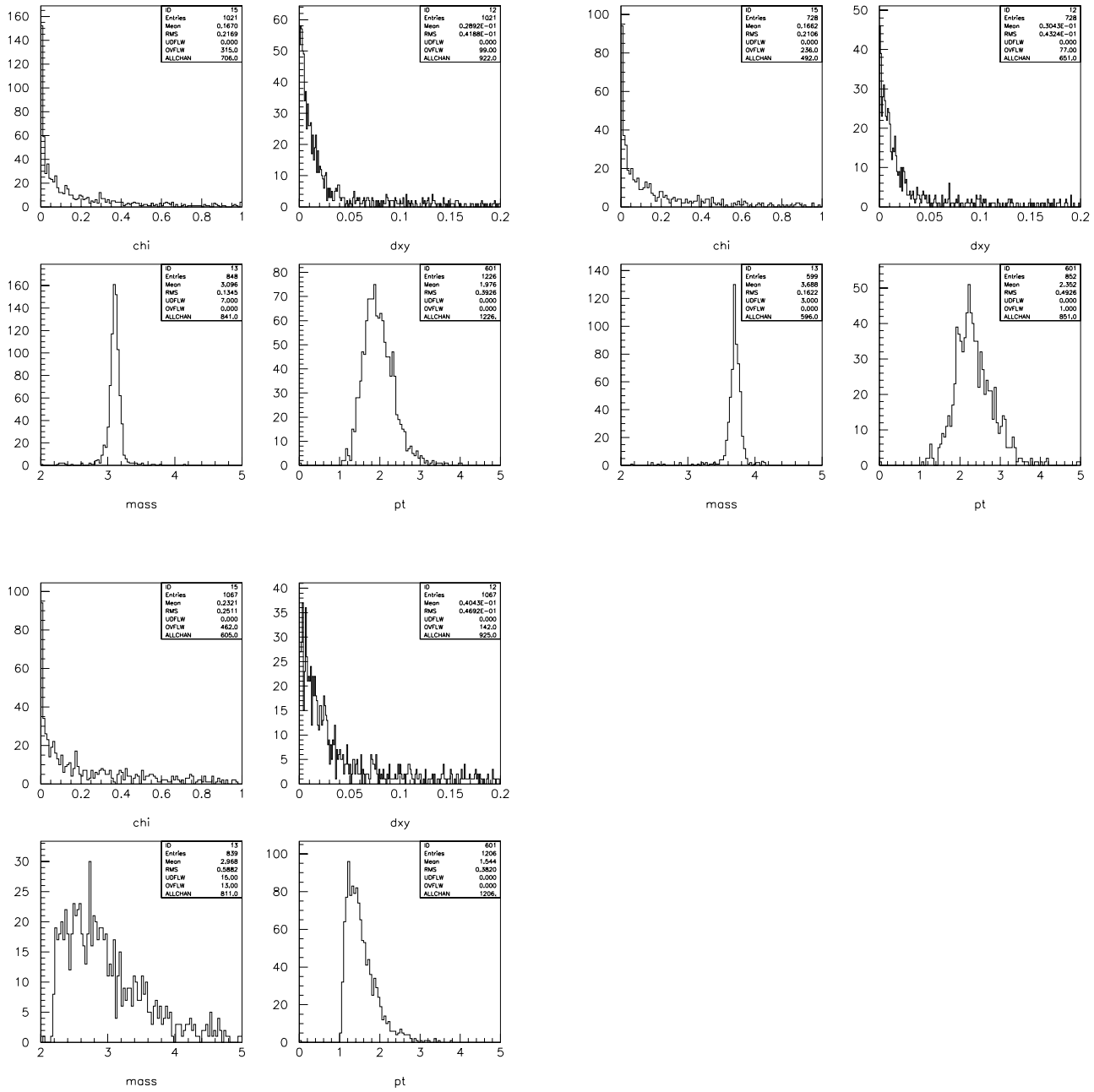

Figure 2.14: *J/ψ (up left), $\psi(2s)$ (up right) and DD (down left) events. Chi square from common vertex fit and distance in the x-y plane at reconstructed vertex (top), invariant mass and highest p_t in event (bottom)*

[8] which has been tested thouroghly on MC, see [22], [28]

Detector scenario

As an hypothetical scenario for this study, done in beginning of 1998, we will use approximately 50% of the final SVD detector setup, inner and middle electromagnetic calorimeter, and no muon tracking device. Therefore the study is concentrated on e^+e^- final state for J/ψ , and the cuts applied in the analysis are, compatibly with having a good signal/background ratio, kept not very tight.

Analysis

The analysis is concentrated on single interaction events, since this is the only realistic type of events to look at, to be able to reconstruct a clean signal with so reduced a detector.

Assuming a 3 MHz single interaction rate (which given the Hera bunch frequency of 8.1 MHz means assuming a mean number of interactions equal to 1), and a running period of 1.33 10^6 sec ($\sim$ 2 weeks), we can calculate the luminosity for that period, assuming to use a carbon wire (A=12)
$L = T_{run} \cdot \frac{IR_{single}}{\sigma_{inel} \cdot A^{0.66}} = 1.33\ 10^6 \cdot \frac{3 \cdot 10^6}{33 \cdot 10^{-3} \cdot A^{0.66}} = 4 \cdot 10^{13}$ barn^{-1}
The plots in the following will be scaled to this reference running time.

The cross sections, and expected production yield for the processes of interest, are shown in table 2.5, where we have taken in consideration for the signal $c\overline{c}$ events the factor $A^{0.92}$ and the branching ratio to two leptons.

process	**cross section**	production yield in 1.33 10^6 sec
Inelastic	33 mb	6.7 10^{12}
$pN \to J/\psi X$	440 nb	12 10^6
$pN \to \psi(2s)X$	70 nb	2.4 10^5
$pN \to \chi_c X, \chi_c \to J/\psi\gamma$	30% total J/ψ	4 10^6
$pN \to DDX$	20 μb	10^8

Table 2.5: *Summary of total cross sections. For cross sections measurements, see [15],[17],[18]*

The amount of direct J/ψ production (see [14], [15] and [16]) is approximately 55% of the total J/ψ yield, 30% comes from χ_c decay and 15% from $\psi(2s)$. Contribution from $b\bar{b}$ events is several order of magnitude lower, and therefore not mentioned. χ_c's will be caught only through the $\psi(1s)$ trigger.

We see in fig.2.14, what are the characteristics of triggered pairs and their reconstructed common vertex (using l2vertex) for signal and background events. We see that they are very similar, coming essentially all from the primary interaction region. For J/ψ and DD the different cross section saves the signal, while for $\psi(2s)$ and DD a further cut on p_t will be probably needed to ensure a safe signal/background for the signal.

2.3.2 Results for $\psi(1s)$ and $\psi(2s)$

Table 2.6 describes the (trigger + reconstruction) efficiency measured on $\psi(1s)$ events and the other important background for this channel, the double semileptonic D decays, which has a cross section approximately 1 order of magnitude larger. We list the percentage of background from D and of signal in a given mass window : $2.9 < M(e^+e^-) < 3.3$ GeV. The pretrigger cut on p_t is at 1 GeV, and the mass cut at 2.2 GeV. The requirement at SLT is 1 hit per view found in SVD.

	$p_t > 1.$	
	ψ(1s)	DD
start	4800	4000
lund prescal		10^{-3}
PRE	1255	1414
FLT	1226	1206
SLT	1031	1068
M(e^+e^-)	800	161
TOT eff	**16 %**	0.4 10^{-4}

Table 2.6: *Results on J/ψ and DD events. The lund prescaling factor needs to be applied since the DD events were generated only if at least 2 leptons with p_t above 1 were in the event, checked at LUND generation level.*

It is interesting to see also how the plot for J/ψ would change if we change the calibration of ECAL to 5%, which is the level expected after the first few weeks of run. See fig. 2.16. It is also interesting to see how the efficiency for J/ψ would change, in this hypothetical 1998 scenario for Hera-B, when requiring more hits in the matching of the ECAL cluster with the SVD. See fig. 2.17. We can see that the efficiency goes down more than a factor of 10, for geometrical reasons essentially, since the SVD setup is quite smaller than what is expected in the final setup.

From table 2.6, in the case of p_t cut at pretrigger at 1 GeV, with a 3 MHz single interaction rate, in a period of 1.33 10^6 sec, we would expect to have a $\frac{S}{\sqrt{B}} \approx (0.16{\cdot}12\ 10^6)/(\sqrt{0.4\ 10^{-4} \cdot 10^8}) =$ 3 10^5.

For $\psi(2s)$, we repeat the same cuts essentially, but we decide to cut tighter on p_t to eliminate DD background in the $\psi(2s)$ window. This saves a good fraction of the signal, and eliminates background which could turn out to be more dangerous because of the lower cross section of $\psi(2s)$ in respect to J/ψ . One can see in table 2.7 the efficiencies obtained. A cut at 1.5 GeV on the transverse energy E_t of the cluster associated to a SVD track seems to be more opportune, to further reduce the combinatorial background and the DD background. In table 2.7 we see also the percentage of events in a mass window $3.3 < M(e^+e^-) < 4.$ GeV.

	$p_t > 1.$	
	ψ(2s)	DD
start	3000	4000
lund prescal		10^{-3}
PRE	871	1414
FLT	852	1206
SLT	765	1068
E_t	307	81
M(e^+e^-)	295	30
TOT eff	**9.8%**	0.7 10^{-5}

Table 2.7: *Results on $\psi(2s)$ and DD events. In comparison to J/ψ (see table 2.6) an additional cut on the transverse energy of the cluster is applied. This reduces the DD background considerably.*

As clearly seen from fig 2.18, the significance of a $\psi(2s)$ measurement in a period of 1.33 10^6 sec will be different from what we have seen for $\psi(1s)$ before, but anyway the signal is still safe.

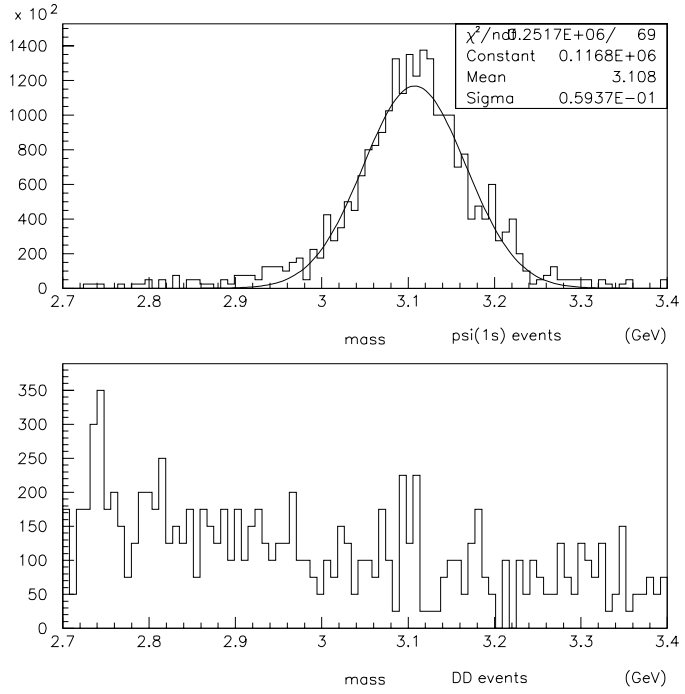

Figure 2.15: *M(e^+e^-) from $\psi(1s)$(upper) and from DD(lower) after the cuts. The bin size is 8 MeV. the plots are scaled to a 1.33 10^6 sec run at 3 MHz. The average number of trigger pairs reconstructed in an events is $\approx$ 1*

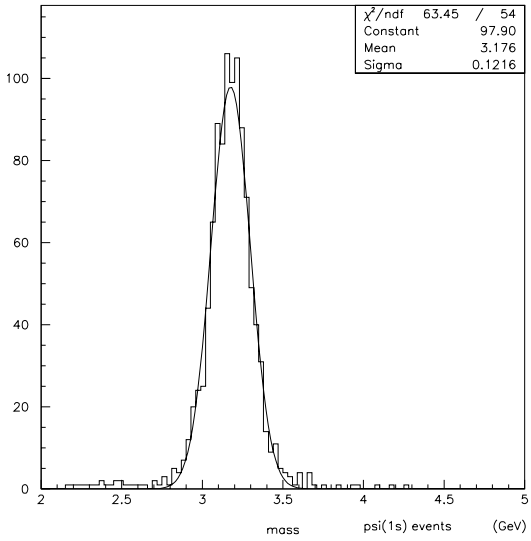

Figure 2.16: *5% miscalibration effect on J/ψ invariant mass*

In fig. 2.18 the plots are scaled for 3 MHz single interaction rate, and 1.33 10^6 sec of run. After the cuts the $\frac{S}{\sqrt{B}} \approx (0.098 \cdot 2.4\ 10^5)/(\sqrt{0.7\ 10^{-5} \cdot 10^8}) = 907$

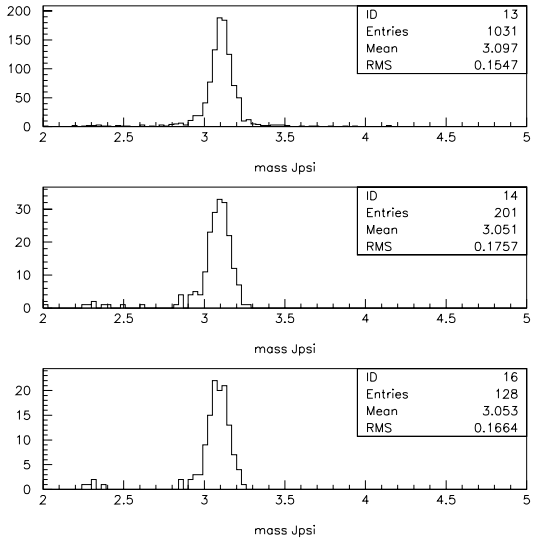

Figure 2.17: *Effect of stronger hit requirements on the SVD tracks forming J/ψ . Top: standard SLT requirement of at least 1 hit per view (x,y) for each track. Middle: a total of 4 hits for each track is required. Bottom: a total of 6 hits for each track is required.*

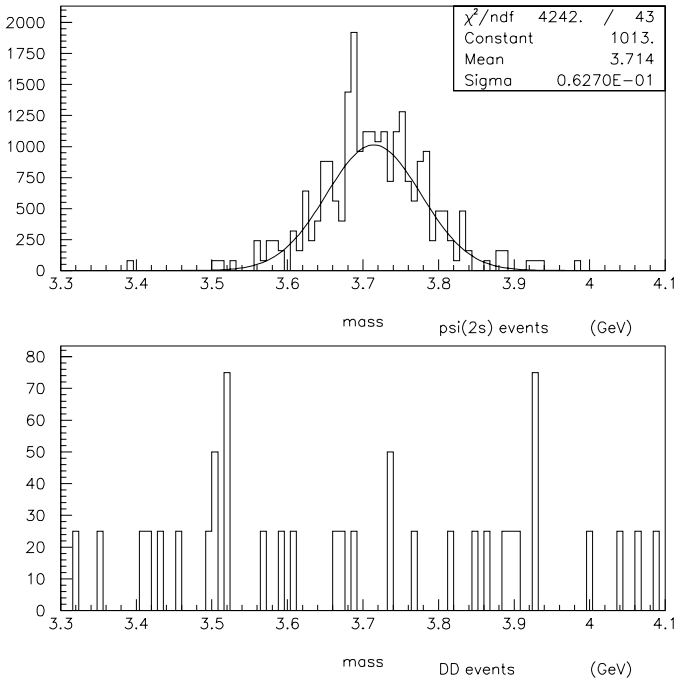

Figure 2.18: *$M(e^+e^-)$ from $\psi(2s)$(upper) and from DD(lower) after the cuts. The bin size is 8 MeV. The plot is scaled to a run of 1.33 10^6 sec at 3 MHz single interaction rate.*

2.3.3 Results for χ_c

Another interesting quantity, when measuring $\psi(1s)$ production, is the fraction of the different sources of production in a sample collected. Here we tried to see if it is possible to disentangle, in a sample of $\psi(1s)$, the $\chi_{c1,2}$ component [9] The results seem very promising.

Since neither RICH nor SVD real reconstruction program was available, at the time of the study, then the strategy to detect χ_c has been to consider, in events where a pair of tracks with invariant mass M(e^+e^-) > 2.5 GeV was found, all the combinations of this pair with the electromagnetic calorimeter clusters reconstructed, after some cuts described below, and then simply plot the invariant mass M($e^+e^-\gamma$) - M(e^+e^-) of all the combinations surviving. The backgrounds considered here to this channel are the internal background, due to combinations, and the directly produced $\psi(1s)$. Applying the same cuts to a sample of the last kind, we see that a significant measurement in a period of 1.33 10^6 sec will be possible, see fig 2.20. The average number of combinations per event is 1.55.
The cuts applied to reduce the internal background consist of:

- cut on the shape of the cluster, to suppress hadronic clusters from electromagnetic clusters, by requiring to use only clusters whose likelihood $LH_{em} > 0.5$ and $LH_{had} < 0.5$.
- cut on the total energy of the cluster, E_{cl} >10 GeV.
- cut on the transverse energy of the cluster, E_{tcl} >0.25 GeV.

No cut on the angular distance of the $\psi(1s)$ with the cluster is required, since the hypothized 1998 setup of the electromagnetic calorimeter in itself is applying this cut. For a brief view of the cuts, see fig 2.19. These cuts manage to have a good efficiency on the signal, and reduce the internal background of a factor 10-15. A closer look at the internal background surviving the cuts above indicates that more than half of it is constitued by photons. The rest is due to e^+,e^-,π^+,π^-, and they can be eventually reduced by use of the RICH. One can look at the size of the electromagnetic signal left there. We want to detect the γ from χ_c which has converted into e^+e^-. We know these two travel very close, and will leave in the RICH a signal significantly higher (in terms of number of photons) than a single background $e^\pm$ or $\pi^\pm$. Therefore we can try to use the height of the signal to discriminate the source of the cluster. In table 2.8 are presented the results observed during the study, for signal and background. Again, the percentage of signal and background in a mass window 0.35 < ΔM=M($e^+e^-\gamma$)-M(e^+e^-) < 0.55 GeV is reported. The two states χ_{c1} and χ_{c2} have the same behaviour, because of the small mass difference between them, and here they are plotted together.

Applying the same cuts to a $\psi(1s)$ sample, what we get is shown in fig. 2.20, after the cuts, and for a 3 MHz single interaction rate and a running period of 1.33 10^6 sec.

From fig. 2.20, is quite clear that the $\chi_{c1,2}$ signal is significantly above the $\psi(1s)$ background.

From table 2.8 we can calculate the $\frac{S}{\sqrt{B}} \approx (0.3 \cdot 12 \cdot 10^6 \cdot 0.12)/(\sqrt{0.55 \cdot 12 \cdot 10^6 \cdot 0.06}) \approx 686$, for 3 MHz int. rate and 1.33 10^6 sec of run.

2.3.4 Conclusions

Assuming some reduced setup for Hera-B detector, as it seemed realistic in the beginning of 1998, we have tried to analyze the charmonium signal and see if a significant measurement can be performed.

[9] The χ_{c0} component is contributing with a cross section 2 order of magnitude smaller than the other two χ_c states, therefore at the moment has been omitted. For what concerns $\psi(2s)$ source, it has not yet been studied. It requires some changes in the PYTHIA generator in order to produce a sample.

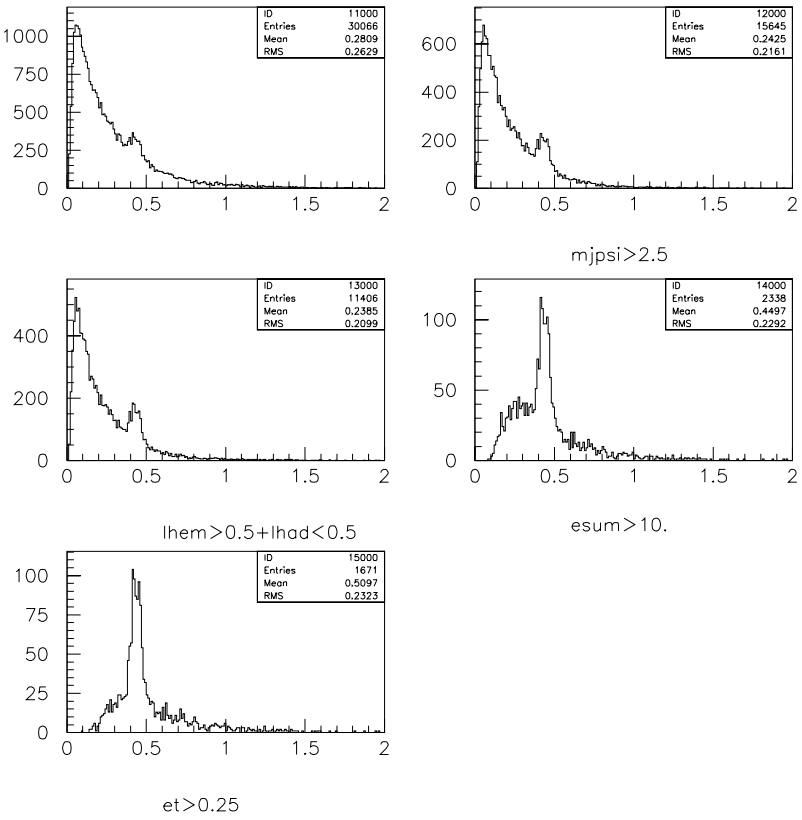

Figure 2.19: *M($e^+e^-\gamma$) - M(e^+e^-) in an event where $\chi_{c1,2}$ has been produced, after the different cuts*

	$p_t > 1.$		$p_t > 1.5$	
	$\psi(1s)$	$\chi_{c1,2}$	$\psi(1s)$	$\chi_{c1,2}$
start	4000	8000	4000	8000
PRE	27%	23%	6%	5%
FLT	99%	98%	99%	100%
SLT	84%	82%	85%	87%
M(e^+e^-)	93%	97%	95%	99%
LH	99%	99%	95%	100%
E_{cl}	63%	79%	63%	80%
E_{tcl}	77%	87%	78%	90%
ΔM	60%	95%	55%	98%
TOT	**6%**	**12%**	**1 %**	**3 %**

Table 2.8: *Results on χ_c and J/ψ . LH is a cut on calorimeter based variable, which helps distinguishing hadrons from electromagnetic clusters. E_{cl}, E_{tcl} are cuts on the total and transverse energy of the cluster*

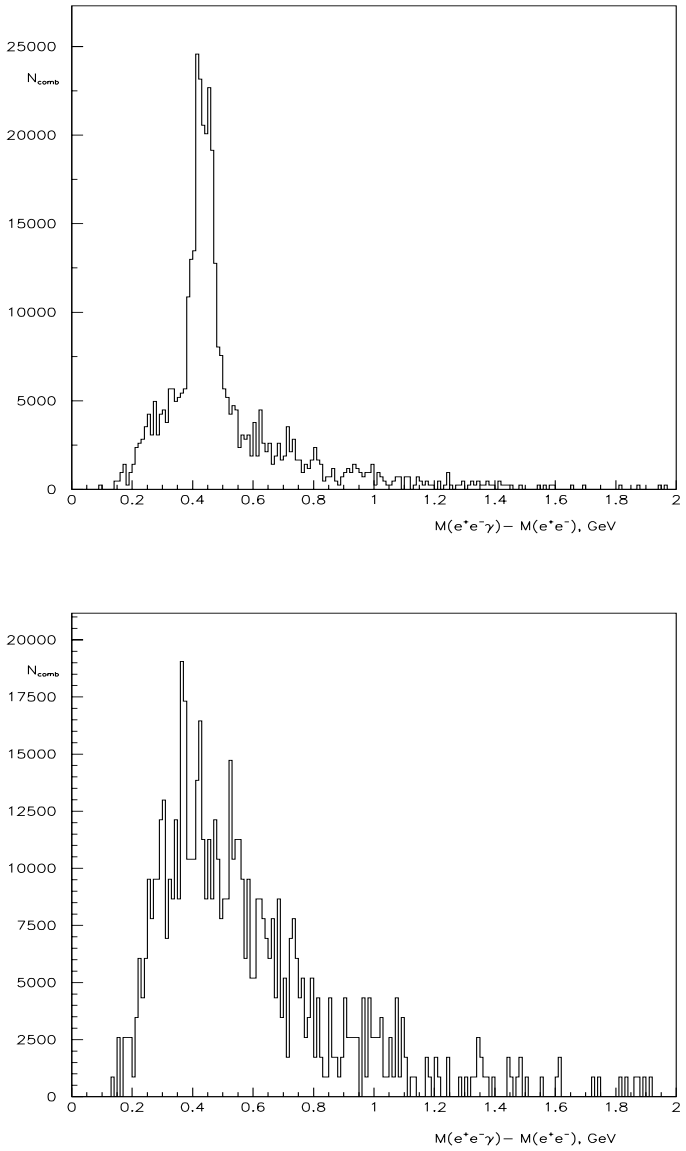

Figure 2.20: *M($e^+e^-\gamma$)-M(e^+e^-) in an event where $\chi_{c1,2}$ (up) and $\psi(1s)$ (down) has been produced. The bin size is 5 MeV*

The background considered here is double semileptonic decays of D mesons, for J/ψ and $\psi(2s)$ signal, and direct J/ψ production for χ_c signal. The background seems to be well contained by the cuts, and the $\frac{S}{B}$ ratio makes us confident that the signal can be observed. But we should make it clear that the real main background, coming from high p_t inelastic events not containing heavy quarks, remains unstudied since it is not realistic to do it within MC simulation, and therefore cannot allow us to conclude that our charmonium signal can be clearly detected, in the period of run we are considering (1.33 10^6 seconds).

Chapter 3

Time to get data!

3.1 The 1998-1999 run

Hera-B has been taking data in 2 periods: from August to December 1998, and from January to May 1999. These two runs have allowed to start testing some of the main components of the detector, and some important systems like pretrigger, first level (FLT) and second level (SLT) trigger, and data acquisition (DAQ). Table 3.1 gives an idea of the status of readout and sharc processing/memory units available for each Hera-B detector component, as it was in February 1999. It is almost 40% of what will be there finally.

component	**readout**	**sharc chips**
SVD	145 (612)	78 (306)
ITR	(468)	(234)
OTR	43 (938)	10 (157)
HIPT	2 (9)	1 (2)
RICH	28 (28)	5 (5)
TRD	1 (32)	1 (6)
ECAL	133 (182)	28 (31)
MUON	24 (32)	5 (7)
SWITCH		72(240)
SLT-PC's		80 (240)
FCS		65 (200)

Table 3.1: *For each Hera-B component, the amount of readout (in units of Front End Drivers, FED), and the amount of SHARC chips devoted to memory buffering for the trigger system, is specified. In parenthesis is reported what will be the number in the final Hera-B setup. In the bottom, also the amount of chips in the switching network of the DAQ/trigger system, the amount of processing computers for the SLT, and the amount of components for the Fast Control System (FCS) of DAQ/trigger is shown*

This run has been the first run with so many different components working together, and with data acquisition and triggering set up as they should be in the final system, only with a reduced number of components. During the 1999 period, more than 5 million high transverse momentum triggered events were taken, using the pretrigger and SLT. In fig. 3.1 we can see a schematic representation of the setup for DAQ/SLT used in 1999. When data are readout from the Hera-B detector (after a pretrigger signal or a clock signal), they are stored in pipelines

(FED), so that the FLT can work on them.

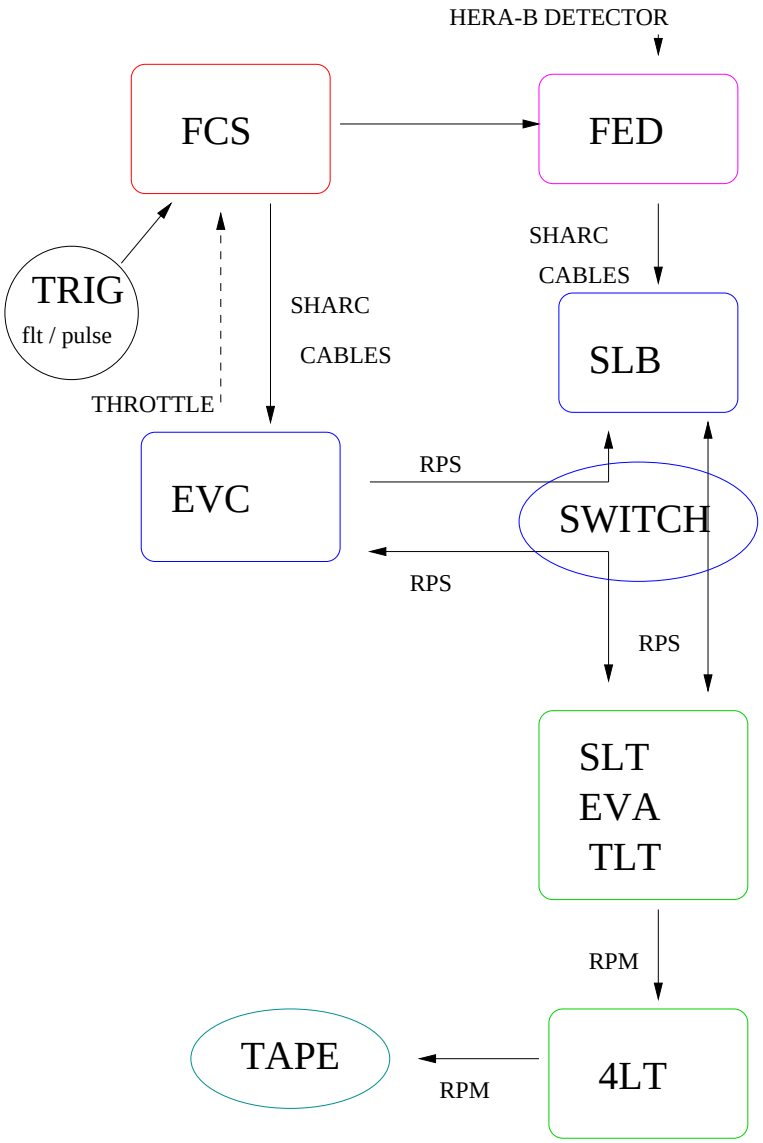

Figure 3.1: *The DAQ/trigger system in 1999. Different colours for different technologies. In pink, the FED, or pipelines where the data are temporaneously stored, before going to the SLT. In red, the fast control system, working between readout, EVC and FLT. In blu, SHARC chips are the building blocks for the event controller (EVC), the memory buffers (SLB) and the switching network (SWITCH). In green, the processors, Pentium Pro 200 MHZ, forming the SLT/TLT processing units, and the reconstruction online farm (4LT).*

In the period of 1999 the pretrigger was a small percentage of what is expected to be in the final setup, and was only based on the electromagnetic calorimeter (so only $J/\psi \to e^+e^-$, no $\mu^+\mu^-$ final decay). The FLT was a small fraction of the final setup as well, and the only decision possible at that level was a count trigger, no mass cut and no formation of Region of Interest for the SLT.

Once the FLT accepts an event, it informs the Fast Control System, which in turn pushes the data into the memory buffers of the SLT (SLB), and tells the Event Controller (EVC) that

the SLT should start. Data go through the switch from SLB's to computers sitting in the SLT farm. If the event is accepted by the SLT, then the event is assembled (EVA) on the SLT farm, and sent to the fourth level farm (4LT), which in 1999 already tried reconstruction online of data, as foreseen for the final system. Then the data are sent to tape. We should note here that a brief period of run was devoted for online tests of the Third Level Trigger (TLT) as well, and tracks were reconstructed online using the data coming from the entire SVD detector available.

The whole chain just described has been shown during 1999 to be working stably for relatively long runs (5-8 hours), and in particular the SLT has been able to trigger with the part of the FLT emulator (i.e. a transverse momentum and mass cut was applied), while the SLT part of the code handling SVD data has been tested online successfully, during the magnet off runs, and an example of online plot can be seen in fig. 3.2. This last test is actually not trivial, it has allowed to test one of the critical points of the experiment, namely the traffic through the switching network during multiple requests of data per event from the processors to the buffers.

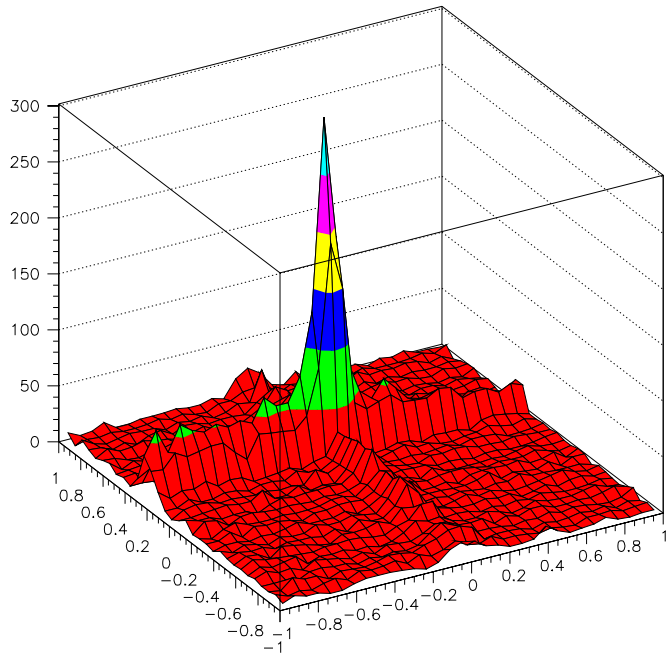

Figure 3.2: *Plot of the tracks found online by the SLT, projected on the (x,y) plane, transverse to the beam line. The tracks are extrapolated at the target position. The coordinate is in cm.*

Two of the detectors available in 1999, particularly interesting for the analysis as we will show later on, are the electromagnetic calorimeter (ECAL), and the vertex detector (VDS). In fig. 3.4 and 3.3 we give a schematic view of them. The available components of SVD were installed in an L shape around the beamline, since studies performed in [28] showed that this would have allowed the maximal acceptance for J/ψ leptons, and the maximal overlap with ECAL, which is important since the leptons are caught in the very first instance by the decision taken at pretrigger/trigger level (which in 1999 has used only ECAL informations).

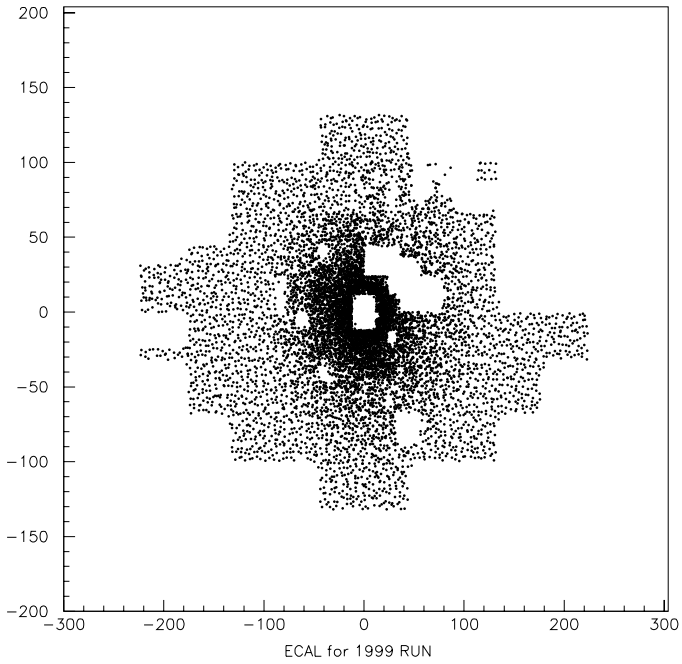

Figure 3.3: *Schematic view in the (x,y) plane (perpendicular to the beam line) of occupancy of ECAL as installed in 1999. The final ECAL should cover a region 6 meter large, and 4 meters high. The coordinate in the plot is cm.*

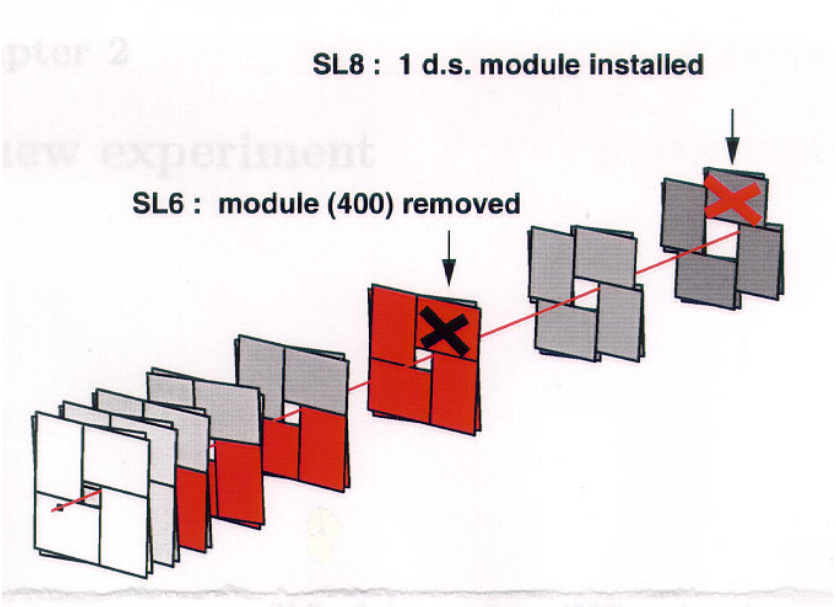

Figure 3.4: *Schematic view of SVD. In red, the modules available for 1999. The line in red crossing the modules is the beam line.*

3.2 The second run : 1999

The run going from January 1999 until May 1999 has been an interesting run. Many improvements in understanding the detector, triggering, alignment and calibration of the detector were achieved. That's why for the following we will concentrate on the data taken during that period, in particular in the long period while the magnet was kept switched off. We shall try first to take a look at the performances of the calorimeter, briefly summarize the performances of the silicon reconstruction software, and then finally use the informations from these 2 parts of the detector to look for J/ψ . We should mention here that the short time that could be dedicated to this analysis has not allowed us to include other interesting informations, like the measurements from the Cherenkov detector. On the other hand, the analysis is concentrated on magnet off data, and in these conditions the RICH performances have been shown to be not optimal, because of too high background from low energetic particles, which in presence of magnetic field would otherwise be bent off the detector.

3.2.1 Study of η and π^0 reconstruction using the electromagnetic calorimeter

As a first approach to a more complicated analysis to look for the J/ψ particle, let's try to see if we can understand the performances of our calorimeter. In particular, we look for π^0 and η particles, which are reconstructible via their decay into two photons and which are produced in relatively high quantity. We look at their general properties in order to understand what we should expect at the J/ψ region.

The reconstruction we use is the standard ECAL reconstruction CARE [35]. The way one reconstructs π^0 and η is by considering pairs of electromagnetic clusters, and requiring them to have at the ECAL position a distance D above some minimal value, to ensure that the 2 photons showers do not overlap, and a minimal transverse momentum p_t (to help clearing up the region around their mass). Then one looks at the invariant mass spectrum resulting. At first, with a p_t requirement at 0.45 and 0.65 for π^0 and η respectively, and a $D > 2$ cells requirement on the distance [1], we get, for runs 4463, 4393, 4437, 4380, the invariant mass plots shown in fig. 3.5,3.6, whose mean and width are summarized in table 3.2.

In fig. 3.5 and 3.6 we separate the particles reconstructed in the inner and middle part of the calorimeter, to get more informations, and also because we expect the inner calorimeter to be better calibrated than the middle one (simply for reason of different statistics accumulated up to now for the two parts). We observe a clear peak for π^0 in both parts of the calorimeter, and we can see a clear η in the inner, and a less clear (for statistics reasons) peak in the middle calorimeter. This makes us confident that we are indeed observing particles, and not some fake effect due to our cuts or to the geometry of the instrumented calorimeter. What is interesting is that we observe lower masses than what we expect, both for π^0 and for η, and a ratio $\frac{\sigma(m)}{m}$ in the inner calorimeter increasing when moving from π^0 to η, which is not what we would expect from looking at the energies and angular separations of the clusters in the region of the peak (see fig. 3.7) and remembering that

$$\frac{\sigma(m)}{m} = \frac{\sigma(\theta)}{\theta} \oplus \frac{1}{2}\left(\frac{\sigma(p_1)}{p_1} \oplus \frac{\sigma(p_2)}{p_2}\right) \tag{3.1}$$

where p_1, p_2 are meant to be the momentum of the highest and lowest photon in the pair. In table 3.2 is a summary of the observations.

[1] The cell size in the inner calorimeter is 2.2 cm, and in the middle is 5.7

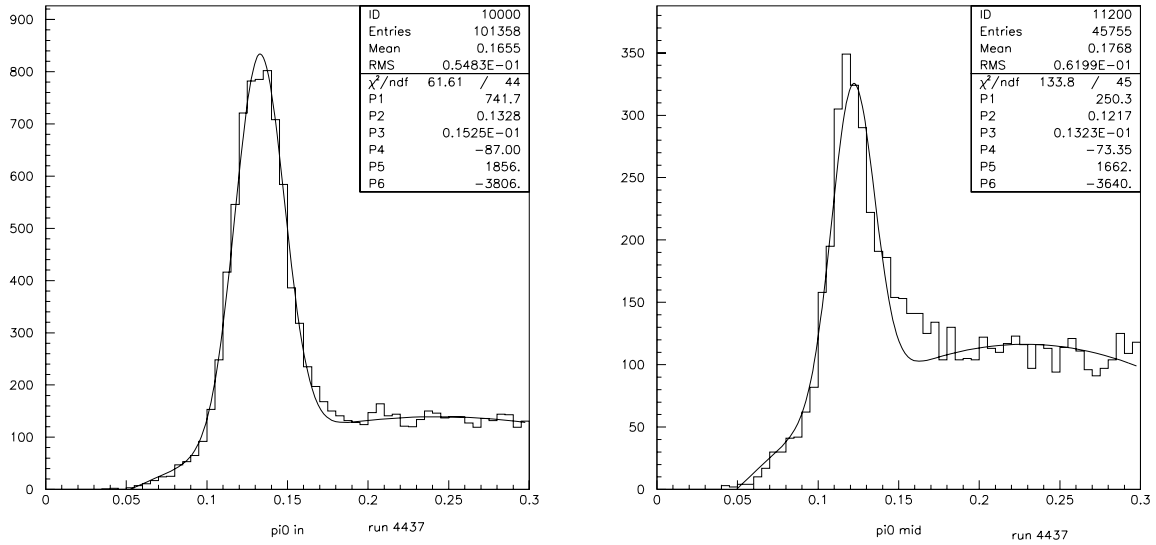

Figure 3.5: π^0 *in inner/middle ecal as obtained by running through half of run 4437*

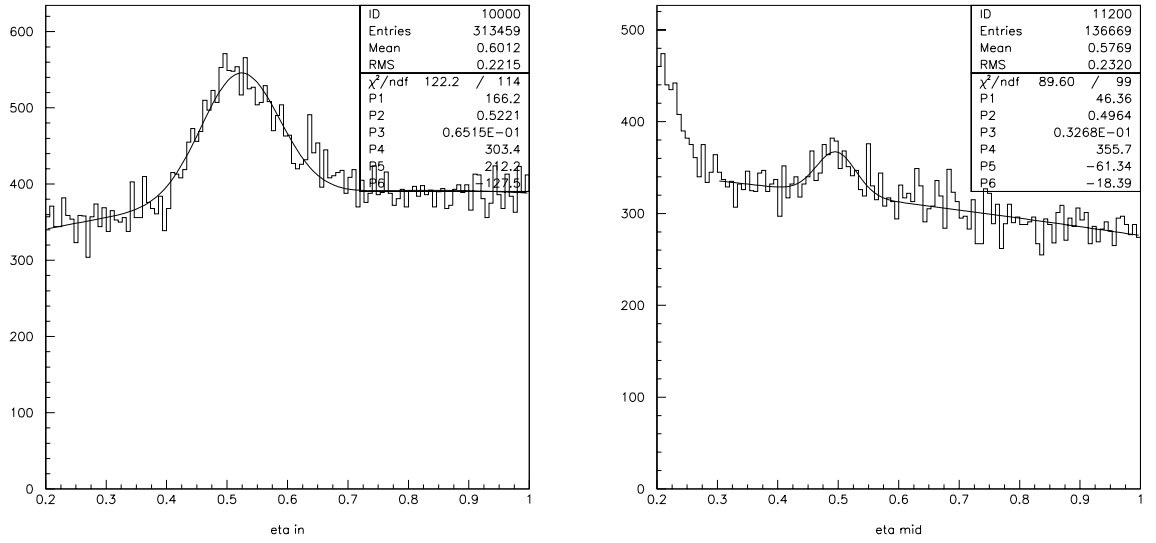

Figure 3.6: η *in inner/middle ecal as obtained by running through half of the statistics of runs 4463,4393,4437,4380*

We also observe an energy dependent behavior of these mass shifts, see fig. 3.8. What one can try to do is then to assume this is a general, energy dependent effect, and try to correct for it, waiting for the ECAL group to tune their calibration with a more appropriate procedure. The reason for an effect like a stronger shift in mass when going from inner to middle calorimeter could be due to the fact that in the middle there is a stronger (than in the inner) systematic error in determining the position of the photon because of the bigger cell size and the non homogeneous energy release in the calorimeter, and if the energy is not properly corrected for accounting for

particle	M (MeV)	$\sigma(m)$ (MeV)	PDG	shift
π^0 inner	132.8	15.2	0.135	2%
π^0 middle	121.7	13.2		10%
η inner	522.1	65.1	0.547	4%
η middle	496.4	32.6		9%

Table 3.2: *Observed masses and widths from plots 3.6,3.5 compared to the Particle Data Group (PDG) values*

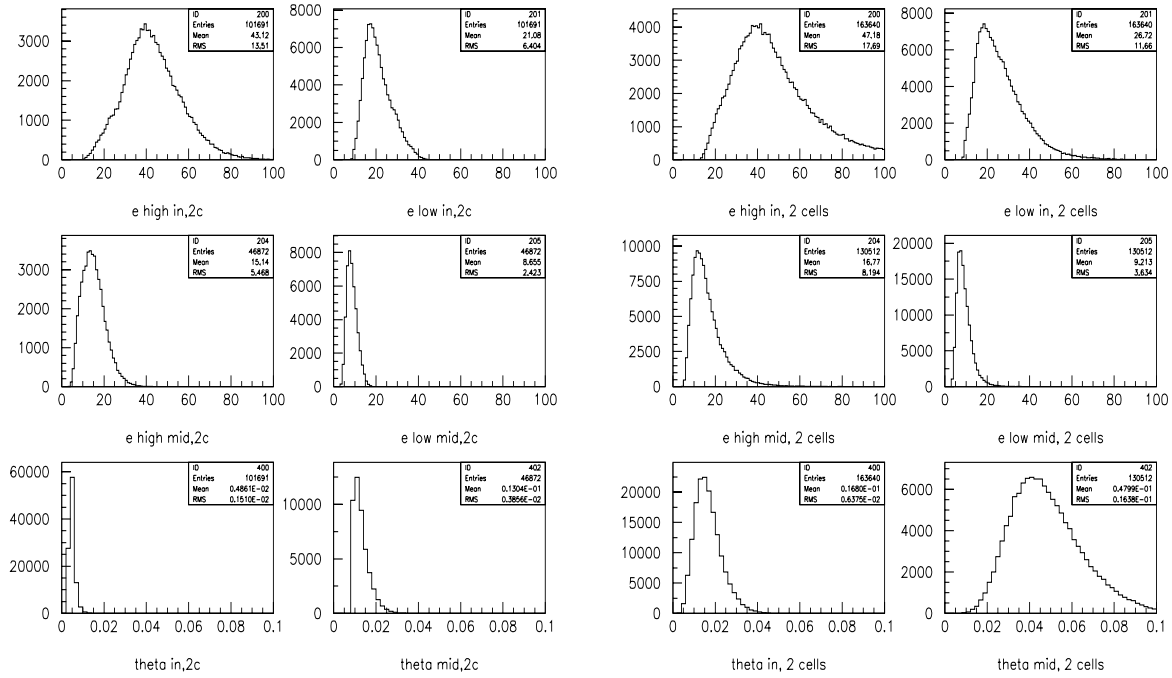

Figure 3.7: *Properties of highest and lowest photon making the π^0 or η, and angular separation. In= inner, mid= middle calorimeter. 2c= cut on distance of 2 clusters greater than 2 cells is applied.*

this effect, the mass could result shifted in respect to the expected value (remembering that $m = m(\pi^0) \simeq \sqrt{p_1 \cdot p_2} \cdot \theta$). The way we decide to apply the correction is to look at π^0's, which have a factor or 10 or so higher statistics than η, and split , for inner and middle calorimeter separately, the candidates where both photons are high or low energy. This correction is a bit hard to apply for the middle calorimeter since the π^0 mass constraint makes the energy of the photons in general lower than in the inner calorimeter. We assume the correction to be of type:

$$E \to E \cdot (\alpha + \beta \cdot E) \tag{3.2}$$

We need therefore to calculate 4 constants all in all, using the results shown in fig. 3.8, and the constants turn out to be like listed in table 3.3.

We then apply the correction and the result can be seen in fig. 3.9. The result of the correction seems to have some effect on the π^0 but not much on the η. In the meanwhile, the ECAL group discovers that what is needed is not a general correction, but rather a specific

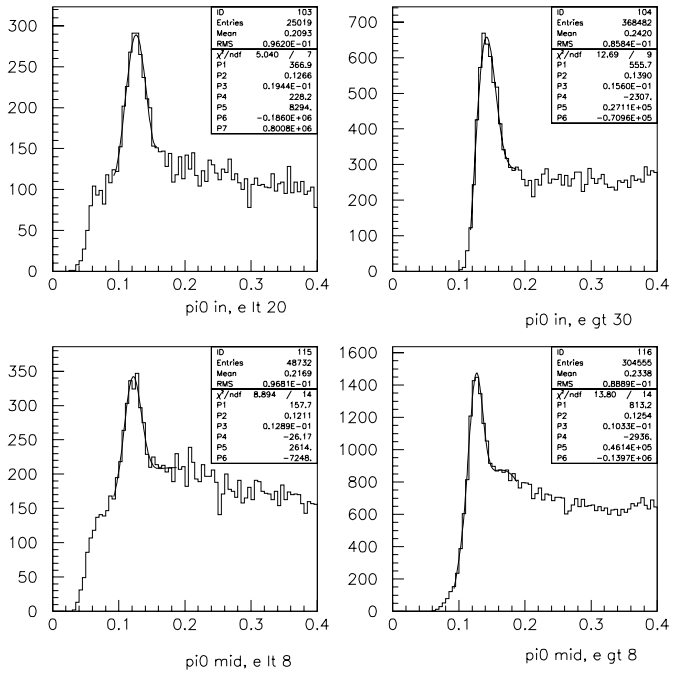

Figure 3.8: *Invariant mass plot for π^0 candidates in inner (up) and middle(down) calorimeter, splitted in low (left) and high (right) energy*

ECAL part	α	β
inner	1.122	$-3.6 \cdot 10^{-3}$
middle	1.133	$-4.5 \cdot 10^{-3}$

Table 3.3: *Correction parameters for energy as extrapolated from observed shift in masses from plots 3.8*

correction on some ECAL boards. After their correction, the situation looks healthier. We show in fig. 3.10, and in table 3.4 the analysis for π^0 and η performed using a minimal p_t requirement at 0.5 GeV, and a minimal distance D of 2 cells. The runs used are run 4380, 4393, 4424, 4486 (full statistics). The calibration is taken from the database after the update of May 12, 1999.

It's nice to see that the widths have shrinked, and the shift in mass has almost disappeared. The only doubt in our opinion remains on the η signal in the middle calorimeter, where the statistics is limited.

A last thing to try before thinking about what we expect for J/ψ , is to check how the observed ratio $\sigma(m)/m$, for π^0 and η matches the expected one, as calculated by using eq. 3.1 and the recent estimates for the relative error on the energy:

$$\frac{\sigma(E)}{E} = 17\%/\sqrt{(E)} \oplus 1.5\% \tag{3.3}$$

for the inner calorimeter [36]. No available estimate for the middle exist. We shall try to use the same constants for the middle, and compare with the data to see how reasonable it is. What we get for $\sigma(m)/m$ is shown in table 3.5. We should remember here that we did not introduce

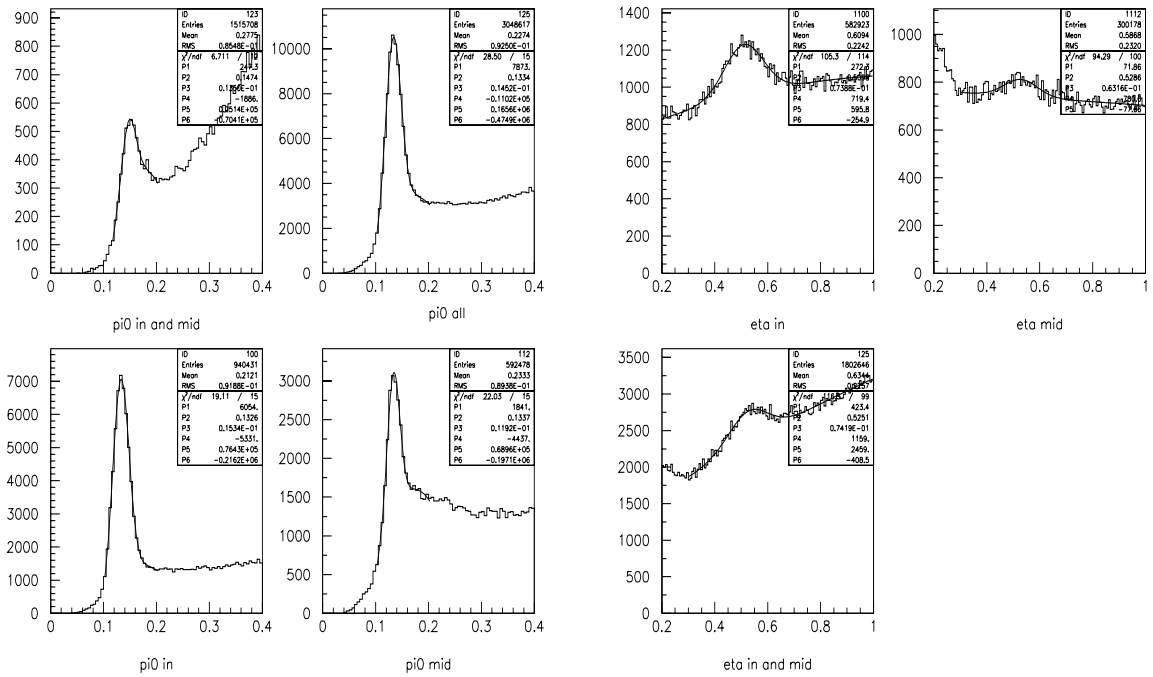

Figure 3.9: *Invariant mass of clusters in π^0 and η region, originating one in inner and one in middle (up left), everywhere (up right), only in inner (down left), and only in middle (down right). After energy correction.*

cuts	**ECAL**	**particle**	**Mass(MeV)**	$\sigma(m)$ **(MeV)**	**shift**	**% error**
$p_t > 0.5$, $D > 2$	inner	π^0	138.2	10.2	2%	7.4%
$p_t > 0.5$, $D > 2$	middle	π^0	140.8	11.8	4%	8.3%
$p_t > 0.5$, $D > 2$	inner	η	552.2	32.3	1%	5.8%
$p_t > 0.5$, $D > 2$	middle	η	562.9	46.7	3%	8.3% (?)

Table 3.4: *Final values (after the very recent calibration update of ECAL) for masses of π^0 and η as observed in inner and middle calorimeter, with the cuts used (D is in cell units). the number are from fig.3.10, where one can see that the limited statistics in the η signal in the middle calorimeter does not really allow us to conclude anything.*

any error contribution from the angle between the 2 clusters. If we try to extrapolate from the results in [37] for the π^0 in the inner, we see that the use of the error on the angle will bring up the calculation for $\sigma(m)/m$ of 1% approximately.

part/ecal	**obs**	**calc**	**factor**
π^0 inner	7.4%	3.3%	2.2
π^0 middle	8.3%	4.6%	1.8
η inner	5.8%	3.3%	1.8

Table 3.5: *Observed and calculated $\sigma(m)/m$ and factor of difference between the two*

If we then use the same formulas, and the informations for J/ψ from MC from fig. 3.11, we

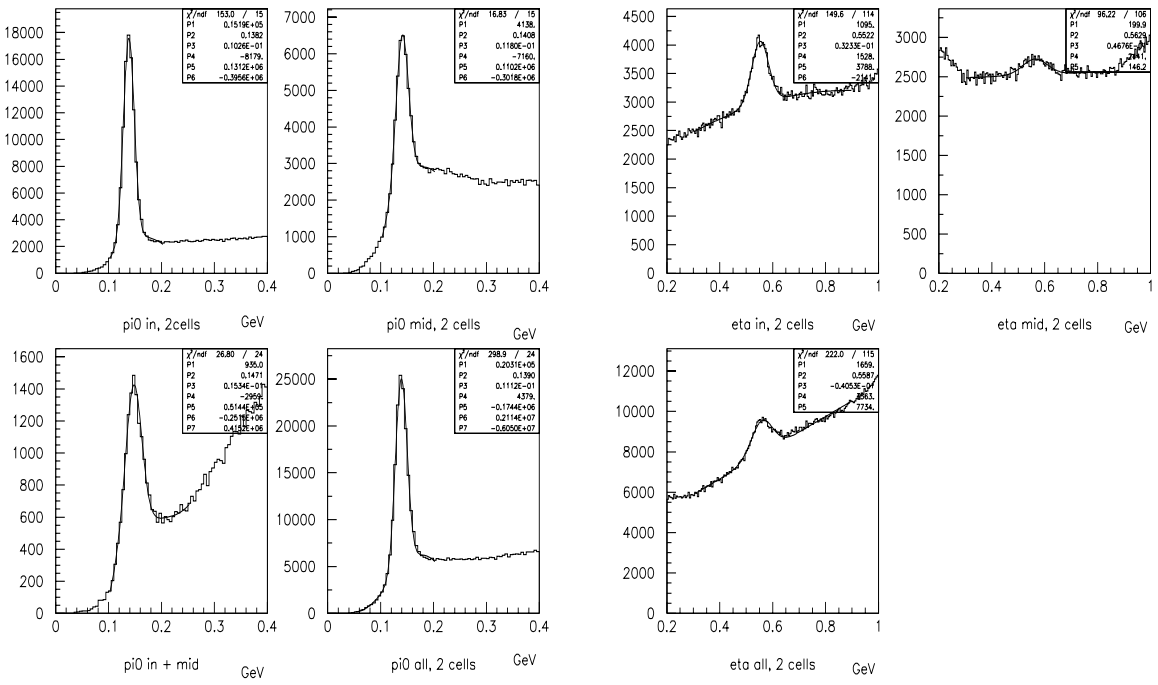

Figure 3.10: *Invariant mass of clusters in π^0 and η region, originating only in inner (up left), only in middle (up right), one in inner and one in middle (down left), and everywhere (down right). After recent ECAL board-specific correction.*

get $\frac{\sigma(m)}{m}$=2.6% and using a factor 2 bigger value, as observed for the other 2 particles we looked at, we predict the width observed to be $\simeq$ 0.15 GeV. As a last comment, we should mention that some recent studies by ECAL group on comparison of π^0 invariant mass spectrum in MC minimum bias events with data show good agreement when the calibration in MC is assumed to be 5%.

3.2.2 Luminosity measurement

Even if Hera-B is not really intended to be a "cross section measurement" experiment (since quantities like CP violation asymmetry, mixing parameters, etc.. do not depend on it), we think it's anyway interesting to try to get a luminosity estimate. Why? For example, at Hera-B we can study the dependence of cross sections of processes like $b\overline{b}$, $c\overline{c}$ open or bound state production for different materials, since our target wires are done of different materials, and this is a nice measurement to add to the other ones in these fields. Further, trying to attempt cross section measurement means also trying to understand our detector and our trigger, and this is for sure a useful exercise.

Very recently more than one way of giving luminosity estimates has become available. Let us first define what is luminosity for us.

$$L \cdot \sigma_{proc} = N_{proc} = N_{BX} \cdot \lambda \tag{3.4}$$

where λ is the number of interactions for a given "process" per bunch crossing (BX). The luminosity L is for us simply the number of interactions of type " proc" in a given time. To

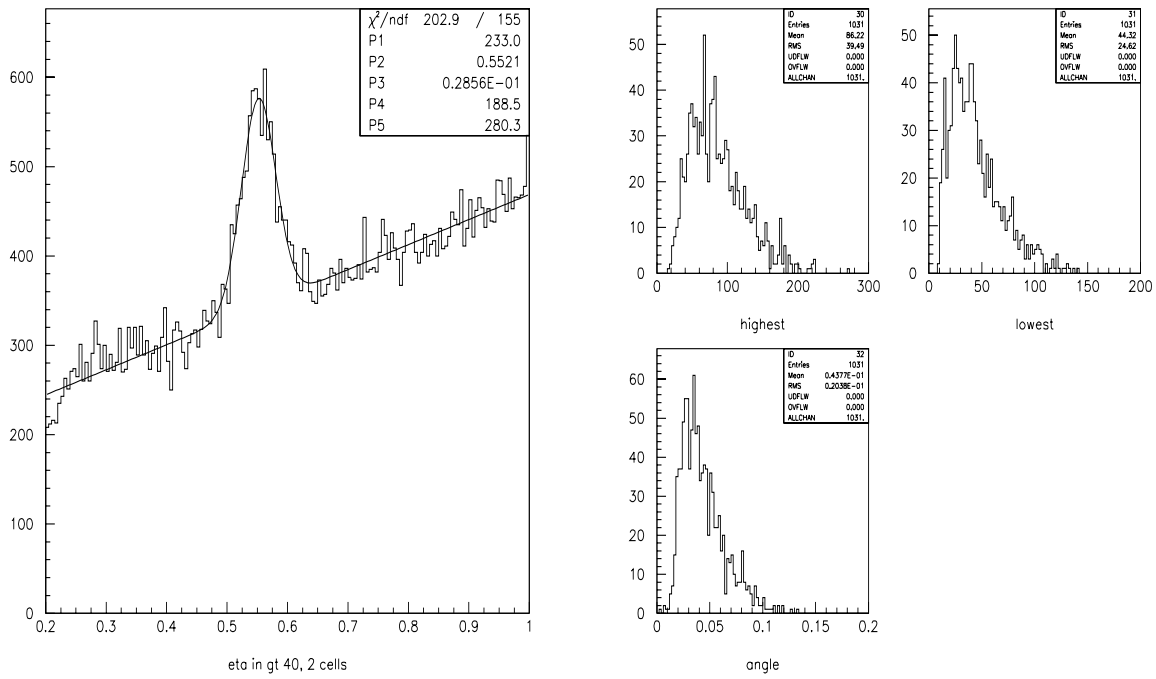

Figure 3.11: *On the left, η signal obtained with the cuts mentioned, plus requiring the two clusters to have high energy ($E > 40$ GeV). On the right, properties in energy and angle of leptons from J/ψ as observed in MC events*

determine it, we use a standard "proc", the inelastic interactions, and then by having λ and knowing N_{BX} from the machine, we get L. Once we have L, we can then use it, together with a cross section measurement for a process from other experiments, to have an idea of how many events containing that process we should expect, or we can use the measured count of events containing that process to estimate the cross section for that process.

One estimate of L in Hera-B comes from the target counters, described in chapter 1, which give us online the interaction rate, but it's nice to find also alternative ways to cross check the results. Another estimate [39] comes from the analysis of the total energy released in ECAL, and the use of it to estimate the mean number of interactions per event. Both methods have still rather large uncertainties (of order 20%). For example, for what concerns the first method, the large acceptance counter had to be removed end of last year, and therefore these scintillator counters are really not good to give an absolute rate calibration. Another method using the information from a charge integrator is being adopted at the moment. The second method on the other hand is very sensitive to background. We don't want to go too much in detail here, we refer to [40] for a review on this. We just say that both methods listed (the charge integrator and the ECAL energy method) give a rate estimate in reasonable agreement with each other, and a factor of 2 lower than the old scintillator method gives (used to monitor the interaction rate online).

We hereby list the values for luminosity determination for the run of our interest, as estimated by the ECAL energy method (and the scintillator method), available up to now. See table 3.7.

We calculate

$$L = N_{BX} \cdot (180/220) \cdot \lambda/\sigma_{inel} \tag{3.5}$$

where 180/220 is due to the fact not all the bunches are filled, and σ_{inel} =222 mb for Carbon, and 620.5 mb for Titanium, taken from [41]. The overall efficiency in table 3.7 takes into account the dead time in the DAQ/trigger system. One should use it when calculating the number of J/ψ expected afterwards.

run	**overall eff.**	**evt(K)**	$N_{BX}(10^9)$	**target rate (MHz)**	λ **ECAL(scint)**	**L pb**$^{-1}$
4393	0.325	212	66.0	5	0.45 (0.58)	0.109
4424	0.3	376	116.1	5	0.41 (0.58)	0.175
4486	0.21	148	45.2	10	0.47 (1.13)	0.078

Table 3.6: *Luminosity estimates has recently become available thanks to [39],[42]. For runs with Carbon target (A=12.01). The luminosity is per nucleus.*

run	**overall eff.**	**evt(K)**	$N_{BX}(10^9)$	**target rate (MHz)**	λ **ECAL(scint)**	**L pb**$^{-1}$
4434	0.46	113	38.4	1.7	0.25(0.20)	0.0126
4436	0.45	71	23.8	2.7	0.24(0.3)	0.0075
4437	0.46	225	74.7	2.2	0.233(0.26)	0.023
4492	0.15	257	88.6	10	0.68 (1.09)	0.079
4496	0.1	234	76.0	10	0.63 (1.01)	0.063

Table 3.7: *Luminosity estimates has recently become available thanks to [39],[42]. For runs with Titanium target (A=47.87). The luminosity is per nucleus.*

3.2.3 A brief look at the VDS reconstruction

Lets' take a look at the vertex detector system, in particular at the reconstruction program using this part of detector informations. At present, the reconstruction program mostly used in Hera-B is called HOLMES [43], and we will use this tool for the analysis on J/ψ . Some of the code performances can be seen in fig 3.12, 3.13, 3.14. In the first one, we see that HOLMES is able to reconstruct tracks. The tracks are projected in the x,y plane at the position of the target, and we clearly see a peak over the background showing tracks coming from the wire. In fig. 3.13 we see how precise HOLMES is in reconstructing the position in x,y,z, of the vertices where these tracks come from. In fig. 3.14 we see how the iterative procedure of lateral alignment of the SVD, which is using the HOLMES package, works. On the left, we see the residual distributions for a track, for each plane seeding the track itself, before any alignment. On the right, the result after the alignment. The internal alignment of the planes is quoted to be $\simeq 50\mu m$. Another important question, how is the alignment of the SVD in respect to ECAL, is answered by fig. 3.15, where the closest SVD track segment projected at the ECAL position for each cluster reconstructed in ECAL is shown. We see that the width is approximately 2 cm, and a clear peak over background is observed. All this makes us relatively comfortable in using this package for our analysis.

3.2.4 J/ψ analysis

As a conclusion of this Ph.D. work, we could not avoid attempting to look at the recently taken data and look for J/ψ . For this we use the data listed in table 3.8.

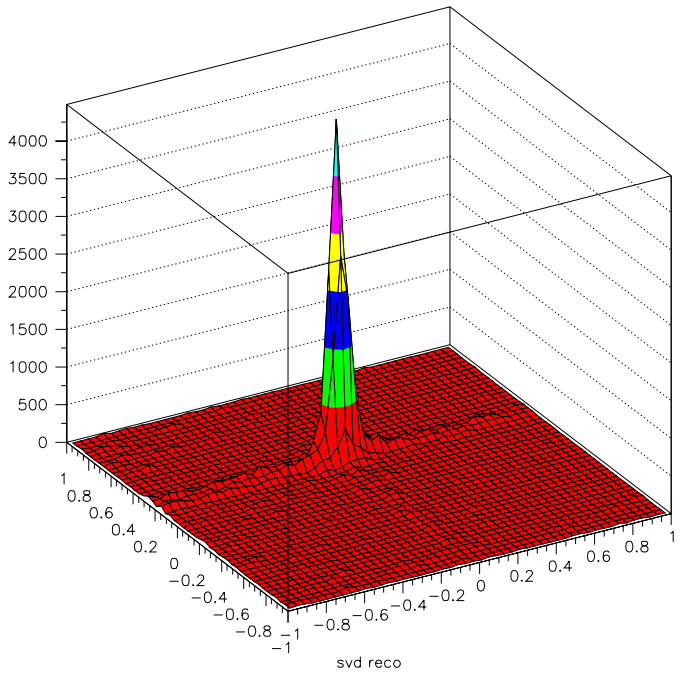

Figure 3.12: *Target spot obtained using tracks reconstructed by the HOLMES package.*

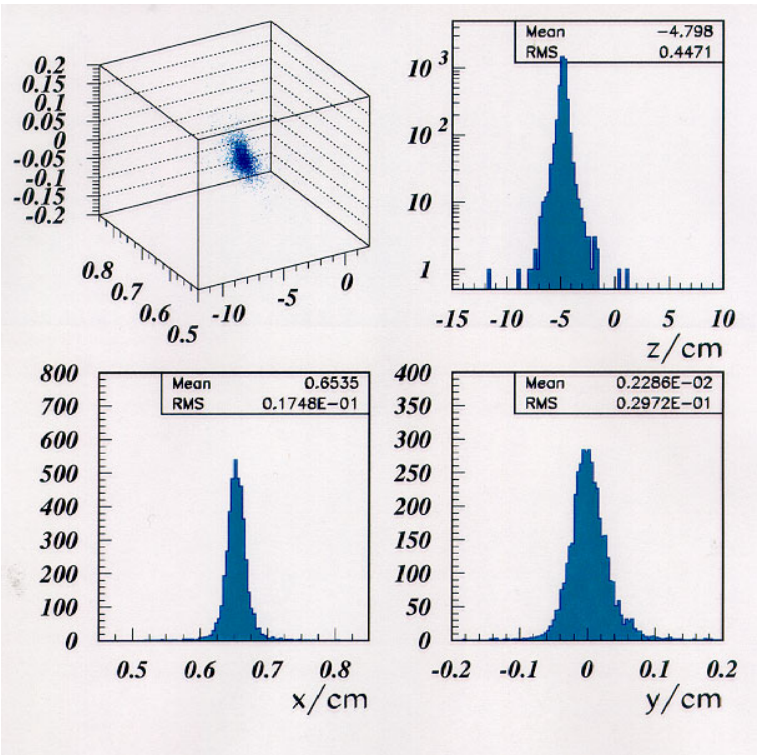

Figure 3.13: *Resolution of HOLMES in finding the primary vertex of interaction.*

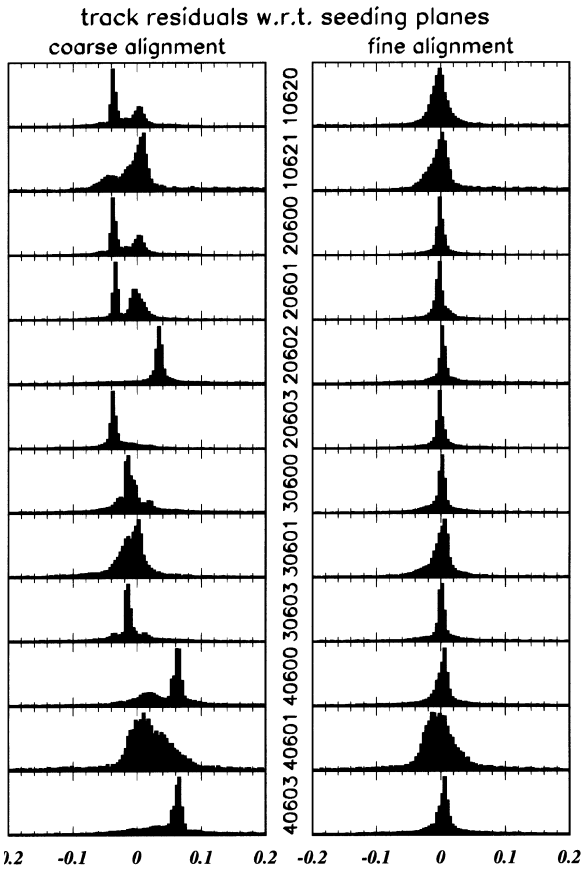

Figure 3.14: *Status of internal alignment of SVD planes before (left) and after (right) the lateral alignment procedure is applied. The procedure uses HOLMES tracks.*

The data

run	target rate(MHz)	period	target material	numb. events per file	numb. files
4026	10.6	2h10'	Carbon	2841	37
4376	9.9	0h50'	Carbon	2841	37
4380	9.9	1h18'	Carbon	2841	57
4382	10.1	0h30'	Carbon	2841	21
4384	10.0	0h40'	Carbon	2841	17
4393	4.9	1h50'	Carbon	2841	75
4424	5.1	3h06'	Carbon	2841	133
4434	1.7	1h02'	Titanium	2841	40
4436	2.7	0h40'	Titanium	2841	26
4437	2.2	2h00'	Titanium	2841	80
4486	10.1	1h13'	Carbon	2841	53
4492	9.7	2h30'	Titanium	2841	88
4496	9.6	2h02'	Titanium	2841	83

Table 3.8: *Summary of data used for the J/ψ analysis here presented*

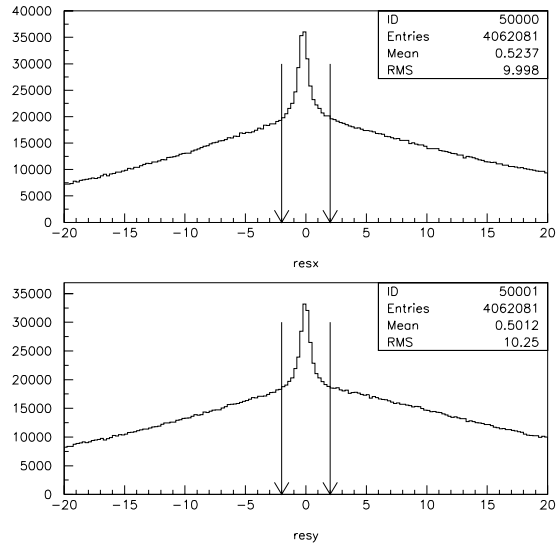

Figure 3.15: *x,y coordinate of a cluster - x,y coordinate of the closest SVD track, projected at the position of the cluster.*

This data have been taken with the detector setup described in the previous sections. Runs 4026-4384 have been take with pretrigger decision: at least 1 track in ECAL with $p_t > 1.1$ GeV, and with trigger decision: at least 2 tracks in ECAL with $p_t > 1.$ GeV, and 1 pair with mass above 2.5 GeV. Runs 4393-4496 have been take with pretrigger decision: at least 1 track in ECAL with $p_t > 1.1$ GeV, and with trigger decision: at least 2 tracks in ECAL with $p_t > 1.$ GeV, and 1 pair with mass above 2.2 GeV.

3.2.5 The strategy and its efficiency tested on MC

To find J/ψ we use the standard reconstruction tools available at the moment, CARE and HOLMES, already described.

Let's look at the cuts we use, and let's try to justify them by looking at a MC J/ψ sample, which has been preliminary pretriggered [36] using in the MC simulation the configuration for readout, pretrigger and noise values from real data. This will bring us at the end with a realistic idea for the J/ψ efficiency for the cuts we apply.

CUTS

- Only clusters with $p_t > 1.$ GeV should be considered. The effect of this cut on the J/ψ leptons can be seen in fig. 3.16, and it has been used to cut on data at the trigger level. One can see from MC study that applying a trigger of this type on signal events has very little probability to select tracks not coming from J/ψ . So there is not point in trying lower cuts for the cluster considered. This will also reduce our internal background.

- We should consider the invariant mass for clusters which have number of cells contributing to them smaller than 9 (this is what is expected for an electromagnetic cluster, we denote the cut with **wid**). Further, a cut on the lateral shape of the cluster (we denote it with

asym in the table), used also in [28] when trying to understand the expected number of J/ψ for the 1998 run, is applied. The cut applied is the following

1) $0.2 < shape < 1.96$ if in inner calorimeter

2) $0.2 < shape < 5.4$ if in middle calorimeter

The shape cut enhances the electromagnetic in respect to hadronic originated clusters in ECAL, which are normally more spreaded. We can see from table 3.9 how this affects our signal in MC.

- From fig. 3.17 we can see what is the expect total momentum for J/ψ in events where both clusters have $p_t > 1$. We decide to use also this cut, and ask the **total energy** of the 2 clusters making the pair to be above 60 GeV.

- we try to require one or both the clusters to match a SVD track, reconstructed by HOLMES, by requiring the SVD track to lay within 2 cm from the cluster position at ECAL. This means we ask the clusters to be originated by charged tracks. This is an important cut, which will sensibly reduce our photon background.

  Further, the number of hits collected for the track should be above 6. Looking at J/ψ leptons after HOLMES, with $p_t > 1$ GeV, see fig. 3.18, we see that this requirement is not hard on the signal, and it helps reducing ghost tracks from the event and not charged tracks, because it essentially means that the track should have 2 points in 2 distinct superlayers. We can see how this requirement affects the J/ψ signal in table 3.9.

In table 3.9 we summarize the efficiency of our cuts.

cut	**events passed**	**percentage**	**events passed**	**percentage**
start	36000	100%	36000	100%
pretrigger	2363	6.6%	2363	6.6%
slt	914	38%	914	38%
asym+wid	442	48%		
tot mom	398	90%		
1 svd match (nhits>6)	368 (359)	92% (90%)	852	93%
2 svd match (nhits>6)	98 (95)	27% (26%)	236	28%
TOTAL		0.27% (0.25%)		0.65%
TOTAL, with plane eff		0.15% (0.14%)		0.5%

Table 3.9: *J/ψ efficiency on MC. With slt we intend the requirement of 2 tracks above $p_t > 1$ GeV from the whole readout region for ecal, and a mass cut at 2.2 (for 2.5 there is no significant change). At the bottom of the table we show the final efficiency, considering also the plane efficiency factor, neglected in the MC simulation. On the right last 2 columns, the efficiency using milder cuts is shown. We will use it for comparing results on plane efficiency from other studies.*

After this, we need to take into account the plane efficiency effect. In the MC simulation it is set to a very high value (98%), but we know that in real life [44], for the 1999 run, it is presently measured to be 60%. The way it has been estimated on real data is by using HOLMES tracks reconstructed without a given plane, projecting a region of interest from the track on that plane, and counting how many times a hit is found, out of all times tried. This method resents of ghosts

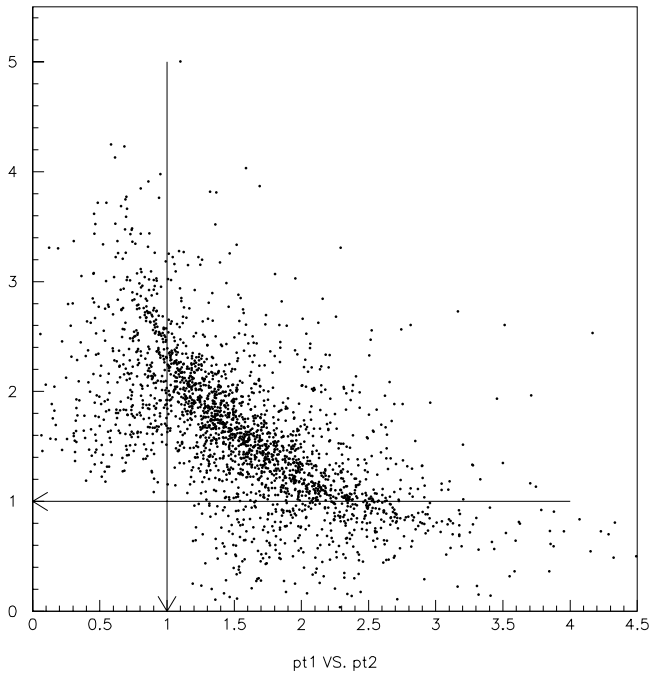

Figure 3.16: *J/ψ lepton1 p_t vs lepton2 p_t from MC, after the pretrigger selection*

tracks[2], in fact when better alignment is introduced (see [45]) then the efficiency goes slightly down. We anyway calculate how the plane efficiency effects our selection by hand, knowing that for the present SVD geometry a track has at maximal 11 planes to traverse (4 layers in SI04, 4 layers in SI05 and 3 layers in SI06) and assuming that a track will only leave hits in 1 sector, and that it will always be able to traverse all the 11 planes. This will overestimate the effect a bit, but we can later compare with another study [46], which uses 60% plane efficiency in the MC, and see how much we differ from them. We calculate the efficiency ϵ of our requirement of N hits in total, out of 11, by the formula

$$\epsilon = \sum_{i=N}^{i=11} \frac{11!}{i! \cdot (11-i)!} (0.6)^i (0.4)^{11-i} \tag{3.6}$$

We get $\epsilon = 89.4\%$ for N=5, and $\epsilon = 74.7\%$ for N=6. Just as a comparison, using the right part of table 3.9 (where no asym cut is asked, only wid), and N=5, we get 2.% and 0.5% for the total efficiency, when requiring single and double SVD match. In [46], using MC simulation to calculate the efficiency for the same cuts, one gets 1% and 0.16% for single and double match. Considering that the assumption we make leads us to an overestimate of the efficiency, the two results are not too far from each other. We shall use therefore our result, keeping in mind the factor of difference with the more detailed MC study, for discussing our final results. As last thing, let's take a look at how and where we expect to reconstruct J/ψ , applying on the MC sample the same cuts we will apply on the real data, introducing a miscalibration of 5%. See

[2]e.g. combination of hits which survive the definition of "track" but do not correspond to the path of a physical track

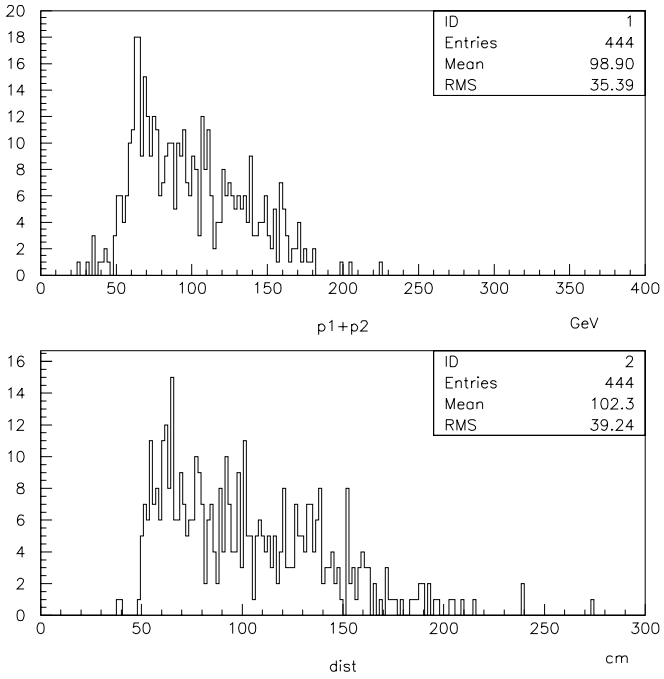

Figure 3.17: *J/ψ leptons total momentum and distance at ECAL from MC, after the pretrigger selection, and asking $p_t > 1$ for both clusters*

fig. 3.19. The invariant mass plots has a mean at 3.09 GeV, and has a width of 0.13 GeV, not far from what we predicted already using the π^0 and η data.

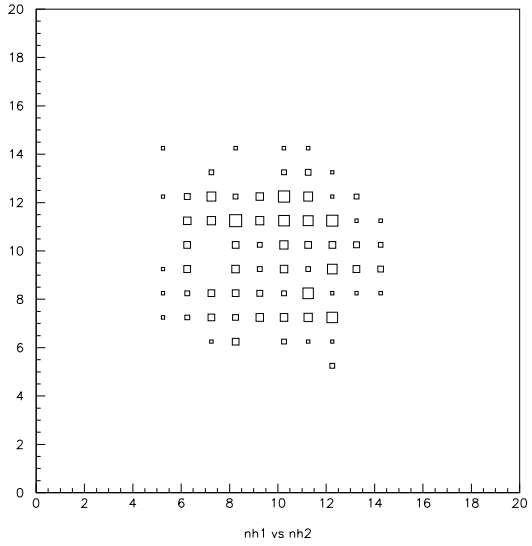

Figure 3.18: *Total number of hits collected using HOLMES for J/ψ lepton1 vs lepton2 from MC*

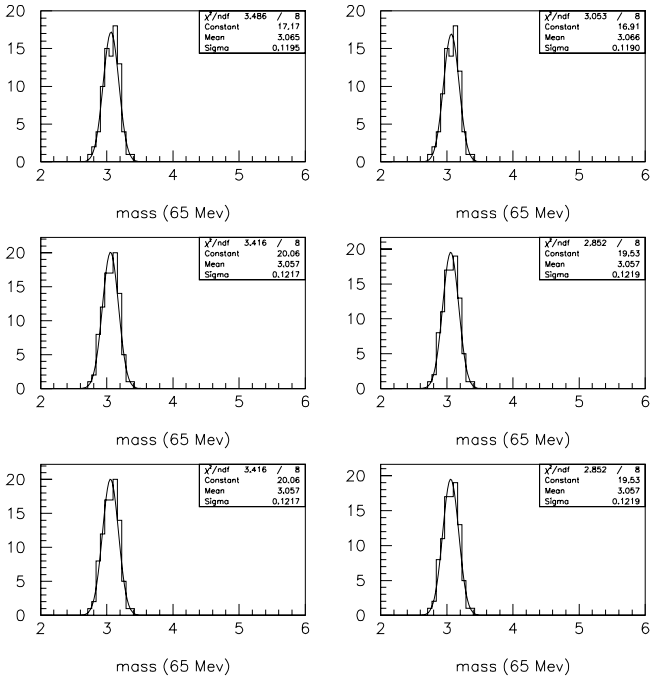

Figure 3.19: *J/ψ resolution for p_t(1-2)= 0.3 GeV, 0.7 GeV, 0. GeV cut (up,middle,below), and total number of hits in SVD $\geq 5, 6$ (left, right column), for SLT triggered J/ψ MC events, after the total momentum and shape cut. Bin size is 65 MeV*

3.2.6 Results

We decided to look separately at the runs where the SLT mass cut was set to 2.2 or to 2.5. The shape of the invariant mass distribution from the last one can show some enhancement around 3 GeV if simply superimposed to the first one, enhancement which is fake, and is simply given by the turn on due to the mass cut which for different luminosities can play funny tricks.

Fig. 3.21 and 3.20 show the full spectrum of invariant mass, and the one where we require 1 or both tracks in the pair to match the SVD detector, after the pretrigger and SLT cuts applied. Already at this stage, the sample with trigger mass cut at 2.5 GeV is left with very little statistics, therefore we decide to concentrate on the runs with trigger mass cut at 2.2.

We decide to concentrate on the double SVD matching strategy, and we start applying the cuts we described in the previous section. Fig. 3.22 and 3.23 show the invariant mass spectrum, and the requirement of the shape cut, the number of hits above 6, and the total momentum above 60 GeV, when both clusters have $p_t > 1$ GeV. The first figure has binning of 75 MeV, the second one of 65 MeV. We shall not try to cut higher in p_t since that would, a part from reducing our signal, spoil the shape of the background around the region we are interested in, and make our analysis more difficult. Anyway, different cuts on p_t attempted (e.g. $p_t(1) > 1., p_t(2) > 1.3GeV$ and $p_t(1) > 1., p_t(2) > 1.7GeV$) show a very similar spectrum in the region around 3.1 GeV. The spectrum from the 2 different binning plots is rather similar. It's interesting to notice how effective the shape cut is, and how it reduces considerably the background.

Let's remember here that the nominal mass for J/ψ is 3.1 GeV.

We saw in the previous subsections, that the masses of π^0 and η were overestimated of few

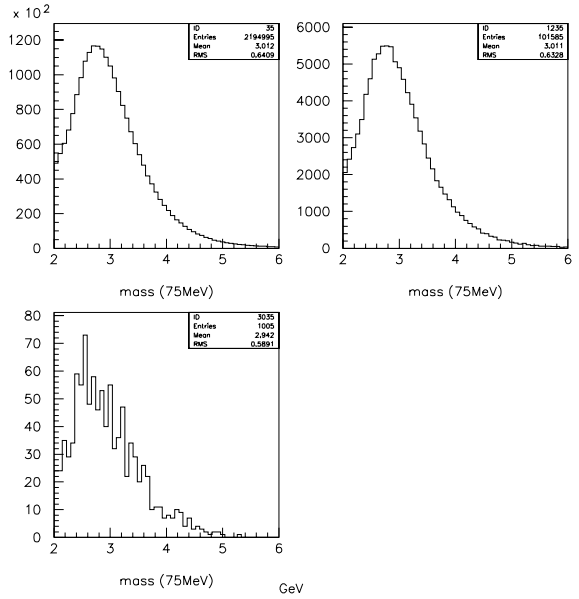

Figure 3.20: *Invariant mass from data. Sample triggered at pt>1 for 2 tracks and M>2.2. Up left: spectrum for cluster pairs without a match to SVD. Up right: spectrum for cluster pairs with at lest 1 match with SVD. Down left: spectrum for both clusters having a match to SVD.Bin width is 75 MeV.*

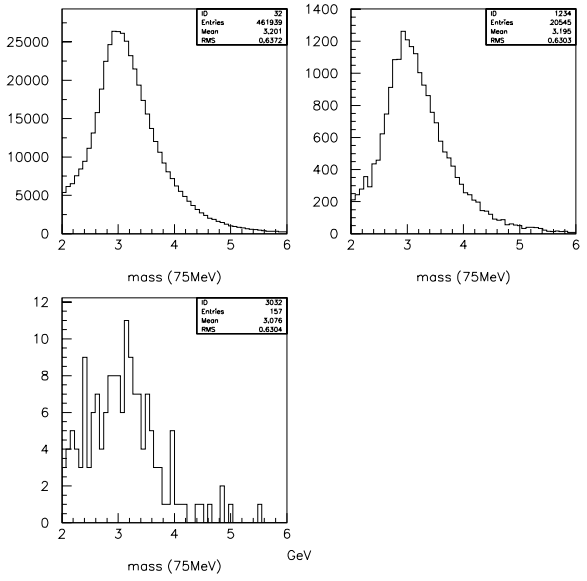

Figure 3.21: *Invariant mass from data. Sample triggered at pt>1 for 2 tracks and M>2.5. Up left: spectrum for cluster pairs without a match to SVD. Up right: spectrum for cluster pairs with at lest 1 match with SVD. Down left: spectrum for both clusters having a match to SVD. Bin width is 75 MeV.*

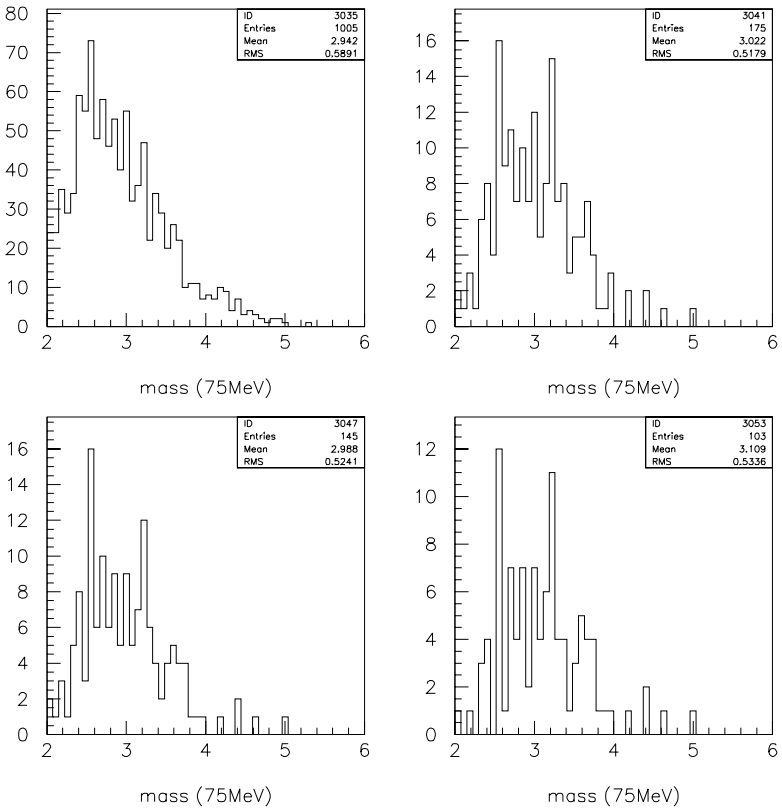

Figure 3.22: *We see how the invariant mass spectrum changes when applying a shape cut (top right), a total number of hits greater or equal than 6 cut (bottom left), and a total momentum cut (bottom right). Bin is 75 MeV. Energy scale is GeV.*

percents, when ending up in the middle calorimeter. We know that the J/ψ , because of the higher mass, and the distance between the 2 leptons, which we showed in fig. 3.17, will probably tend to have at least 1 of the 2 clusters in the middle. Therefore a possible overestimation of few percents should be allowed. Let's try to take a look more in detail at these plots. As already mentioned, no background MC sample is available, to study how we would expect the shape to be in the region around 3.1 GeV after our cuts. It would require an enourmous amount of MC production. One possibility to consider would be to try to get the idea of the background by mixing events, but a good procedure for doing this has not been tried yet, since it is not trivial to mix properly triggered events (where already a structure has been required in the event). The limited time available for our analysis suggests us that we should try to guess the shape of the background from our plot. Anyway, it is rather clear that the extremely limited statistics available at this point will not allow us to claim anything.

In fig. 3.24 we show two fits: one done by imposing the shape to be a gaussian around 3.15 plus an exponential, and the second one simply trying to fit an exponential. In fig. 3.25 we show the histogram with errors, with the fit superimposed. Just to cross check with binning, we redo fig. 3.25, just with a different binning. We can see the result in fig. 3.26.

It looks like the chi square of the fit does not change much when trying one or the other

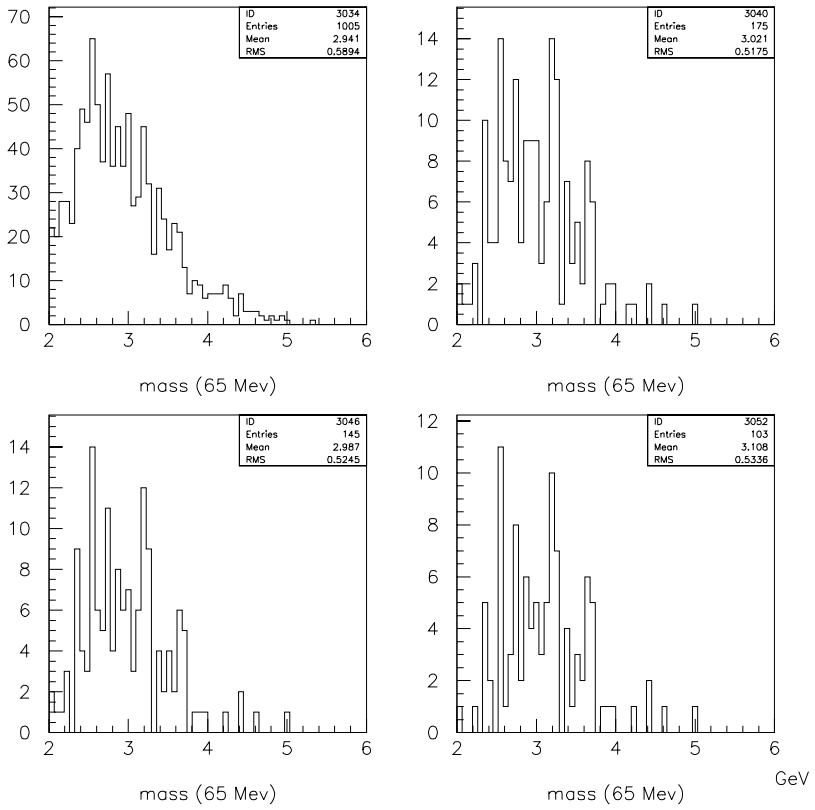

Figure 3.23: *We see how the invarinat mass spectrum changes when applying a shape cut (top right), a total number of hits greater or equal than 6 cut (bottom left), and a total momentum cut (bottom right). Bin is 65 MeV. Energy scale is GeV.*

possibility, indicating that what could look like an enhancement around 3.2 GeV does not have yet the strength enough to discriminate the shape of the spectrum. Remember anyway the amount of statistics we are looking at. Around 3.2 GeV we see a point standing 1.5-2 standard deviations out of the fitted curve, and this still is true when changing binning. The amount of events standing above the exponential, in correspondence to 3.2 GeV, is about 10, as can be seen in fig. 3.24, and the same amount can be counted in the similar plot, with binning 65 MeV.

Wondering a bit more about the reason for seeing any enhancement around 3.2, which is a few percent higher than the nominal mass, we try to use the position of the cluster at ECAL, instead of the direction from the silicon track matching, to construct the invariant mass. The reason for doing this is first of all for curiosity, as an additional check. Secondly, we remember what we discussed about shift in mass of π^0 and η in the beginning of the chapter, and how the calibration procedure could introduce a systematic error on the energy, due to a systematic error done on the angle. If one uses the direction measured from other parts of the detector, like the SVD, together with the energy from ECAL, the consistency of the picture could fail and things could look different.

By redoing our plots, we obtain what is shown in fig. 3.27 and fig. 3.28. The enhancement which we observed at 3.21 before, is now at 3.17 GeV, 2% away from the nominal value of the

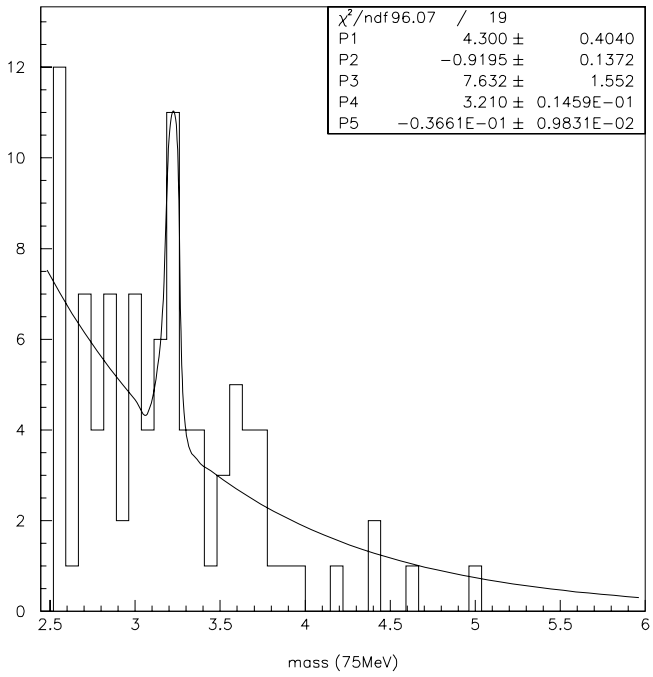

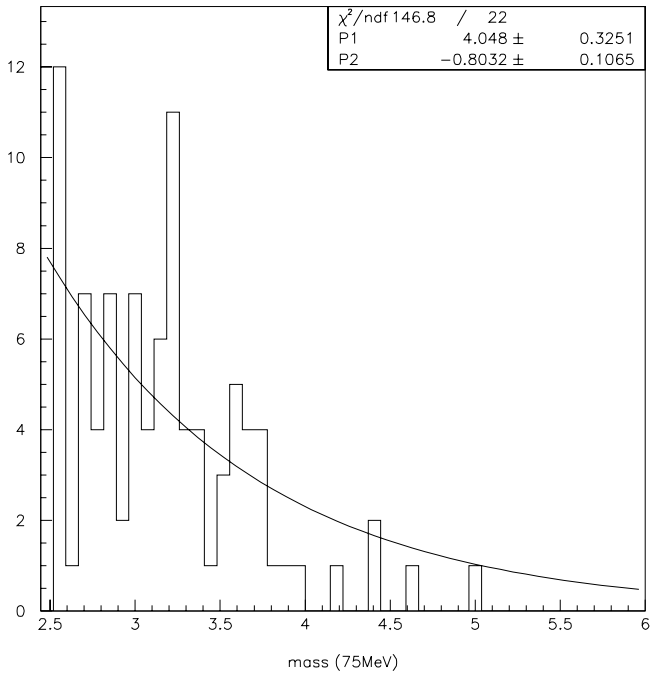

Figure 3.24: *Invariant mass spectrum obtained after applying our cuts on the data sample analyzed. A fit of type* $P_1\ exp(P_2\ (m - m0)) + P_3\ exp(-(m - P_4)^2/(2\ P_5^2))$ *and one of type* $P_1\ exp(P_2\ (m - m0))$ *is attempted. The binning is 75 MeV. Energy scale is GeV.*

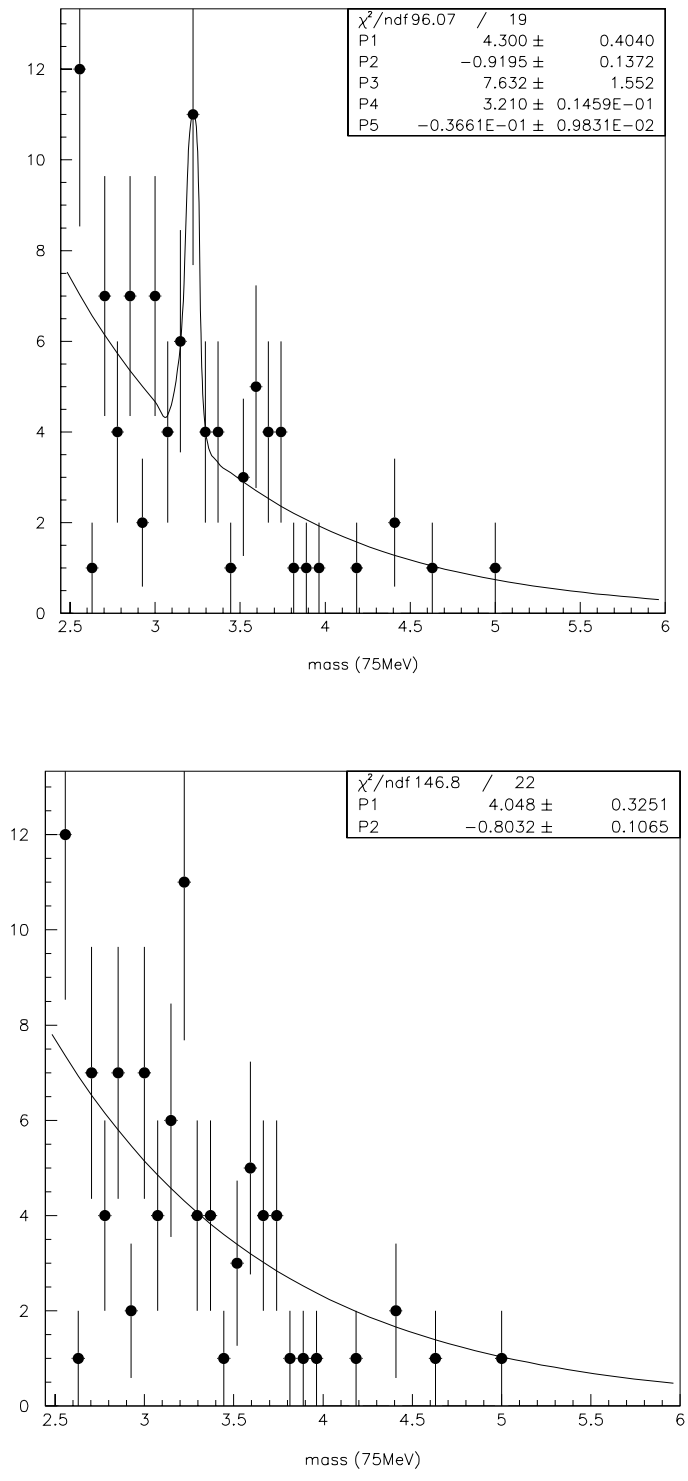

Figure 3.25: *Fig. 3.24 is here shown, with the experimental points and their error bars. The 2 fitting functions are superimposed. Energy scale is GeV.*

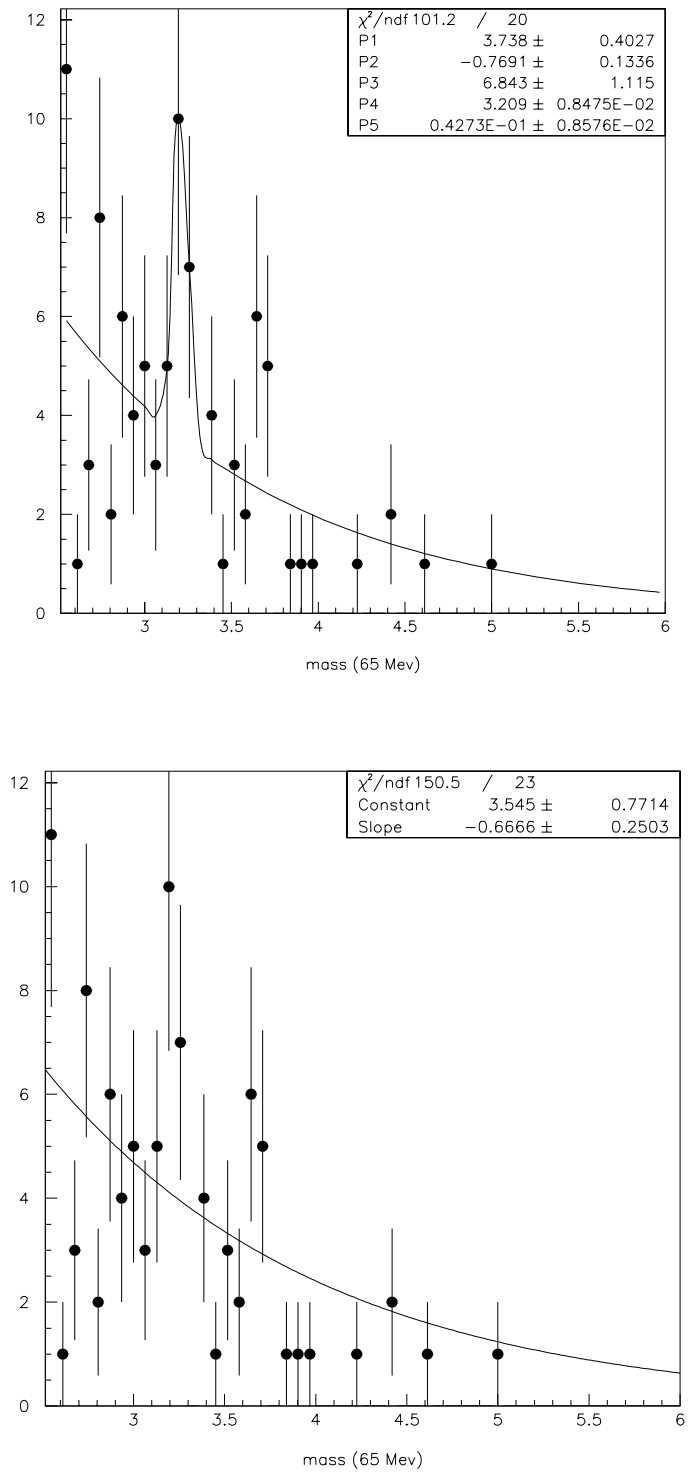

Figure 3.26: *Fig. 3.24 is here shown, but the binning has changed. Now the binning is 65 MeV. Energy scale is GeV.*

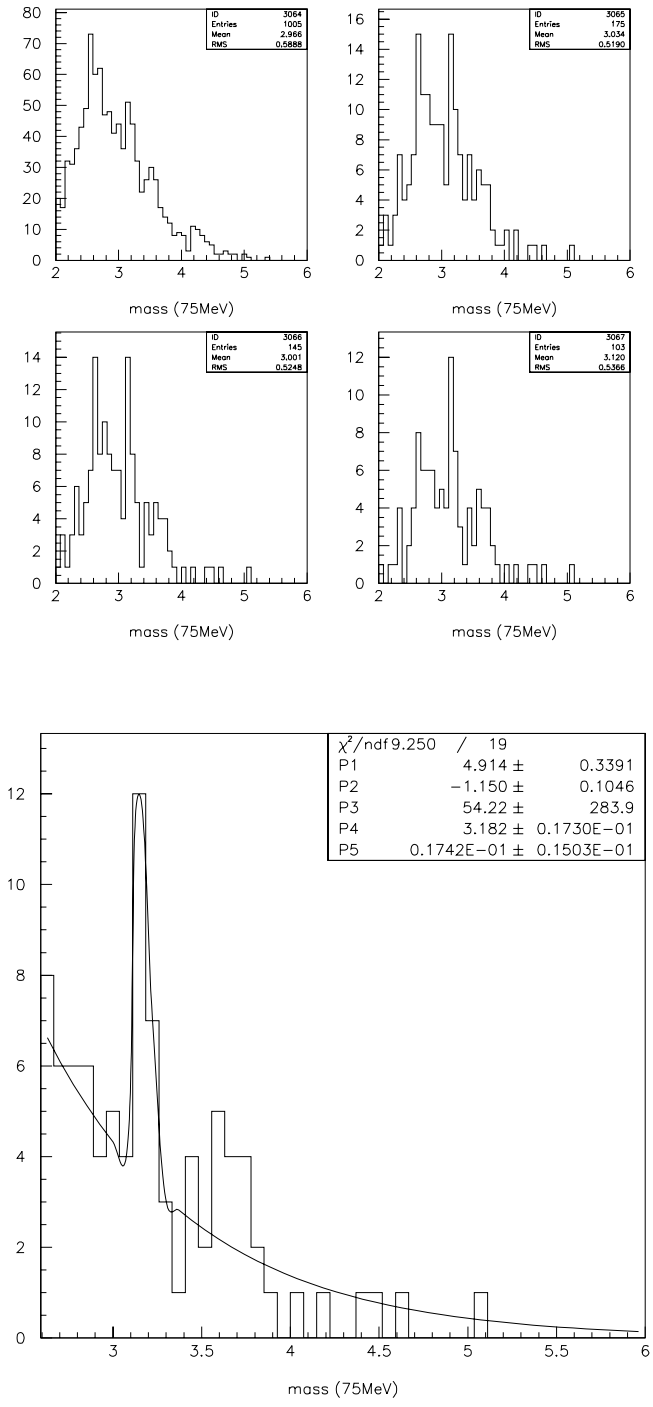

Figure 3.27: *Top: Invariant mass spectrum while applying the shape cut (top right), the requirement on the number of hits (down left), the total momentum cut (down right). Here the position at ECAL, not the SVD track direction, is used to build up the invariant mass. Bottom: fit of an exponential plus a gaussian, as done in fig. 3.24. Binning is 75 MeV. Energy scale is GeV.*

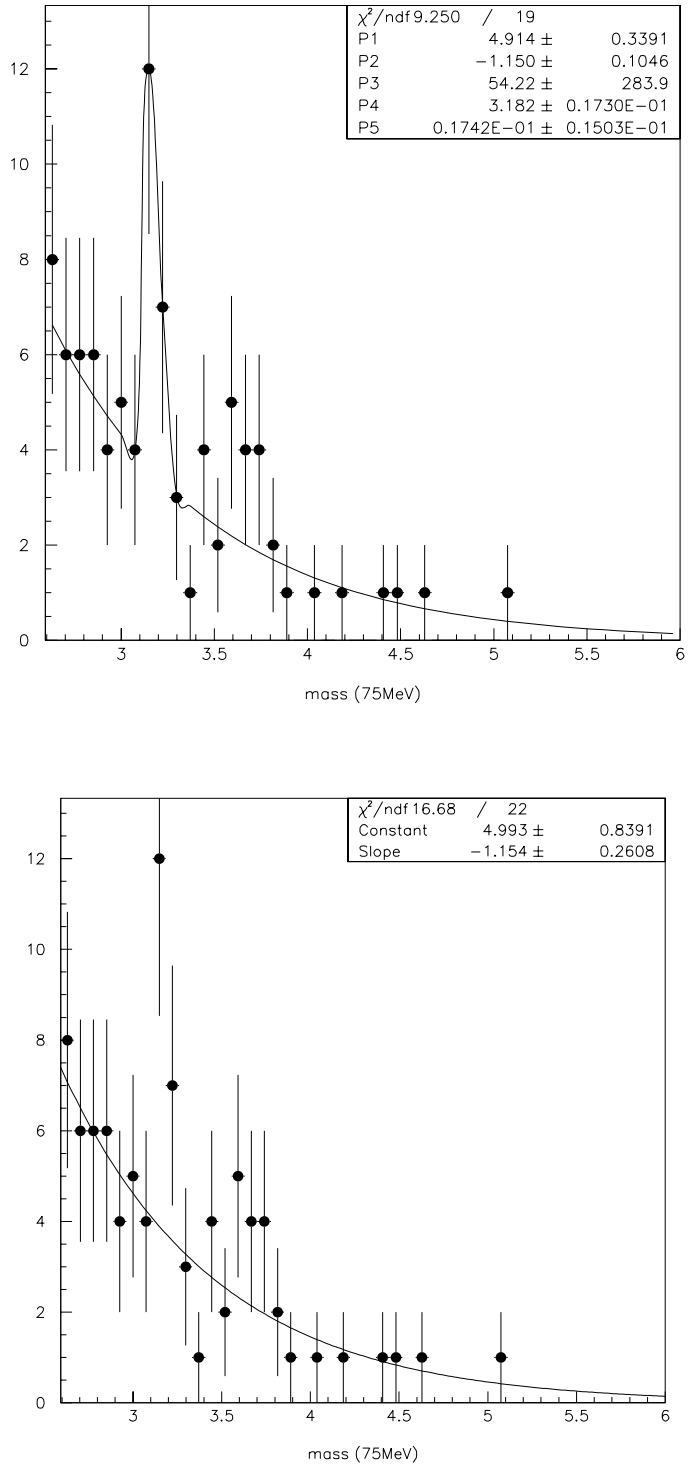

Figure 3.28: *Bottom of fig. 3.27 is here showed with experimental points and their errors, and the fitted function (exp+gaussian or simple exponential) is superimposed. Energy scale is GeV.*

J/ψ mass, and the number of events above the " peak" has increased of few units. It is now 13 approximately. The enhancement is a bit more than 2 standard deviations up in respect to the background level, from the exponential fit.

Another thing we want to try with our data, before passing to the final section. We take the data in fig.3.27, in the region around 3.17 GeV where an enhancement is observed, and we try to construct the 3 body invariant mass of the pair entering fig.3.27 and of a photon laying everywhere else in the calorimeter in the same event. To pick up the photon we look for clusters which show an SVD anticoincidence [3]. We then plot the difference in mass between the 3 body invariant mass and the mass of the pair. This is very similar to what we did in chapter 2 when trying to look for χ_c. Let's remind here that the χ_c states have masses around 3.55 GeV, 0.45 GeV away from the J/ψ mass value.

The result of the search is shown in fig. 3.29, on top we have considered all the possible combinations of photons with a given pair, and on the bottom we show the combination which gives the minimal mass difference in the event. By the number of entries in the region of the enhancement of fig. 3.27 ($\simeq 13$), we would expect 30% of these candidates "J/ψ "'s to come from χ_c's. So we would expect 4 χ_c's at most, considering the inefficiency to detect the photon. If we look at fig. 3.29, in the interval 0.35 - 0.55 GeV, and we look how many events contribute to the 29 entries there, we get a total number of 12 events. This doesn't contraddict our calculation. Once again, we cannot really claim anything since the statistics is so poor.

One last thing we should now try to do, before finishing this section. We shall try to use the luminosity measurements now available, and our efficiency estimate from the MC study, to get an idea of how many J/ψ we would expect anyway.

3.2.7 Conclusions

We try now to use table 3.7, where the luminosity are listed, and table 3.9, where the MC efficiency is listed, to calculate how many J/ψ we expect. We do the calculation only for the runs with trigger requirement on mass at 2.2 GeV, since the luminosity is available only for those.

The formula we use is the following:

$$N_{J/\psi} = (\sum L \cdot \epsilon_{dt}) \cdot \sigma_{J/\psi} \cdot A^{0.92} \cdot Br(J/\psi \to ee) \cdot \epsilon_{J/\psi} \epsilon_s \tag{3.7}$$

where we should sum over the product of the luminosity for a given run and the dead time for that run (ϵ_{dt}), we should correct the J/ψ cross section for the atomic number A of the target material used in that run, we should multiply by the MC estimated efficiency to reconstruct J/ψ with our cuts, and by the fraction ϵ_s of events analyzed for that run. For $\sigma_{J/\psi}$ we use 440 nbarn, as measured by [15].

We finally get the value of **30** expected J/ψ 's. This number has a large uncertainty, we already mentioned that the luminosity measurement itself has at least a 20% error. The efficiency estimated from MC has also some uncertainty, since the MC is not really treating the serious problems we encounter in real life, like misalignement and plane inefficiency, which further are not constant, but change during a run. So, considering all this, and remembering what we just observed on the data, we believe that there is no real contradiction between the expected yield of J/ψ and what we see in the data. One thing is clear, this measurement cries for more statistics, and we hope that soon, already in the beginning of the next run, someone will repeat this same analysis and do not have to worry how to fit an histogram with 100 entries in total left.

[3] No SVD track in the event, if projected at the cluster position, lies closer than 2. cm from the cluster

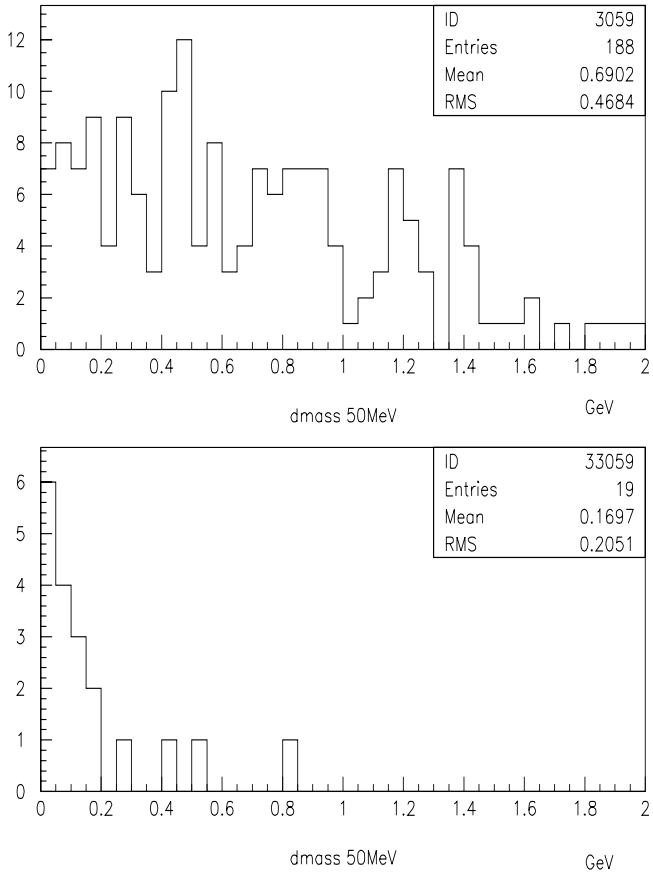

Figure 3.29: *M(123) - M(12), where (12) is a pair of ECAL clusters matching SVD, satysfing our cuts for J/ψ search and giving a invariant mass around 3.17 GeV, and (3) is a cluster from the event, for which an anticoincidence cut with SVD has been required. Top: all the combinations for a given pair are considered. Bottom: only the combination which gives the minimal M(123) - M(12) in the event is shown*

	98 study	**99 experiment**	**factor**
J/ψ events	12 $10^6 \cdot 16\% \cdot 10\%$	90	$2.1 \cdot 10^3$
Trigger+reco eff	1.6%	0.16%	10
DAQ time	10^6 sec	$5 \cdot 10^4$	20
dead time	1.	0.1 - 0.5	10 - 2
total			400 - 2000

Table 3.10: *Comparison between 1998 expected number of J/ψ and up to date calculation based on realistic 1999 detector conditions. The number of J/ψ calculated in chapter 2 is the number of produced ones (tab. 2.5) times the efficiency (tab. 2.6) times the reduction when asking 5 hits (extrapolated from fig. 2.17).*

As a very last remark, let's just try to take what we got in chapter 2, for the estimated

yield of J/ψ with the expected 1998 detector, and roughly compare it with the present expected number, and see if consistent when taking into account how different the run time and the detector efficiency has turned out to be during the real 1999 run. See table 3.10. We shall use not really our number (30), but the number we would get by simply requiring pretrigger, SLT, and nhits above 5 for 2 SVD matchings. This is easier to compare to the numbers in chapter 2. This gives approximately 90 J/ψ 's expected for the 1999 experiment run (one can get it looking at the ratio of final efficiencies on the left and on the right lower part of table 3.9 in this chapter). As one can see in table 3.10 there is no real disagreement between the reduction in the number of expected J/ψ , and the reduction in the detector performances, so it really seems that a good explanation for not having a clear J/ψ signal can be accounted by a lower period of run than expected in beginning of 1998, by a dead time in the DAQ/trigger system, introduced to handle the rate to tape since the whole trigger system was not yet ready, and by detector efficiency and acceptance smaller than expected in beginning of 1998.

CONCLUSION

Hera-B is an interesting experiment, for the physics that can be detected and for the challenge the high radiation environment gives to the detector. The preliminary results from the run of end 1998 - beginning of 1999 make us look forward to the next period of data taking at the end of 1999.
Our first contribution to this experiment has been the development and test of a section of the second level trigger algorithm on simulated data. The section, called l2magnet, performs properly within MC simulation, and needs to wait for the next Hera-B data taking run to be tested online.
Another contribution has been the study, performed in the beginning of 1998 on simulated data, of the expected yield of charmonium states detectable with the detector setup of the 1998 run. This study has shown that no real dangerous background for charmonium measurements exists, except maybe high transverse momentum inelastic events not containing heavy quarks, which cannot be realistically studied within simulation. The study has also shown that in Hera-B we can disentangle the source of direct and indirect (via χ_c) production of J/ψ.
Finally, in this report is also summarized the analysis work done to understand the newly taken data by trying to measure the production of particles like π^0, η and J/ψ. As for the last point, the results should be considered preliminary, given the short time passed from the end of the data taking period and the time of the analysis.
Nonetheless, these results show that we are gaining a good understanding of some of the components of the detector, and that we need more statistics for studying properly charmonium production.

ACKNOWLEDGMENTS

I would like to express my gratitude to my advisor, Professor Jørn Dines Hansen, for his support throughout all my Ph.D. work. I enjoy working with him, and I admire his way of doing physics. I will treasure all the things I've learned from him.
The atmosphere at work has always been very relaxed as well as inspiring, and I would like to thank the High Energy Physics group at the Niels Bohr Institute, and in particular Rasmus, Mogens and Søren for this. It has been a pleasure to know them and work with them.
I would like to express my thanks to the people in Hera-B I've been working and discussing physics with most of the time: Mike, Jenny, Peter and Mauro.
Finally, I wish to thank with all my heart my family and Steen, this work would not have been possible without their support and encouragement.

NAMING CONVENTIONS

ARTE : Software for MC generation, reconstruction and trigger simulation
ATLAS: high energy experiemnt which will take place at LHC (CERN)
BABAR : high energy experiment at SLAC
CARE : CAlorimeter REconstruction
CEM : Color Evaporation Model
CERN: Eruopean Centre for Nuclear Research
CKM : Cabibbo, Kobaiashi, Maskawa
CMS: high energy experiemnt which will take place at LHC (CERN)
COM : Color Octet Model
CSM : Color Singlet Model
DAQ : Data Acquisition
DESY : High energy physics laboratory in Hamburg, DE
ECAL: Electromagnetic CALorimeter
EVC : Event Controller
FCS : Fast Control System
FED : Front End Driver
FERMILAB : High energy physics laboratory in Batavia, US
FLT : First Level Trigger
4LT : Fourth Level Trigger
HOLMES : Reconstruction package for SVD
HPT : High PT chambers
IR : Interaction Rate
ITR : Inner TRacker
L2SIMU : Second Level Trigger simulation software
LHC : Large Hadron Collider
MC : Monte Carlo
MSGC: MicroStrip Gaseous Chambers
OTR : Outer TRacker
PC: Portable Computer
PDG : Particle Data Group
RICH: Ring Imaging CHerenkov detector
SHARC : Super Harvard ARchitecture Computer
SLB : Second Level Buffer
SLT : Second Level Trigger
SM : Standard Model
SVD : Silicon Vertex Detector (same as VDS)
TLT : Third Level Trigger
TRD : Transition Radiation Detector
VDS : Vertex Detector System

Bibliography

[1] H.Albrecht et al., *An experiment to study CP violation in the B system using an internal target at the HERA proton ring*, DESY-PRC 94/02, May 1994.

[2] http://www-hera-b.desy.de

[3] L.Wolfenstein, *Phys. Rev. Lett.* **51** (1983) 1945

[4] J.L.Rosner, *Present and future aspects of CP violation*, hep-ph/9506364

[5] Y.Nir, *Recent developmnets in Theory of CP violation*, hep-ph/9709301

[6] M.Dam, *Rare decays at Hera-B*, Hera-B note 99-049

[7] C.Quigg, *Realizing the potential of quarkonium*, fermilab-conf-97/266-T

[8] P.Hoyer, *Charmonium production at ELFE energies*, hep-ph/9702385.

[9] E. Braaten, *Charmonium production in high energy collisions*, hep-ph/9608370

[10] G.A.Schuler, *Quarkonium production and decays*, cern-th.7170/94

[11] P.Hoyer, S.Peigne, *Rescattering effects in quarkonium production*, NORDITA-97/37 P. Jan. 14,1998

[12] D.M.Kaplan, *Charmonium production in Fermilab E789*, hep-ex/9610003

[13] M.Beneke, *Non relativistic effective theory for quarkonium production in hadron collisions*, hep-ph/9703429

[14] A.Sansoni, *Quarkonia production at Fermilab*, Fermilab-Conf-95/263-F

[15] T. Alexopoulos et al., *Production of J/Psi and Psi' and Upsilon in 800 GeV/c proton - silicon interactions*, Phys Lett B 374, 271 (1996)

[16] The E771 collaboration, *Charmonium production in 800 GeV/c pSi interactions*, XXVII Int. Conf. on H.E.P., Glasgow, July 1994

[17] R. Bonciani, S. Catani, M.L. Mangano, P. Nason, *NLL resummation of the heavy-quark hadroproduction cross-section*, hep-ph/9801375

[18] Phys. Rev. D, *Particles and fields*, July,1 1996, Part I.

[19] F. Ratnikov, *Status of FLT* , Hera-B note 97-127

[20] M.Medinnis, D.Ressing, *Proposal for an all-SHARC SLT for Hera-B* , Hera-B note 96-247, Sept. 27, 1996.

[21] The NBI group, *Proposal for a DS-link based SLT for Hera-B* , Hera-B note 96-248, Sept. 27, 1996.

[22] J.D.Hansen, M.Medinnis, S.Schmidt, S.Xella, *SLT performance in the 1998 scenario* , Hera-B note 98-148

[23] M.Medinnis , *L2simu overview*, Hera-B note 95-019

[24] M.Medinnis , *Slicer overview*, Hera-B note 96-102

[25] H.Thurn , *Refit overview*, Hera-B note 96-102

[26] See presentations by M.Medinnis, S.Xella and S.Schmidt at last physics meeting (May 1998, Zeuthen) and collaboration meeting (February 1998, Hamburg)

[27] S.Scharein, *TLT performances*, Hera-B note in preparation

[28] I.Arinyo et al., *Hera-B physics options in the 1998 run*, Hera-B note 98-132.

[29] J.Ivarsson, T.Lohse, P.Kreuzer, *PYTHIA and FRITIOF: Event generators for Hera-B*, Hera-B note 99-067

[30] T.Sjostrand, Computer Physics Comm. **82** (1994) 74, hep-ph/9508391

[31] H.Pi, Computer Physics Comm. **71** (1992) 173

[32] H.Albrecht, *ARTE*, Hera-B document (see http://www-hera-b.desy.de/)

[33] CND, *GEANT - Detector description and simulation tool* , CERN writeup W5013

[34] R.Mankel, *Kalman Filter - black magic or triviality*, Hera-B seminar, http://www-hera-b.desy.de/general/seminar/herab/kalman.pdf, Jan. 27, 1999.

[35] M.Villa, *Progress Report on the ECAL Reconstruction Software.*, Hera-B note 97-135

[36] M.Villa, private communication

[37] M.Villa, *ECAL reconstruction: status update*, Hera-B note 99-030

[38] V.Alberico et al., *The reconstruction for the electromagnetic calorimeter of the Hera-B experiment*, Hera-B document

[39] A.Somov, *Lumi measuring with ECAL*, Hera-B note 99-096

[40] R.Mankel, *Approaches to luminosity determination for Hera-B*, PRC meeting, May 1999.

[41] A.Carrol et al. , *Absorption cross sections of* $\pi^{\pm}, K^{\pm}, \overline{p}$ *and* p *on nuclei bewteen 60 and 280 GeV/c*, Phys. Lett. 80B, 3 (1979), pag. 319

[42] S.Spratte and M.Symalla, *Target luminosity determination*, Hera-B note 99-096

[43] M.Schmelling, *HOLMES reconstruction package*, Hera-B note 99-086

[44] T.Glebe, *Study of SVD plane efficiency*, Hera-B note 99-096

[45] M.Brauer, *Alignement and track reco*, Hera-B note 99-089

[46] C. Borgmeier, private communication